UNIVERSITÀ
DEGLI STUDI
FIRENZE

DOTTORATO DI RICERCA IN
FISICA E ASTRONOMIA

CICLO XXX

COORDINATORE Prof. Raffaello D'Alessandro

Exploring quantum phase slips in 1D bosonic systems

Settore Scientifico Disciplinare FIS/03 Fisica della materia

Dottorando
Dott. Simona Scaffidi Abbate

Tutore
Prof. Giovanni Modugno

Tutore
Dr. Chiara D'Errico

Coordinatore
Prof. Raffaello D'Alessandro

Anni 2014/2017

UNIVERSITÀ
DEGLI STUDI
FIRENZE

PhD. Thesis in Physics and Astrophysics

XXX CYCLE FIS/03

Exploring quantum phase slips in 1D bosonic systems

Presented by

Simona Scaffidi Abbate

Supervisor: Chiara D'Errico

Supervisor : Giovanni Modugno

Coordinator: Raffaello D'alessandro

Alla mia famiglia, per avermi supportato
A Marisa, per avermi sopportato
A Jacopo e Simone, per avermi fatto sempre sorridere
A Marco, per avermi incoraggiato e per avere sempre avuto fiducia in me

Contents

Introduction

Phase slips, i.e. phase fluctuations of the superfluid order parameter, are the primary excitations of one-dimensional superfluids and superconductors, in the presence of an obstacle for the superflow and supercurrent [1, 2, 3, 4, 5, 6, 7]. These excitations are particularly abundant in one-dimensional systems because of their fragility and vulnerability to the presence of perturbations and fluctuations compared to higher dimensional systems. The phenomenon of phase slips has been originally studied in the field of superconductors, and only recently it has been investigated also in the field of ultracold quantum gases, which are offering an unprecedented opportunity of exploring important quantum phenomena. They are, in fact, very versatile and powerful tools and good candidates to be suitable quantum simulators of several phenomena concerning condensed matter, superfluidity and superconductivity, thanks to the control and manipulation of key properties such as dimensionality and interactions that can be changed by using optical lattices and Feshbach resonances [8].

The first theoretical proposal for the phase slips phenomenon was made by Little in 1967 [1] in order to describe the finite resistance of thin wires below the critical temperature for superconductivity. He supposed that each segment of a thin wire has a finite probability to become, for a very short time, a normal conductor. Due to these fluctuations, which are originated by thermal effects, the persistent current is disrupted and a non-zero resistance in the wire arises. In this situation, the excitations are known as thermally activated phase slips (TAPS). However, the resistance may remain finite also at zero temperature, due to the presence of quantum phase slips (QPS), which may occur via quantum tunnelling events.

Phase slips, both thermal and quantum, have been deeply investigated, both from a theoretical and experimental point of view, in different condensed-matter systems. In particular, they have been observed in superconducting nanowires [11, 9, 10, 12, 13, 14] and Josephson junction arrays [15].

The phenomenon of phase slips became of interest also in the field of superfluids based on ultracold quantum gases. This kind of systems, in fact, gives the possibility to investigate

aspects of phase slips that are not accessible in other systems, thanks to their extreme tunability. For example, by tuning the interactions among the particles of the Bose-Einstein condensate (BEC) thanks to Feshbach resonances [16, 17], it is possible to understand if the interactions can modify the nucleation rate of phase slips or if they can influence the generation of quantum phase slips rather than the nucleation of thermally activated ones. In condensed-matter physics, in fact, tuning the interactions between the Cooper pairs is difficult to achieve. Moreover, it is possible to study the phenomenon of phase slips also in one dimensional system with different geometry. Recently, both theory and experiments investigated the phase slips mechanisms not only in a one-dimensional superfluids [5] but also in a ring geometry [7].

In the case of ultracold quantum gases the presence of phase slips induces a finite dissipation, which is the analogous of the resistance in condensed matter systems. So, the goal in the presence of BEC is to study the dissipation induced by phase slips as a function of the interaction, temperature and velocity. Despite several theoretical models concerning the phenomenon of phase slips in ultracold quantum gases have been made, an experimental exhaustive picture of QPS in ultracold superfluids has not been obtained until few years ago. The first signatures of QPS obtained so far are the observation of a regime of temperature-independent dissipation for a Bose-Einstein condensate in a 3D optical lattice in the group of Brian DeMarco [18], and our recent observation of velocity-dependent dissipation in one dimensional lattices (1D) [19, 20, 21]. Theoretical studies that attempt to reproduce the experiments are underway [22, 23].

As in the case of condensed matter systems, also in the presence of ultracold quantum gases there are experimental obstacles, which make the observation of the phase slips difficult. For example, the occurrence of the Mott insulating phase [24] prevents the observation of phase slips in the strongly interacting regime. In fact, when the system is a Mott insulator the superfluidity of the system, which is the key ingredient to study how fluctuations affect the transport properties of the superfluid, is lost. Moreover, it is also difficult to explore a wide range of currents, i.e. superfluid velocities, due to the occurrence of two different dissipation phenomena: the Landau instability and dynamical instability. The first phenomenon is related to the Landau's criterion of the superfluidity [25, 26], i.e. if the system flows slower than a critical velocity v_c, which correspond to the sound velocity, no excitations can be created and the system does not dissipate. As soon as the system exceeds the critical velocity, phonons will be emitted, inducing thus a energy lost for the superfluid. The latter phenomenon is related to the divergence of the phase slips nucleation rate: if the system velocity is larger than a critical velocity for the dynamical instability, the system enters a dynamically unstable regime driven

by a divergence of the phase slip rate and strongly dissipates.

In order to observe the presence of QPS and to study how this kind of fluctuations modifies the behaviour of our system, we performed transport measurements by using a trap oscillation technique in the presence of a 1D optical lattice, and we studied the time evolution of the quasi-momentum of the system. We observe two different behaviours depending on the momentum reached during the oscillation. For momenta smaller than the critical momentum for the dynamical instability we observe that our system oscillates with a damping due to the presence of phase slips. For large momenta we observe instead an overdamped motion, which we attribute to the occurrence of the dynamical instability that can be described in term of a divergence of the phase-slips rate at the critical velocity for the dynamical instability. In the first part of my theses, I will show the experimental results regarding this two different phenomena, obtained by exciting the sloshing motion of the system for different values of interactions, velocities and temperature. In the second part of my thesis, I will focus the attention on transport measurements performed at constant velocity. By employing this new experimental technique, we can overcome some experimental limits occurring when we excite the sloshing motion of the system, and we can investigate the system dissipation in the regime of low velocity and strong interactions. In both cases of weak and deep 1D optical lattice, we observe a finite dissipation, not only in the superfluid regime, but also in the Mott insulating one. We attribute this dissipation when the system is in the Mott insulating regime to the nucleation of phase slips of the residual superfluid phase, which is due to the fact that we have an inhomogeneous system.

The presentation of the thesis is organized as follows. In the first chapter I will introduce the main instruments related to the physics of BECs. I will discuss the Bose Einstein condensation theoretical model and I will focus the attention on the experimental techniques employed to independently control interactions and dimensionality, i.e. Feshbach resonances and optical lattices. In the end of this chapter I will talk about the physics of a particle in an optical lattice.

In the second chapter, I will focus the attention on one-dimensional systems. Initially I will describe the importance and the basic features of one-dimensional systems. Then I will introduce the theoretical frameworks of a one dimensional systems in the presence of an optical lattice, i.e. the Bose Hubbard model and the Sine Gordon ones. I will show that depending on the competition between the interaction energy and the tunnelling one, the systems may behave as an insulator rather than a superfluid.

The third chapter concerns the phenomenon of phase slips in 1D systems. First I will introduce the phenomenon in superconductors and I will show both the theoretical and the

experimental results regarding thermally activated phase slips and quantum ones. Then I will briefly discuss the first experimental signatures of QPS in superfluids and I will focus the attention on the theoretical model of phase slips in 1D atomic superfluids.

The last chapter is the core of my theses, and it is dedicated to our experimental results regarding the observation of phase slips (both quantum and thermal). In the first part I will briefly describe how we realize the 1D superfluids by starting from a three-dimensional ^{39}K BEC. Then, I will initially focus the attention on the transport measurements performed by using the trap oscillation technique, and subsequently I will describe the transport measurements performed at constant velocity.

Chapter 1

Bose-Einstein Condensate

Bose-Einstein Condensates (BECs) are extremely versatile and powerful tools which can be employed in order to investigate quantum problems related to different branches of physics. The phenomenon of BEC occurs when a high fraction of bosonic particles in thermal equilibrium occupies the same single particle ground state. In this situation, they are observable macroscopic objects behaving according to the laws of quantum mechanics.

The phenomenon of BEC was predicted in 1924 by Bose and Einstein [27, 28] and it was experimentally observed for the first time in 1995, almost simultaneously in three different groups [29, 30, 31] which employed Alkali atoms.

In order to better understand the Bose Einstein condensation, let us consider a gas of N bosons in the continuum confined in a 3-dimensional box with volume V, which in thermal equilibrium are characterized by a density $n = d^{-1/3}$, being d the mean distance between

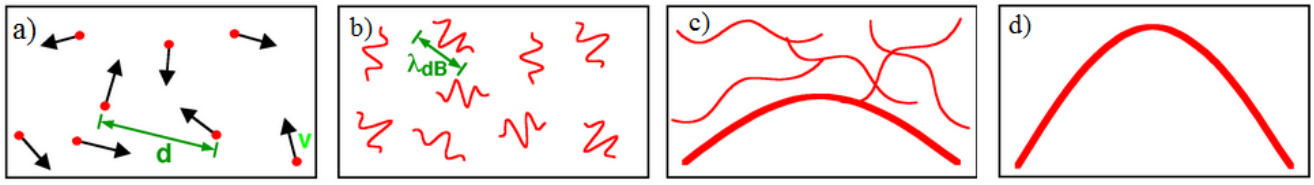

Figure 1.1: Phase transition to the BEC. (a) When $T \gg T_c$, the distance between the particles, d , is large than the De Broglie wavelength λ_{DB} and the particles obey to the Boltzmann statistics. (b) By decreasing the temperature the quantum nature of the particles must be taken into account and they must be described by using a wave function. (c) At $T \simeq T_c$ the wave functions start overlapping and a macroscopic number of particles occupy the lowest-energy quantum state giving rise to the BEC. (d) At $T = 0$, all particles are in the same quantum state, giving rise at a pure BEC without any thermal component

the particles, and by a thermal velocity v. At high temperature, they can be considered as distinguishable point-like particles, obeying to the Boltzmann statistics (Fig.1.1a). Decreasing the temperature, the quantum nature of the particles must be taken into account and they must be described by using a wave function, which is symmetric under interchange of any pair of particle, due to the bosonic nature of the particles (Fig.1.1b). In this situation, the spatial extension of a particle can be suitably described in terms of its De Broglie wavelength

$$\lambda_{DB} = \sqrt{\frac{2\pi\hbar^2}{mk_BT}} \tag{1.1}$$

where m is the particle mass, T the temperature and $\hbar$ and k_B are, respectively, the Planck and the Boltzmann constants. Decreasing the temperature below a critical temperature T_c, the De Broglie wavelength becomes of the order of the mean distance between the particles, i.e. $\left(\frac{V}{N}\right)^{1/3} \approx \lambda_{DB}$, the wave functions start overlapping, the particles cannot be considered distinguishable any longer and a phase transition occurs. In particular, a macroscopic number of particles occupies the lowest-energy quantum state , giving rise to the BEC (Fig.1.1c). Ideally, at $T = 0$, all particles are in the same quantum state, giving rise at a pure BEC without any thermal component (Fig.1.1d). At the phase transition, n and T are related via

$$n\lambda_{DB}^3 = 2.612, \tag{1.2}$$

where $n\lambda_{DB}^3$ is the phase-space density, which is defined as the number of atoms in a box with a volume equal to λ_{DB}^3. In this way, depending on the value of the phase-space density, it is possible to know if the system behaves according to the laws of quantum or classical mechanics. For example, a system of ^{87}Rb at $T = 300$ K and $P = 1$ Atm, behaves according to the laws of classical mechanics, due to the fact that the phase-space density $n\lambda_{DB}^3 \approx 10^{-8}$ is eight order of magnitude smaller than the phase-space density at the phase transition. In order to reach the BEC phase, one can act on the phase-space density either by increasing the density or decreasing the temperature. However, by increasing the density, the probability of three-body recombination increases as well and this results in an increase of atoms losses. In fact, when three atoms are close to each other, two of them may form a dimer, which is usually in an excited vibrational state, whereas the third atom carries away the released energy. Due to the fact that this energy is much larger than the typical depth of the trap confining the atoms, the three atoms are lost and the system is subject to heating.

In addition, not only the increase of the density but also the decrease of the temperature gives rise to a problem. By decreasing the temperature, in fact, all the known interacting systems undergo a phase transition to the solid phase, with the exception of the helium. Both

problems can be solved by employing dilute gases which are defined as systems with a density many thousand times more dilute than air, where the mean interparticle distance is much greater than the scattering length a for s-wave collisions, i.e.

$$n \ll \frac{1}{a^3}. \tag{1.3}$$

In this condition, the probability for three-body collisions to occur is severely reduced and at the same time the samples can be cooled down to very low temperatures (of the order of 1μK or less) due to the fact that the still probable two-body collisions keep the gas in a metastable state, avoiding the transition to the solid phase.

1.1 Non-interacting particles: ideal BEC

Let's consider an ideal system of non interacting bosons at the thermodynamic equilibrium. As it is well known, the mean occupation number of bosons in the single-particle state ν is given by the Bose-Einstein distribution [27, 28, 32]

$$\bar{f}(\epsilon_\nu) = \frac{1}{e^{(\epsilon_\nu - \mu)/k_B T} - 1} \tag{1.4}$$

where T is the temperature, ϵ_ν is the energy of the ν^{th} single particle energy state and μ is the chemical potential. The latter depends on the total number of particles N and on the temperature T via the normalization condition, which imposes that the total number of particles must be equal to the sum of the occupancies of the individual levels. At high temperature, the chemical potential is much smaller than the ground state energy ϵ_{min}, due to the fact that the mean occupation number of the single-particle state is less than unity, and the Bose statistics eq. 1.4 reduces to the Maxwell-Boltzmann statistics. By decreasing the temperature, the chemical potential increases as well as the mean occupation numbers. However, μ cannot exceed the ground state energy, due to the fact that if $\mu > \epsilon_{min}$, $\bar{f}(\epsilon_\nu)$ becomes negative and loses its physical meaning. Consequently, μ must be always lower than ϵ_{min} and the mean occupation number of any excited single-particle state is superiorly limited by the value $\frac{1}{e^{(\epsilon_\nu - \epsilon_{min})/k_B T} - 1}$.

In general, at a fixed temperature T, the constant total number of particles N_{tot} is given via $N_{tot} = N_{exc} + N_0$ where N_{exc} is the number of particles in the excited state and N_0 is the number of particles remaining in the ground state. If the number of particles in the ground state is arbitrarily large, the system has a BEC and this happens when the chemical potential approaches the ground state energy. The highest temperature at which the ground state is macroscopically occupied is known as Bose Einstein transition temperature T_c and it is defined

via

$$N_{exct}(T_c, \mu = \epsilon_{min}) = N_{tot} \tag{1.5}$$

More in detail, at the transition N_{ext} is given by the equation

$$N_{exct}(T_c, \mu = 0) = N_{tot} = \int_0^\infty d\epsilon g(\epsilon) \frac{1}{e^{(\epsilon)/k_B T_c} - 1} \tag{1.6}$$

where the ground state energy $\epsilon_{min} = 0$[1]. In the Eq. 1.6 $g(\epsilon)$ is the density of the state, defined as $g(\epsilon) = \frac{dG(\epsilon)}{d\epsilon}$ where $G(\epsilon)$ is the total number of states with energy less than ϵ. Depending on the system boundary condition, the density of the states depends differently on the energy. In particular, in the ideal situation of a non-interacting d-dimensional system in thermal equilibrium and at zero temperature, the density of state depends on the energy via $g(\epsilon) \propto \epsilon^{d/2-1}$, which implies that in a two-dimensional system the density of the states does not depend on the energy. Instead, in the situation of non-interacting identical bosons in a d-dimensional harmonic confining potential $V(\mathbf{r}) = \frac{1}{2} m \sum_{i=1}^{d} \omega_i^2 x_i^{2}$[2] with frequency ω_i, the density of states depends on the energy via $g(\epsilon) = \frac{\epsilon^{d-1}}{(d-1)\prod_i \hbar\omega_i}$. As a consequence, the critical temperature behaves differently depending on the system dimensionality. In general it can be written as

$$kT_c = \frac{N_{tot}^{1/\alpha}}{[C_\alpha \Gamma(\alpha)\zeta(\alpha)]^{1/\alpha}}. \tag{1.7}$$

Here $\Gamma(\alpha)$ and $\zeta(\alpha)$ are, respectively, the gamma and the Riemann zeta functions and both depend on the index α which is related to the system dimensionality: in the presence of a d-dimensional system $\alpha = d/2$, whereas in the presence of a d-dimensional harmonic confining potential $\alpha = d$ (Tab. 1.1).

Also the constant C_α depends on the index α and behaves differently in the two considered cases. In caseof a box of volume V

$$C_\alpha = \frac{V m^\alpha}{2^{1/2}\pi^2\hbar^3}, \tag{1.8}$$

whereas in the case of a harmonic potential

[1]This assumption is valid also in the presence of an harmonic potential if the number of particles is large enough to neglect the zero-point energy.

[2]The case of N particles in an harmonic potential is of interest due to the fact that, from an experimental point of view, the BEC is always realized in an external confining potential

$$C_\alpha = \frac{1}{(\alpha-1)\prod_i \hbar\omega_i}. \tag{1.9}$$

In 3-dimension, in both cases, the temperature at which the transition occurs is finite. In the first case it is related to the number of particles N_{tot} via

$$k_B T_C \approx 3.31 \frac{\hbar^2}{m}\left(\frac{N}{V}\right)^{2/3} \tag{1.10}$$

whereas in the latter case

$$k_B T_C \approx 0.94 \hbar\bar{\omega} N^{1/3} \tag{1.11}$$

where $\bar{\omega} = (\omega_1\omega_2\omega_3)^{1/3}$ is the geometric mean of the three oscillator frequencies. Let's focus our attention on the low dimensional cases. For a $\alpha \leq 1$, the zeta Riemann function diverges and this implies that for a uniform gas in one or two dimensions and for a one dimensional harmonic potential, the condensation can occur only at $T_C = 0$. Differently, for a two dimensional harmonic potential, $\zeta(2)$ is finite, and consequently the system undergoes the transition to the BEC phase at finite temperature. The one-dimensional systems will be treated in more detail in Chapter 2.

From the transition temperature it is possible to obtain the number of particles in the excited state and, consequently, the number of particles in the ground state via

$$N_0(T) = N_{tot} - N_{exc}(T). \tag{1.12}$$

By considering only the three-dimensional cases, in the presence of a uniform gas, the number of particles in the condensate phase depends on T/T_c via

$$N_0 = N\left[1 - \left(\frac{T}{T_c}\right)^{3/2}\right] \tag{1.13}$$

α	$\Gamma(\alpha)$	$\zeta(\alpha)$
1	1	∞
1.5	0.886	2.612
2	1	1.645
2.5	1.329	1.341
3	2	1.202
3.5	3.323	1.127
4	6	1.082

Table 1.1: Gamma and Riemann zeta functions for different values of the α parameter.

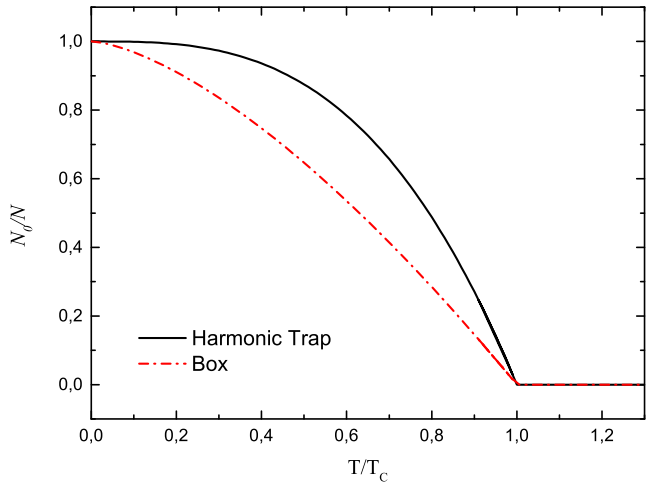

Figure 1.2: Condensate fraction in the presence of a 3D box (red dotted line) and in the presence of an harmonic potential (black continue line). Adapted from [33]

whereas in the presence of an harmonic potential

$$N_0 = N\left[1 - \left(\frac{T}{T_c}\right)^3\right] \tag{1.14}$$

1.2 Interacting particles

So far we have considered the ideal case of a system of non interacting particles. In this section, instead, we will address the case of interacting particles, and we will derive the wave equation describing the behaviour of this kind of systems which is called Gross-Pitaevskii equation [32]. As it was shown before, in a dilute gas, it is possible to neglect the three-body collisions and to consider the binary collisions as the only relevant. In general, in this systems, the interactions are very small for typical interparticle separation, but they become important if two atoms are close together. If the two particles have small total energy in the centre-of-mass frame, the interaction is dominated by the s-wave contribution and the collision properties can be described in terms of the scattering length a, which is the only relevant parameter [32].

In this situation, the binary collisions can be written in terms of a contact pseudopotential as

$$U(\mathbf{r} - \mathbf{r'}) = g\delta(\mathbf{r} - \mathbf{r'}) \tag{1.15}$$

where $(\mathbf{r} - \mathbf{r'})$ is the distance between the two atoms, and g

$$g = \frac{4\pi\hbar^2}{m}a \tag{1.16}$$

is the constant coupling. This quantity depends on the atom mass m and on the scattering length a, which can assume both positive that negative values: in the first case the interaction among bosons is attractive, whereas in the latter the particles repel each others.
In second quantization, the many-body Hamiltonian operator describing a system of N interacting bosons, where the interaction is described by using the pseudopotential in the Eq.1.15, in an external potential V_{ext}, is given by

$$\hat{H} = \int d\mathbf{r}\hat{\Psi}(\mathbf{r})^\dagger \left[-\frac{\hbar^2}{2m}\nabla^2 + V(\mathbf{r})\right]\hat{\Psi}(\mathbf{r}) + \frac{g}{2}\int d\mathbf{r}\hat{\Psi}(\mathbf{r})^\dagger\hat{\Psi}(\mathbf{r})^\dagger\hat{\Psi}(\mathbf{r})\hat{\Psi}(\mathbf{r}). \tag{1.17}$$

Here $\hat{\Psi}(\mathbf{r})$ is the field operator, and its evolution is determined by the Heisenberg equation

$$i\hbar\frac{\partial}{\partial t}\hat{\Psi}(\mathbf{r},t) = \left[\hat{\Psi}(\mathbf{r}), \hat{H}\right] \tag{1.18}$$

which can be written as

$$i\hbar\frac{\partial}{\partial t}\hat{\Psi}(\mathbf{r},t) = \left[-\frac{\hbar^2}{2m}\nabla^2 + V(\mathbf{r}) + g\hat{\Psi}(\mathbf{r},t)^\dagger\hat{\Psi}(\mathbf{r},t)\right]\hat{\Psi}(\mathbf{r},t) \tag{1.19}$$

by using the commutation rules. In a semiclassical theory, the field operator can be written as

$$\hat{\Psi} = \langle\hat{\Psi}\rangle + \delta\hat{\Psi} \tag{1.20}$$

where $\phi = \langle\hat{\Psi}\rangle$ is the expectation value on the quantum state of the system and $\delta\hat{\Psi}$ are the quantum fluctuations.[3] The expectation value $\phi = \langle\hat{\Psi}\rangle$ is the *order parameter* related to the phenomenon of Bose-Einstein condensation and correspond to the BEC wave function. The order parameter describes the degree of symmetry of the system and assumes a different value depending on whether the system is in an ordered or in a disordered phase. In particular, for $T < T_C$, i.e. when the system is in the ordered BEC phase, it has a finite value whereas it becomes zero for $T > T_C$, as a result of a spontaneous symmetry breaking. The quantum fluctuations $\delta\hat{\Psi}$ correspond to the non condensed particles and, by using a mean field approach, they can be neglected at very low temperature ($T \approx 0$), when a macroscopic number of particles occupies the ground state. By putting the Eq. 1.20 in the Eq.1.19, we find the Gross-Pitaevskii equation

[3]For definition, $\langle\delta\hat{\Psi}\rangle = 0$

$$i\hbar\frac{\partial}{\partial t}\phi(\mathbf{r},t) = \left[-\frac{\hbar^2}{2m}\nabla^2 + V(\mathbf{r}) + g|\phi(\mathbf{r},t)|^2\right]\phi(\mathbf{r},t) \tag{1.21}$$

This equation, due to the interaction term, is a non linear *Schrödinger* equation and it describes the time evolution of the BEC wavefunction which is connected to the BEC density distribution via

$$\rho(\mathbf{r},t) = |\phi(\mathbf{r},t)|^2 \tag{1.22}$$

The Gross-Pitaevskii equation 1.21 can be also obtained by minimizing the energy functional

$$E[\phi] = \int \phi(\mathbf{r},t)\left[-\frac{\hbar^2}{2m}\nabla^2 + V(\mathbf{r})\phi(\mathbf{r},t)\right]\phi(\mathbf{r},t) + \frac{g}{2}|\phi(\mathbf{r},t)|^4, \tag{1.23}$$

where the first term is the kinetic energy, the second one is the potential energy and the last one is the interaction term, respect to infinitesimal variations of ϕ.

The ground state of the system, i.e. the stationary solution of the Gross-Pitaebskii equation 1.21, can be obtained by substituting the ansatz wavefunction

$$\phi(\mathbf{r},t) = \phi(\mathbf{r})e^{-i\mu t/\hbar}, \tag{1.24}$$

where μ is the chemical potential, in the Eq. 1.21. In this way, we found the time-independent Gross-Pitaewskii equation

$$\left[\frac{-\hbar^2}{2m}\nabla^2 + V(\mathbf{r}) + g|\phi(\mathbf{r})|^2\right]\phi(\mathbf{r}) = \mu\phi(\mathbf{r}) \tag{1.25}$$

which is a *Schrödinger*-like equation, where the potential acting on a atom at the position $\mathbf{r}$ is given by the sum of an external potential V and an effective mean potential generated by the remaining bosons at that point. In the equation the eigenvalue is the chemical potential μ, which it is different from the case of a linear *Schrödinger* equation where the eigenvalue is the energy. In fact, if for non-interacting particles all in the same state the chemical potential is equal to the energy per particle, in the interacting case it is not.

Let's consider the Gross-Pitaevskii equation in the presence of an external harmonic potential $V(x_1,x_2,x_3) = \frac{m}{2}\sum_{i=1}^{3}\omega_i^2 x_i^2$. In the case of N non interacting particles, the wave function of the system is given by the normalized product of the ground state wave functions of the single-particle harmonic oscillator, i.e.

$$\phi_0(r) = \frac{1}{\pi^{3/2}a_{ho}^{3/2}}e^{\frac{1}{2}\sum_{i=1}^{3}\frac{x_i^2}{a_{ho}^2}} \tag{1.26}$$

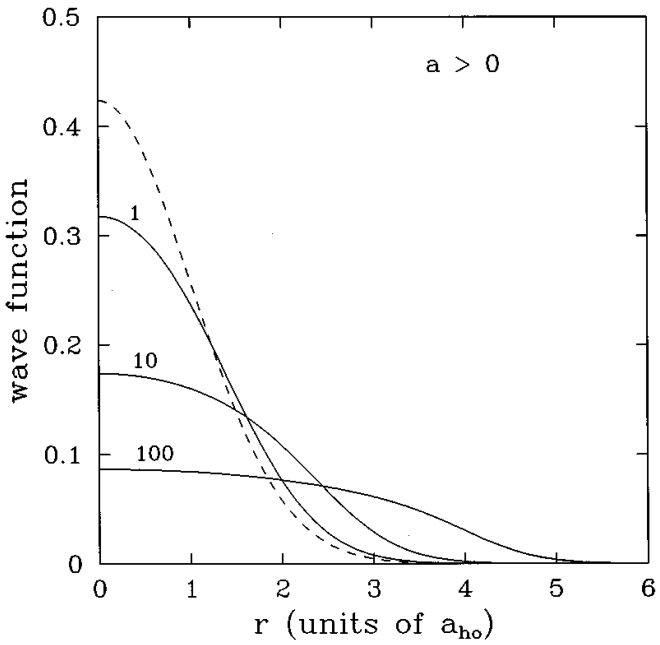

Figure 1.3: BEC density distribution for different values of positive scattering length (repulsive interaction). In the non interacting case the density distribution is a Gaussian (dotted line) whereas, by increasing the interaction it takes the form of an inverted parabola with a broadening which depends on the interactions strength. Adapted from [34]

with $a_{ho} = \sqrt{\hbar/m\omega_{ho}}$ the harmonic oscillator length, and the BEC density distribution has the form

$$n_0(\mathbf{r}) = N|\phi_0(\mathbf{r})|^2. \tag{1.27}$$

In the limit of strong interactions, i.e. $Na \gg a_{ho}$, the interaction energy term in the time-independent Gross-Pitaevskii equation is the dominant one and the kinetic energy term can be neglected ($Thomas - Fermi\ Approximation$). In this situation, the equation takes the form

$$\left[V(\mathbf{r}) + \frac{4\pi\hbar a}{m}|\phi(\mathbf{r})|\right]\phi(\mathbf{r}) = \mu\phi(\mathbf{r}) \tag{1.28}$$

and it can be analytically solved. In this situation the solution is

$$n_0(\mathbf{r}) = \begin{cases} \frac{1}{g}[\mu - V(\mathbf{r})] & \mu > V(\mathbf{r}) \\ 0 & \mu < V(\mathbf{r}) \end{cases} \tag{1.29}$$

which implies that for an harmonic potential the density distribution assumes the shape of an inverted parabola

$$n_0(\mathbf{r}) = -\frac{\mu}{g}\left(1 - \sum_{i=1}^{3} \frac{x_i^2}{R_i}\right) \tag{1.30}$$

where $R_i = \sqrt{\frac{2\mu}{m\omega_i^2}}$ is the Thomas-Fermi radius in the i^{th} direction.

In Fig.1.3 is shown how the repulsive interaction between atoms modifies the density distribution: it has not the form of the gaussian wavefunction of the harmonic oscillator ground state anymore, as in the case of non interacting particles, but it is a broader inverted parabola with a broadening depending on the interactions strength.

1.3 Feshbach resonances

How it was introduced in the previous section, the effective interaction among the particles in a dilute bosonic gas at low temperatures can be described in terms of a single parameter, i.e. the scattering length a. This quantity can assume both positive and negative value and the interaction between two particles is, respectively, attractive or repulsive. Anyway, there is the possibility to change the scattering length value, and switching from a regime to an other, by using Feshbach resonances. This property was studied for the first time in 1958 by Feshbach in the field of nuclear physics [17], and it is important also in the field of cold atoms [16, 35, 36]. In fact, thanks to the presence of these resonances, it is possible to tune the interparticle interaction by simply changing a magnetic field acting on the atoms.

Let us talk about Feshbach resonances more in details and let us consider two diatomic molecular potential curves, the ground state V_{bg} and the excited state V_{exc}, which correspond to two different spin configurations[4] (Fig.1.4). At large interparticle distances, i.e. for $R \to \infty$, the potential V_{bg} correspond to the energy of two free atoms and it is used as reference energy ($V_\infty = 0$). When two atoms collide, with a small energy E, the potential curve V_{bg} correspond to the accessible channel for collisional processes and it is called "open channel". The other channel, which is known as "closed channel", it is not accessible, but it may have a bound molecular state close to 0. If the two atoms have the possibility to make a temporary transition to this the bound state, then their scattering cross section can extremely increase.

Let us suppose that the magnetic moment of the atoms in the two channels is different. In this case, it is possible to change the energy difference between the two state by simply varying a magnetic field B thanks to the fact that the two potential curves have a different response

[4]In general, a molecule has more than two potential curves, each of which corresponds to an hyperfine or Zeeman level. For simplicity the description considers one excited state and it describes appropriately the case of a single resonance.

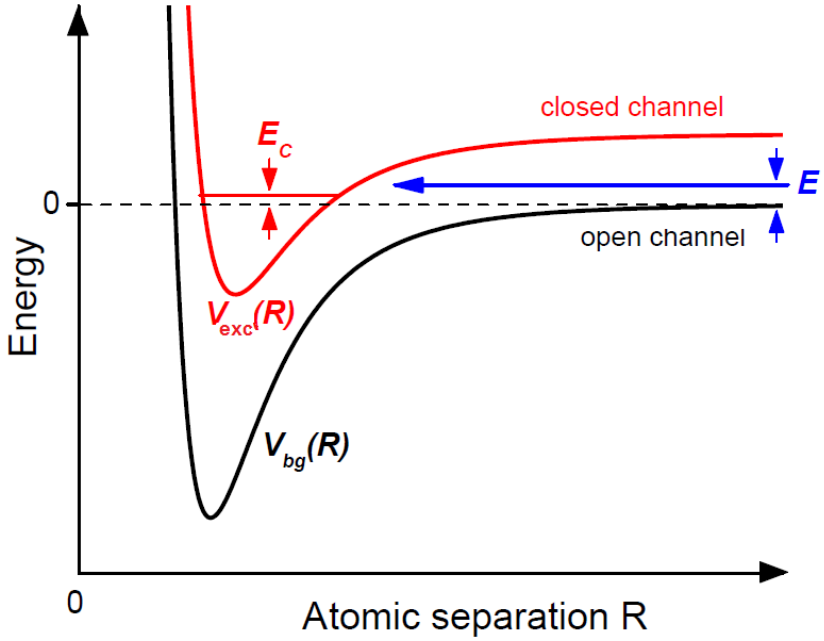

Figure 1.4: Model of the Feshbach resonance. The atoms in the open channel $V_{bg}(R)$ collide with a small energy E. If the collisional energy approaches the energy of the molecular bound state in the closed channel $V_{ext(R)}$ (at the Feshbach resonance) the scattering cross section increases. By tuning a magnetic field, it is possible to the energy level of the closed channel, with respect to the open one. Adapted from [36]

to the application of the field due to the Zeeman effect. In particular, by tuning the magnetic field, it is possible to change the energy level of the closed channel, with respect to the open one. At the (Feshbach) resonance, the energy of the two colliding atoms E approaches the energy of the molecular bound state, by causing the increase of the scattering cross section. The scattering length depends on the magnetic field B via

$$a(B) = a_{bg}\left(1 - \frac{\Delta}{B - B_0}\right) \tag{1.31}$$

where B_0 is resonance center, Δ the resonance width and a_{bg} the background scattering length, i.e. the scattering length far from the resonance.

It is important to note that if the resonance is a general phenomenon, the parameters B_0, Δ and a_{bg} depend on the atomic specie. Let us consider the specific case of the ^{39}K,i.e. the atom that we employ in the experiments. It has a background scattering length negative ($a_{bg} = -44a_0$, with a_0 the Bohr radius), corresponding to an attractive interaction, which would provoke the BEC collapse. However, it has also a wide Feshbach resonance and it is possible

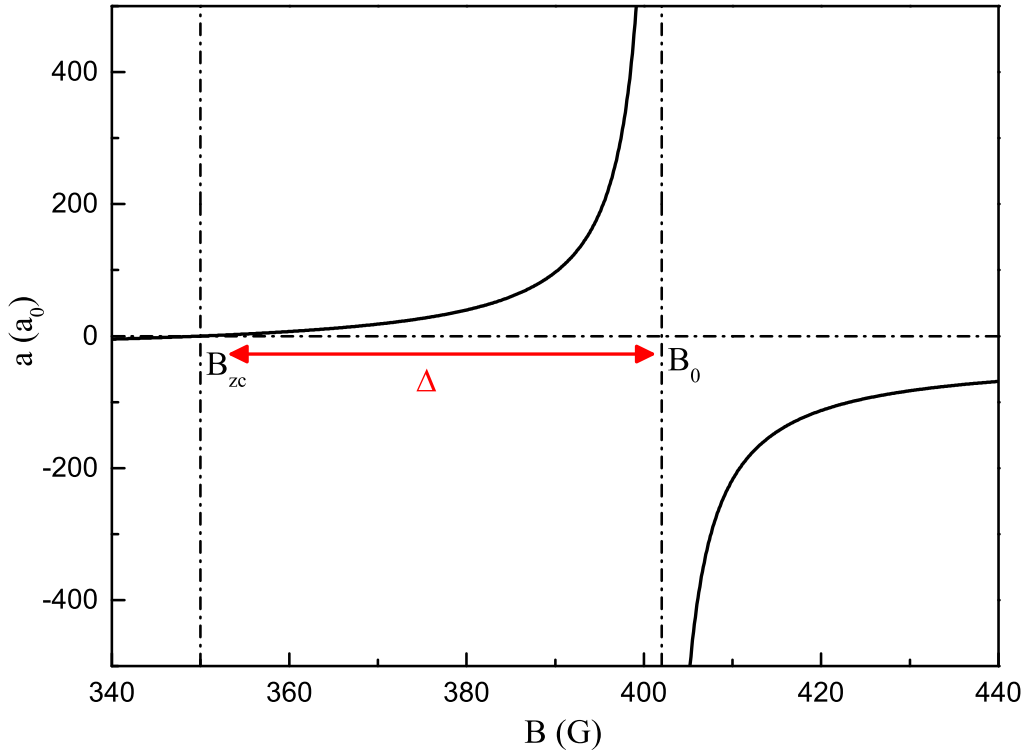

Figure 1.5: Scattering length a, in unit of Bohr radius, as a function of the magnetic field B for ^{39}K atoms. The Feshbach resonance occurs at $B_0 \sim 400G$. B_{zc} and Δ are zero-crossing magnetic field and the resonance width respectively.

to tune the value of the scattering length until it reaches positive value. Fig.1.5 shows a plot of the scattering length a as a function of the magnetic field B of the ^{39}K in the substate $|F = 1, m_F = 1\rangle$. In this situation $B_0 \simeq 402G$ and $\Delta \simeq -52G$. As it is shown in Fig 1.5, the scattering length vanishes at a certain value of the magnetic field. It is known as zero-crossing magnetic field $B_{zc} = B_0 + \Delta$ and it is related to the scattering length via

$$a(B) = \frac{a_{bg}}{\Delta}(B - B_{zc}) \tag{1.32}$$

if $B \to B_{zc}$. It is important to not that by tuning the value of $\frac{a_{bg}}{\Delta}$ we control the interaction around the vanishing interaction point. In particular, by decreasing the ratio we improve the accuracy for tuning the interaction. In the case of ^{39}K atoms, the sensitivity around $B_{zc} = 350G$ is $da/dB \simeq 0.56a_0/G$ and this implies that if the stability of the magnetic field is for example 1G, the interactions of the BEC can be nulled with an uncertainty of about half a Bohr radius.

1.4 Optical dipole potentials: red detuned trap

Another important feature of the Bose-Einstein condensates is the possibility to easily manipulate and trap the atoms by using laser light. In order to understand how it is possible, let us focus on the interaction between the atoms and a monochromatic electron magnetic radiation. The presence of an electric field

$$\mathbf{E}(\mathbf{r},t) = \hat{e}\tilde{E}(\mathbf{r})e^{-i\omega t} + h.c. \tag{1.33}$$

induces on the atoms a dipole momentum, which oscillates at the same driving frequency ω of the electric field $\mathbf{E}$

$$\mathbf{p}(\mathbf{r},t) = \hat{e}\tilde{p}(\mathbf{r})e^{-i\omega t} + h.c. \tag{1.34}$$

Both in the electric field equation that in the dipole momentum one, $\hat{e}$ is the unit polarization vector and $\tilde{E}$ and $\tilde{p}$ are, respectively, the amplitude of the electric field and of the dipole momentum, which are related via $\tilde{p} = \alpha\tilde{E}$, with $\alpha = \alpha(\omega)$ the complex polarizability.

Due to the interaction between $\mathbf{E}$ and $\mathbf{p}$, a conservative dipole potential

$$U_{dip} = -\frac{1}{2}\langle \mathbf{pE} \rangle \tag{1.35}$$

is present.

It is possible to demonstrate [37] that if the diving frequency ω is far from the atomic resonance frequency ω_0, which is the case of main practical interest, the dipole potential U_{dip} takes the simple form

$$U_{dip} = \frac{3\pi c^2}{2\omega_0^3}\left(\frac{\Gamma}{\Delta}\right) I(\mathbf{r}) \tag{1.36}$$

where $\Delta = \omega - \omega_0$ is the detuning,

$$\Gamma = \frac{3\pi c^2}{2\hbar\omega_0^3}\left(\frac{\Gamma}{\Delta}\right)^2 I(\mathbf{r}) \tag{1.37}$$

is the scattering rate due to the far-detuned photon absorption and subsequent spontaneous reemission by the atoms and $I(\mathbf{r}) = 2\epsilon_0 c|\tilde{E}|^2$ is the field intensity. In order to reduce the value of the scattering rate in the experiments, large detuning and high intensities are used, due to the fact that $U_{dip} \propto \left(\frac{\Gamma}{\Delta}\right)$, whereas $\Gamma = \left(\frac{\Gamma}{\Delta}\right)^2$

The detuning Δ can assume both positive that negative value. In the first case, which is

known as "blue detuning", the dipole potential is positive, the interaction is repulsive and the light intensity maxima correspond to the potential maxima. In the latter case, which is known as "red detuning", the light intensity maxima correspond to the potential minima and the interaction attracts atoms into the light field. In this pictures we can talk about blue-detuned traps and red-detuned traps. We focus our attention on the latter case.

In the experiment, red detuned gaussian laser beams are employed in order to produced optical trap. The spatial intensity distribution of a gaussian beam, which propagates along the z direction is given by

$$I(r,z) = \frac{2P}{\pi w^2(z)} e^{-2\frac{r^2}{w^2(z)}} \tag{1.38}$$

where r is the radial coordinate and P the power of the beam. $w(z)$ is the radial distance where the maximum intensity is reduced of a factor e^{-2} and it depends on the coordinate z via

$$w(z) = w_0 = \sqrt{1 + (\frac{z}{z_R})^2} \tag{1.39}$$

where w_0 is the waist of the beam, i.e. the minimum radius, and $z_R = \pi\omega_0^2/\lambda$ is the Rayleigh length. Both w_0 and z_R give an estimation of the divergence of the Gaussian beam, and in particular large values of w_0 and z_R implicate a collimated beam.

From the beam intensity profile it is possible to obtain the dipole potential via Eq.1.36. Under the assumption that the atom thermal energy k_BT is lower than the potential depth $V_{trap} = V(r = 0, z = 0)$ (which can vary from few kHz to 1MHz), it is correct to assume that the dimensions of the gas are smaller than the divergence length scale. In this situation the optical potential can be approximated with a harmonic oscillator with a cylindrical symmetry

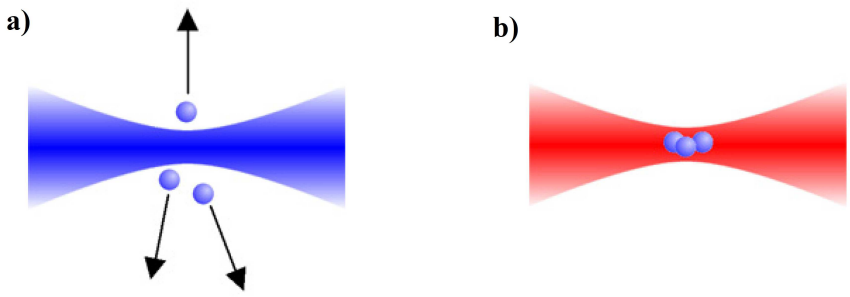

Figure 1.6: Blue- detuned and red-detuned traps. (a) In Blue-detuned traps the atoms are repelled from the blue detuned dipol light field. (b) In red-detuned traps the atoms are attracted into the light field. Adapted from [38].

$$V_{dip} \approx -V_{trap}\left[1 - 2\left(\frac{r}{w_0}\right)^2 - \left(\frac{z}{z_R}\right)^2\right] \tag{1.40}$$

whose oscillation frequencies are

$$\omega_r = \left(\frac{4V_{trap}}{mw_0^2}\right)^{1/2} \tag{1.41}$$

and

$$\omega_z = \left(\frac{2V_{trap}}{mz_R^2}\right)^{1/2}. \tag{1.42}$$

It is important to know that the Rayleigh length z_R is $\pi w_0/\lambda$ larger than the minimum waist w_0 and consequently the force acting on the atoms along the longitudinal direction is lower than that acting along the radial direction. This implies that it is essential to use more than one single laser beam to tightly confine the atoms along all of the spatial directions.

1.5 Optical lattices

By using laser light it is possible to realize optical lattices, which are the perfectly periodic potential for neutral atoms. As the optical trap, they can be employed to trap and to manipulate the atoms.

Optical which are realized by superimposing two counter propagating laser beams. The interference of the two laser beams produces a standing wave with a period equal to $\lambda/2$, where it is possible to trap the atoms. In order to have a standing wave with a larger period, the angle between the two beams must be smaller than 180. In the presence of Gaussian laser beams, the potential trap is

$$V(r,z) \approx -V_0 e^{-2r^2/w^2(z)} sin^2(kz) \tag{1.43}$$

where $k = 2\pi/\lambda$ is the lattice wave vector and V_0 is the potential depth which can be written in term of the recoil energy $E_r = \frac{\hbar^2 k^2}{2m}$ as

$$s = \frac{V_0}{E_r}. \tag{1.44}$$

It is important to note that if all of the parameters of the two laser beams are the same, V_0 is four times larger than V_{trap}. This is the simplest case of 1D optical lattice, but it is also possible to realize 2D or 3D optical lattices by superimposing, respectively, two or three orthogonal standing waves, in order to avoid the interference term. In this situation, the potential depth

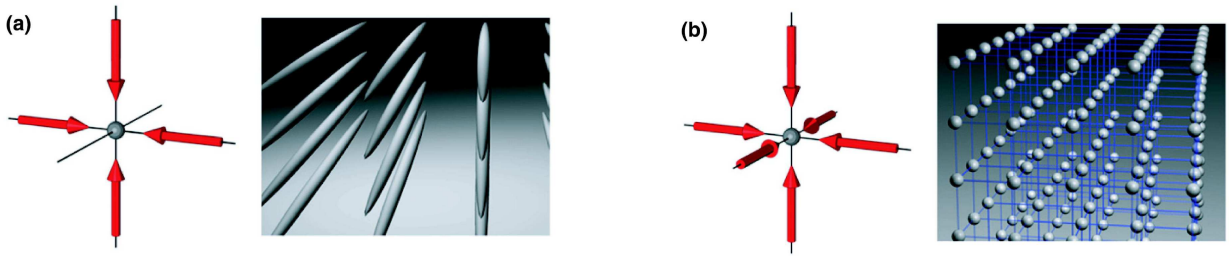

Figure 1.7: Optical lattices scheme. (a)In the 2D case, a matrix of 1D tubes is created by superimposing two orthogonal standing waves. (b) A 3D optical lattice is created by superimposing three orthogonal standing waves. Adapted from [38].

in the center is, respectively, the sum of the two or three standing waves. Obviously, if the beams are not exactly orthogonal, the interference term is finite and the potential changes in time depending on the time phase.

In the 2D case, the atoms are trapped to an array of tightly confining 1D potential tubes (Fig. 1.7(a)), whereas in the 3D one, the optical lattice can be approximated by a 3D simple cubic array of tightly confining harmonic-oscillator potentials at each lattice site (Fig. 1.7(b)).

Due to the fact that optical lattices are easily controllable and manipulable, they are considered a powerful tool that has a relevant role in the field of ultracold quantum gases. In particular, the ensemble of optical lattices, which are perfect lattices without defects or lattice vibrations, and BEC gives rise to a quantum simulator, which can be used to study various phenomena concerning several branches of the physics.

1.5.1 Bloch Theorem

Let us now focus the attention on a particle in the presence of an optical lattice, which we consider one-dimensional for simplicity. The evolution of the system is due to the Hamiltonian

$$H = \frac{p^2}{2m} + V_{latt} \tag{1.45}$$

which contains the kinetic energy of the particle, $E_k = \frac{p^2}{2m}$, and another term related to the presence of the optical lattice which satisfies the condition $V_{latt}(x) = V_{latt}(x + d)$, with d the lattice periodicity.

In this situation, the static *Schrödinger* equation takes the form

$$H\Psi = \left(-\frac{\hbar^2}{2m}\frac{\partial^2}{\partial x^2} + V_{latt}\right)\Psi = E\Psi \tag{1.46}$$

whose solution, according to the Bloch theory [39], is a periodic plane wave,

$$\Psi_{n,q} = u_{n,q}(x)e^{iqx} \tag{1.47}$$

where the periodic term $u_{n,q}(x) = u_{n,q}(x+d)$ has the same lattice periodicity d.

As a consequence of the system periodicity, the eigenfunctions $\Psi_{n,q}$ of the *Schrödinger* equation and the eigenvalues $E_{n,q}$ are characterized by two quantum numbers q and n. The first one is called "quasi-momentum" and it is related to the translational symmetry of the optical lattice.

It is important to note that the periodicity of the optical lattice is reflected also in the reciprocal lattice, whose periodicity si $G = 2\pi/d$, and consequently

$$E_{n,q}(x) = E_{n,q+G}(x) \tag{1.48}$$

$$\Psi_{n,q}(x) = \Psi_{n,q+G}(x) \tag{1.49}$$

As a consequence of the reciprocal lattice periodicity, only the first Brillouin zone, i.e. the elementary cell of the reciprocal lattice which ranges from $q = -G/2$ and $q = G/2$, is relevant. The second quantum number, n, is called "band index": for a given quasimomentum q, there are several solution $E_n(q)$ (which are continuous function of q) identified by the index n. This solution are called "energy bands" and they are separated by forbidden zones, called energy gaps. The energy bands behaves differently depending on the optical lattice depth. In the case of weak optical lattice, i.e. $s \leq 5$, the energy bands depends strongly on the quasimomentum q and they takes the form

$$\frac{E(\tilde{q})}{E_R} = \tilde{q}^2 \mp \sqrt{4\tilde{q} + \frac{s^2}{16}} \tag{1.50}$$

where $\tilde{q} = q/\pi/d - 1$ and the minus sign is referred to the lower energy band whereas the plus sign is referred to the first excited band. (Fig.1.8 (a-c) Under the assumption of weak optical lattice, the only bound states belong to the first two energy band and this is due to the fact that the gap energy between the n^{th} band and the $n + 1^{th}$ once scales as V_0^{n+1}. The particles in the other excited state, instead, behaves as free particles. We observe the energy gap at the end of the Brillouin zone, where $q = \pi/d$, and its value is $\Delta E_{gap} = \frac{sE_R}{2}$.

For deep optical lattices, i.e. for $s \geq 5$, we are in the "tight-binding regime" and the energy bands depend slightly on the quasimomentum as

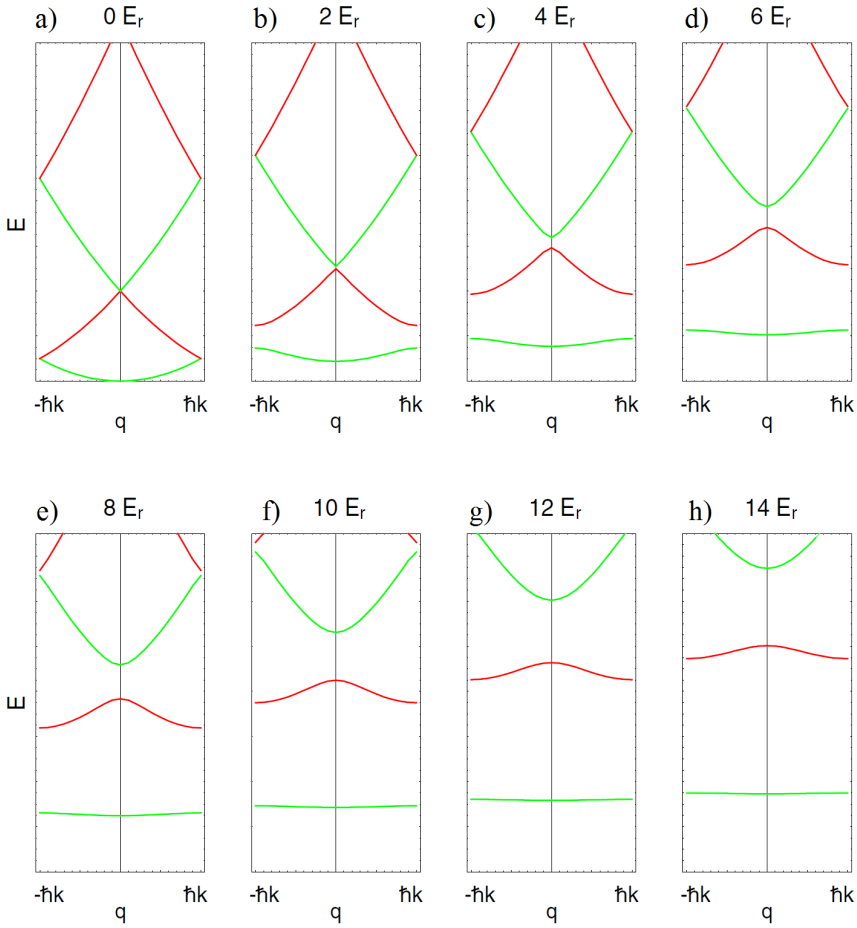

Figure 1.8: Energy of the Bloch state as function of the quasimomentum q for different values of lattice depth in the first Brillouin zone. (a-c) in the presence of a weak optical lattice , i.e. for $V_0 < 5E_r$, the lowest band strongly depends on the quasimomentum, whereas in the presence of a deep optical lattice (d-h), it becomes almost flat. Adapted from [38].

$$\frac{E(q)}{E_R} = \sqrt{s} - 2J\cos qd \tag{1.51}$$

where J is the tunneling energy, which represents the probability for an atom to hop from one lattice site to the neighbour one(Fig.1.8 (d-h)). In this situation it is convenient to write the n^{th} eigenfunction as a superposition of many wavefunctions maximally localized on the potential minima

$$\Psi_{n,q}(x) = \sum_{j=-\infty}^{j=\infty} e^{ix_j q} w_n(x - x_j) \tag{1.52}$$

where $w_{n,j}(x)$ are the Wannier functions (Fig.1.9), which can be approximated with a Gaus-

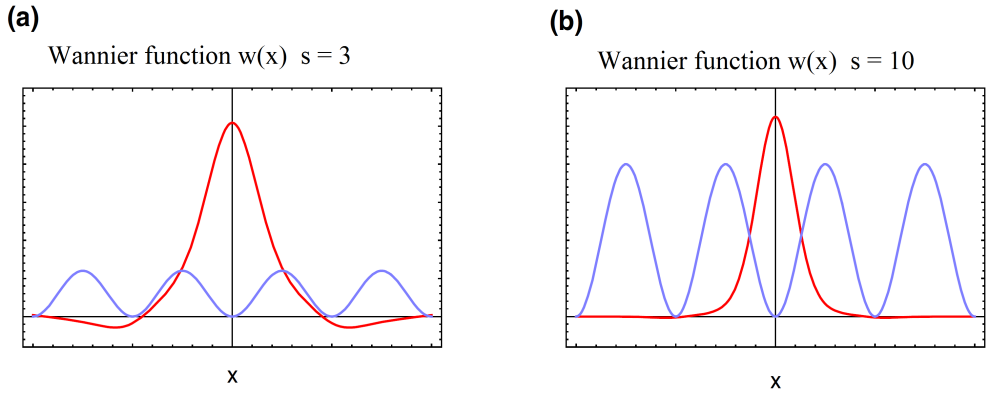

Figure 1.9: Wannier functions (red) for two different value of lattice height s: (a) $s = 3$ and (b) $s = 10$. For $s = 3$ the sidelobes are visible, whereas in the other case they become very small corresponding to a tunneling probability decreases. Figure adapted from [38].

sian at the x_j^{th} lattice site.

1.5.2 Semi-Classical Dynamics

Let us now considerer the dynamics of a particle subjected to an external force F_{ext}. If the external force varies slowly over the dimensions of the Bloch wave packet and it is weak enough not to provoke interband transition, we can use the semiclassical model. From a classical point of view, the behaviour of a particle subjected to an external force F_{ext}, which is related to a potential gradient, is setted by the Hamilton equation

$$\dot{x} = \frac{\partial H}{\partial p} \tag{1.53}$$

$$\dot{p} = -\frac{\partial H}{\partial q}. \tag{1.54}$$

By assuming the analogy between the quasimomentum q and the momentum p, the semi-classical equation of a wave packet in the first energy band can be written as

$$\dot{x} = v^{(0)} = \frac{1}{\hbar}\frac{dE}{dq}, \tag{1.55}$$

i.e. the Bloch velocity $v_n(q) = \frac{1}{\hbar}\frac{\partial E_n(q)}{\partial q}$ expressed in terms of the average position of the wave packet x, and

$$\hbar\dot{q} = -\frac{dV(x)}{dx}. \tag{1.56}$$

According to the semiclassical model, if the external force does not cause an interband transition, it leaves the energy spectrum, due to the periodic potential, unchanged and only the position and the quasimomentum of the particle are changed.

By comparing Eq.1.56, which is related to the particle acceleration, with the second Newton law $m\ddot{x} = -dV(x)/dx$, it is possible to introduce a new mass,

$$\frac{1}{m*} = \frac{1}{\hbar^2}\frac{d^2}{dq^2}E_q^0. \tag{1.57}$$

It is called the effective mass and it depends on the band curvature. Eventually, it may become negative near the Brillouin zones boundaries, meaning that the external forces induce the particle to accelerate in the opposite direction.

In the tight binding limit, by considering the behaviour of the energy spectrum in the Eq. 1.51, the effective mass has the form

$$m^* = m\left(\frac{E_R}{J}\right)\frac{1}{\pi^2\cos(qd)} \tag{1.58}$$

In particular, it depends on the energy band curvature and it tends to the real mass m in the case of a free particle parabolic spectrum. The effective mass is an useful tool in order to describe the dynamical behaviour of a particle in a periodic potential. The interest in this concept is due to the fact that it is possible to use the classical mechanics to describe the particle behaviour only if the mass of the particle is substituted with the effective mass which takes into account the forces due to the presence of the periodic potential.

Chapter 2

Physics of 1D BEC

2.1 1D Quasi-condensate

As it was shown in Section 1.1, an important feature of one-dimensional systems is that in 1D it is not possible to define a finite critical temperature T_c below which the ground state of the system is macroscopically occupied and the transition to the BEC phase doesn't occurs [32]. In fact for one-dimensional systems the critical temperature for Bose-Einstein condensation is the absolute zero, and so no BEC can exist at a finite temperature. Anyway, a degeneracy temperature below which the quantum nature of particles cannot be ignored can be defined and it takes the form

$$T_D = \frac{\hbar^2}{m k_B} n_{1D}^2 \tag{2.1}$$

where $n_{1D} = N/L$ is the 1D density, with L the system length. Below this temperature, the thermal De Broglie wavelength is comparable to the interparticle separation, the wavefunctions of the particles are overlapped, but they do not share the same single-particle ground state. For $T < T_D$ the system is in a new phase of matter, i.e. the quasi-condensate phase, which is characterized by correlation properties different from those on 3D systems.

From a theoretical point of view, the correlation function between two wavefunctions separated by at distance $\mathbf{r}$ is defined as

$$\rho(\mathbf{r}) = \langle \Psi(\mathbf{r})^\dagger \Psi(0) \rangle \,. \tag{2.2}$$

For a pure 3D BEC with density of atoms in the ground state n_0, the condition for Bose-Einstein condensation is

$$\lim_{|\mathbf{r}|\to\infty} \rho(\mathbf{r}) = n_0 \tag{2.3}$$

that is the correlation function is finite even at infinite distances. In fact the 3D BEC is a macroscopic coherent object whose phase $\Phi(\mathbf{r})$ is well defined in the entire system. For temperature above the critical temperature, the correlation function decays exponentially, as in the classical systems. For a 1D system the situation is a bit different, due to the fact that the strong phase fluctuations can destroy the long-range order of the system. As a matter of the fact, the mean square fluctuations of the phase for 1D systems are expected to linearly diverge at large distances

$$\lim_{|r|\to\infty} \langle \Delta\Phi(r)^2 \rangle = \lim_{|r|\to\infty} \frac{m k_B T}{n_{1D}\hbar^2} |r| \to \infty, \tag{2.4}$$

whereas the correlation function decays exponentially

$$\rho(r) n_{1D} e^{\frac{|r|}{2\xi}} \tag{2.5}$$

where ξ is the correlation length

$$\xi = \frac{n_{1D}\hbar^2}{m k_B} \frac{1}{T} \tag{2.6}$$

describing the distance over which the system is coherent. It is important to note that the correlation length increases as the temperature decreases. As a consequence, lowering the temperature, the gas behaves more and more like a true condensate. As it was introduced above, in 1D there is no condensation due to the fact the correlation function approaches zero at large distances. Anyway, if the correlation length is sufficiently large compared to the system size L, i.e. $\xi \ll L$, the phase coherence is preserved throughout the system, which thus behaves as a real condensate. In the intermediate case, i.e. $\xi > n_{1D}$, the correlation function is zero only for some particles, whereas is finite for the others. As a consequence, the gas is locally coherent and the correlation is broken on the entire length scale. This phase is called "quasi-condensate" phase and the system has intermediate properties between a real condensate and a normal system. In term of degeneracy temperature, the condition required to observed a quasi condensate phase is

$$\frac{T}{T_D} = \frac{L/N}{\xi} < 1 \tag{2.7}$$

In Fig. 2.1 the conditions for the different regimes are shown.

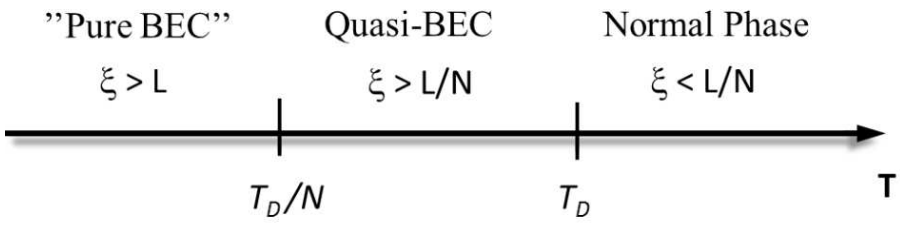

Figure 2.1: Different regimes of a 1D system of N bosons. For $T > T_D$, $\xi < L/N$ and the system is the normal phase. For $T_D/N < T < T_D$, $\xi > L/N$ and the system has intermediate properties between a real BEC and a normal system and it is in the "Quasi-Bec" phase. For $T < T_D/N$ the system is a real BEC. Figure adapted from [40].

2.2 Experimental 1D system

In general, a system can be considered 1D both from a thermodynamic point of view that a collisional one. In the first case, the particles are free to move along one direction (axial) but their movement is frozen along the others two directions (radial). This means that the energy difference between the ground state and the first excited state in the radial direction, $E_{rad} = \hbar\omega_r$ where ω_r is the radial frequency ω_r, is larger than the thermal energy k_BT i.e., $E_{rad} \gg k_BT$ (Fig.2.2).

In our experiments we employ optical lattices in order to freeze the particles movements along the radial direction. In particular, the transverse trapping energy $\hbar\omega_r = h \times 40$ kHz is much larger than all other energy scales, realizing effectively one-dimensional systems. Under the condition of a 1D system (along z) , the wavefunction takes the form

$$\Psi(r, z) = \Psi(z)\phi(r) \tag{2.8}$$

i.e. it can be factorized into a radial part, i.e. $\phi(r) \propto e^{-r^2/2a_r}$ with a_r the harmonic oscillator length if we consider an harmonic confining potential, and an axial one, whose form depends on the specific potential along z. The simplest case is an axial confinement due to an optical harmonic trap, with frequency $\omega_z = 2\pi \times 150$ Hz in our experiments.

A system can be considered 1D also from a collisional point of view and this happens if the dimensions of the confining direction are smaller than the 3D scattering length. Anyway, in the experiment $a_r \approx 70nm$, if $\omega_r = 2\pi \times 50$ kHz, whereas $a = 100a_0 \approx 5nm$ and, in first approximation, the collisional properties of the 1D system are 3D. In this picture, we can

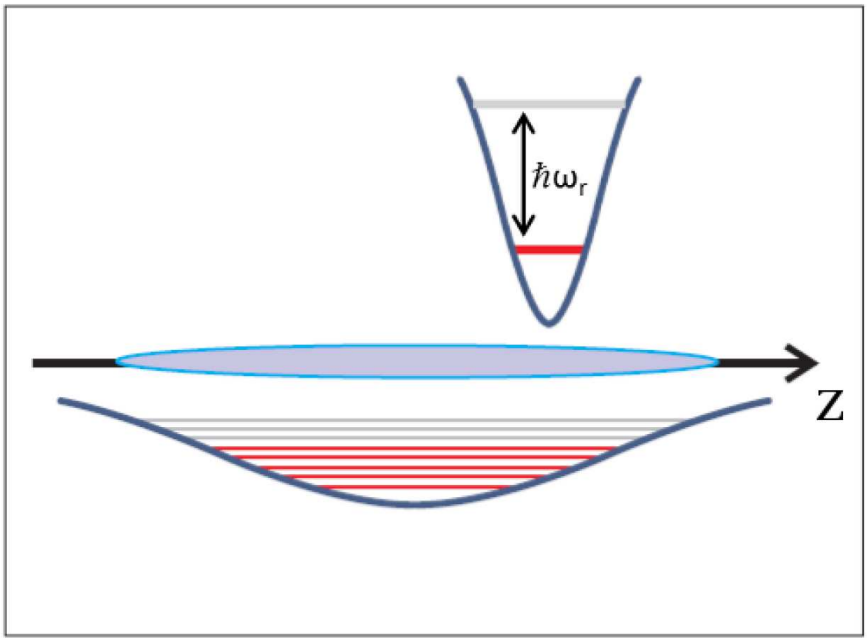

Figure 2.2: In 1D the particles are free to move along one direction (axial) but their movement is frozen along the others two directions (radial). Due to the strong transverse harmonic confinement, i.e. $\hbar\omega_r$ is larger than all other energy scales, only the radial ground state is occupied. In the axial direction, also the excited states can be occupied. Occupied levels are represented in red, empty levels in gray. [40]

introduce a new constant coupling

$$g_{1D} = \frac{2\hbar}{m}\frac{a}{a_r^2} = \frac{2\hbar}{m a_{1D}} \tag{2.9}$$

with $a_{1D} = \frac{a_r^2}{a}$ is the 1D scattering length under the condition $a_r \gg a$. If this condition is not satisfy, as near the Feshbach resonance, the 1D scattering length takes the form

$$a_{1D} = \frac{a_r^2}{2a}\left(a - C\frac{a}{a_r}\right) \tag{2.10}$$

with $C = 1.0326$ [41]. This formula works for any value of a/a_r.

2.3 Momentum distribution and correlation

In our experimental system, the experimental observable employed to study the correlation properties of our system is the momentum distribution $\rho(p)$, which is related to the spatially

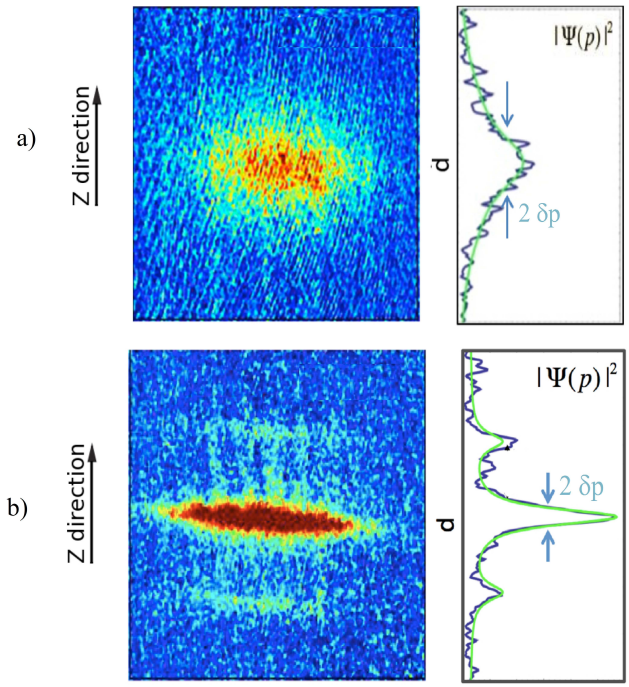

Figure 2.3: (a) On the left, TOF image of the momentum distribution$\rho(p)$ for an insulator atomic sample in a 1D lattice along the z direction. On the right, the image has been integrated along the horizontal direction. A large width δp of the momentum distribution is an evidence of loss of phase coherence of the sample. (b) On the left, TOF image of the momentum distribution$\rho(p)$ for an superfluid atomic sample in a 1D lattice along the z direction. On the right, the image has been integrated along the horizontal direction and it has been fitted with 3 Lorentian functions. It is important to note the sharp width δp of the momentum distribution which is an evidence of the phase coherence of the sample.

averaged correlation function $g(x) = \int \rho(x', x + x')dx'$ via the Wiener-Khinchin theorem

$$g(x) = F^{-1}[\rho(p)] \tag{2.11}$$

i.e. the correlation function is the inverse Fourier transform of the momentum distribution.

In the experiment, $\rho(p)$ is obtained performing time of flight (tof) absorption imaging, i.e. by releasing the atomic cloud from the optical potentials and letting it free to expand before acquiring the image. If the expansion time is sufficient large and the interaction can be neglected the image reproduces the density distribution $n_{tof} \sim \rho(p)$.

Due to the fact that the correlation function decays exponentially on the length scale ξ, $\rho(p)$ is a Lorentzian function

$$\rho(p) \propto \frac{1}{p^2 + \delta p^2} \tag{2.12}$$

whose half width at half maximum δp is related to ξ via

$$\delta p = \frac{0.63\hbar}{\xi} \tag{2.13}$$

The behaviour of δp gives information related to the system nature. A large width of the momentum distribution is an evidence of loss of phase coherence of the sample. In this situation the correlation function decays on a length scale ξ lower than the lattice spacing d. Consequently when the system is in an insulating phase, we observe a large δp (Fig.2.3a). If the system is in the superfluid phase, the momentum distribution has a sharp δp (Fig.2.3b), which is an useful tool to obtain information about the temperature of the sample. In fact, as the coherence length ξ, also the momentum distribution δp depends on temperature, and, in particular, an increase of the temperature provokes an increase of δp.

2.4 Theoretical model for 1D systems

2.4.1 Luttinger Liquid

One-dimensional interacting fluids, both bosonic and fermionic, belong to a universality class known as "Luttinger liquid" [42]. This kind of systems are characterized by low energy excitations, which are collective modes with a linear dispersion relation. A simple explanation of the collective behaviour is the following: due to the interactions among the particles and the strong confinement in the radial direction, if a particle moves in the only allowed direction, it pushes the neighbour one, which in turn moves the next one and so on, turning into a collective motion the movement of a individual particle. Thanks to the presence of this collective modes, it is possible to use the bosonization technique [43, 44], which is efficient both for bosons and fermions, to study the one-dimensional systems. In this construction, the one-dimensional fluids are described in terms of a field operator $\hat{\Phi}_l(z)$ which is a continuous function of the position z. In 1D, the field operator is well defined, unlike that in 3D, due to the fact that in the first case there is a unique way to enumerate the particles, by starting from $z = -\infty$ and proceeding to the right direction. In the case of bosons, a suitable definition of the field operator is [43]

$$\hat{\Phi}_l(z) = 2\pi n_{1D} z - 2\phi(z) \tag{2.14}$$

where $n_{1D} = N/L$ is the mean density of the system and $\hat{\phi}(z)$ is a slowly varying quantum field related to a perfect crystalline 1D structure. In terms of this field, the density operator $\hat{\rho}(z)$ takes the form

$$\hat{\rho}(z) = (n_{1D} - \frac{1}{\pi}\partial_z\hat{\phi}(z)) \sum_m \alpha_m e^{2im(\pi n_{1D} z - \hat{\phi}(z))} \tag{2.15}$$

where m is an integer number and α_m is a non-universal coefficient which depends on the system details. In this situation, the single particle creation operator $\hat{\Psi}^\dagger(z)$ can be written as

$$\hat{\Psi}^\dagger(z) = \sqrt{\hat{\rho}(z)} e^{i\hat{\theta}(z)} \tag{2.16}$$

where $\hat{\theta}(z)$ is an operator which depends on the system details. In the case of a BEC, it is the superfluid phase. In general, the evolution of a system of N interacting boson in an optical lattice $V_{latt}(\mathbf{r})$, subjected to an external potential $V_{ext}(\mathbf{r})$ is driven by the Hamiltonian $\hat{H}$, which in second quantization takes the form

$$\hat{H} = \int d\mathbf{r}\hat{\Psi}^\dagger \left(\frac{-\hbar^2}{2m}\nabla^2 + V_{ext}(\mathbf{r}) + V_{latt}(\mathbf{r}) \right) \hat{\Psi} + \frac{g}{2} \int d\mathbf{r}\hat{\Psi}^\dagger\hat{\Psi}^\dagger\hat{\Psi}\hat{\Psi} \tag{2.17}$$

A representation of the Hamiltonian for the 1D interacting bosons, can be obtained by putting the field operator 2.16 into the Hamiltonian 2.17. Under the assumptions that $V_{ext}(\mathbf{r}) = V_{latt}(\mathbf{r}) = 0$, it takes the form of a quadratic Hamiltonian

$$\hat{H}_{LL} = \frac{\hbar}{2\pi} \int dz [v_s K (\partial_z\hat{\theta}(z))^2 + \frac{v_s}{K}(\partial_z\hat{\phi}(z))^2] \tag{2.18}$$

where v_s and K are the "Luttinger parameters". The two parameters are linked to each other via

$$v_s K = \frac{\pi\hbar n_{1D}}{m} \tag{2.19}$$

$$\frac{v_s}{K} = \frac{U}{\pi\hbar} \tag{2.20}$$

where U is the interaction energy. Both parameters characterized entirely a 1D system. In particular v_s is the sound velocity of the system excitations which are sound-like density-waves with a linear dispersion relation $\omega \sim vk$, whereas the parameter K is an adimensional quantity, related do correlation at long distances, whose value is between 1 and ∞. If $K = \infty$ the bosons are non interacting. On the contrary, if $1 < K < \infty$, the boson are interacting and the correlation function decays as the Luttinger parameter K increases as $(2K)^{-1}$. In the limit case of $K = 1$ the system is strongly interacting and it behaves as spinless fermions (Tonks-Girardeau gas [45]): in order to minimize their mutual repulsion, the particles tend to occupy a fixed position and the wavefunctions of the particles cannot overlap. This behaviour

is similar to the fermions one which cannot stay in the same place in order to satisfy the Pauli exclusion principle. Obviously, the particles are bosons, and the system wavefunction is always symmetric under the exchange of two particles.

2.4.2 Lieb-Liniger Model

As we shown in section 1.2, in the presence of a system of N interacting bosons strongly confined in the radial directions, only the binary collisions among the particles play a relevant role which can be written in terms of the contact pseudopotential

$$U = g_{1D}\delta(z_i - z_j) \tag{2.21}$$

where g_{1D} is the one-dimensional constant coupling (Eq. 2.9). In this scenario, under the assumption that the external potential $V_{ext}(\mathbf{z}) = 0$, the Hamiltonian driving the system evolution takes the form

$$\hat{H} = \sum_{i=1}^{N} -\frac{\hbar}{2m}\frac{\partial^2}{\partial z_i^2} + g\sum_{i<j=1}^{N}\delta(z_i - z_j) \tag{2.22}$$

This model, introduced by Lieb and Liniger in 1963 [46, 47], is the simplest non-trivial model of interacting bosons in the continuum and it can be solved by using the using the Bethe ansatz. It is useful to describe the system by using an adimensional parameter, known as "Lieb-Liniger parameter"

$$\gamma = \frac{mg_{1D}}{\hbar^2 n_{1D}}, \tag{2.23}$$

which represents the ratio between the interaction energy, $E_{int} \approx g_{1D}n_{1D}$, and the kinetic energy required to take a particle at a distance $d = n_{1D}^{-1}$, $E_{cin} \approx \hbar^2 n_{1D}^2/m$. It is important to note that the Lieb-Liniger parameter increases as the mean density decreases. Therefore, in one-dimension, the interaction energy increases with respect to the kinetic energy when the density decreases, unlike that in three dimension. The Luttinger parameters which was introduced in the previous section, can be written in term of the Lieb-Liniger parameter. In particular if $\gamma \ll 1$

$$v_s = v_F\frac{\sqrt{\gamma}}{\pi}\left(1 - \frac{\sqrt{\gamma}}{2\pi}\right)^{1/2} \tag{2.24}$$

$$K = \frac{\pi}{\sqrt{\gamma}}\left(1 - \frac{\sqrt{\gamma}}{2\pi}\right)^{-1/2} \tag{2.25}$$

and the system is in the bosonic limit, whereas if $\gamma \gg 1$ (in the presence of low density or strong interaction)

$$v_s = v_F\left(1 - \frac{4}{\gamma}\right) \tag{2.26}$$

$$K = \left(1 + \frac{4}{\gamma}\right). \tag{2.27}$$

and the system is a Tonks-Girardeau gas.

2.4.3 Bose-Hubbard Model

In order to describe the system of N interacting boson in a deep optical lattices $V_{latt}(\mathbf{r})$ ($s > 5$) subjected to an external potential $V_{ext}(\mathbf{r})$, it is useful to use the Bose-Hubbard model.

The system evolution is driven by the Hamiltonian $\hat{H}$, which in second quantization takes the form

$$\hat{H} = \int d\mathbf{r}\hat{\Psi}^\dagger\left(\frac{-\hbar^2}{2m}\nabla^2 + V_{ext}(\mathbf{r}) + V_{latt}(\mathbf{r})\right)\hat{\Psi} + \frac{g}{2}\int d\mathbf{r}\hat{\Psi}^\dagger\hat{\Psi}^\dagger\hat{\Psi}\hat{\Psi} \tag{2.28}$$

In the tight binding regime, the field operator Ψ can be written as a combination of Wannier functions of the lowest Bloch energy band

$$\hat{\Psi}(\mathbf{r}) \approx \sum_i w_i(\mathbf{r})\hat{b}_i, \tag{2.29}$$

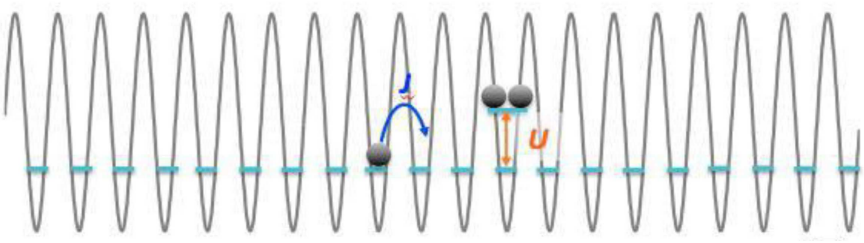

Figure 2.4: Homogeneous Bose-Hubbard model ($\epsilon_i = const$). J is the tunneling energy and U the on-site interaction energy. Adding a particle into a populated neighbour site costs the energy U due to the repulsive interaction between two atoms sharing the same site.

where $\hat{b}_i$ is the annihilation operator of the i^{th} site, and the Hamiltonian takes the form

$$\hat{H} = -J\sum_i(\hat{b}_i^\dagger\hat{b}_{i+1} + h.c) + \frac{U}{2}\sum_i \hat{n}_i(\hat{n}_i - 1) + \sum_i(\epsilon_i - \mu)\hat{n}_i \tag{2.30}$$

where $\hat{b}_i$ is the creation operator of the i^{th} site, $\hat{n}_i = \hat{b}_i^\dagger\hat{b}_i$ is the number operator related to the site occupancy and μ is the chemical potential. This Hamiltonian is known as Bose-Hubbard Hamiltonian

Let's focus the attention on the single terms of the Hamiltonian (Fig.2.4). The first one is the kinetic energy of the system, which is proportional to the tunneling energy

$$J = -\int d\mathbf{r} w * (\mathbf{r} - \mathbf{r}_i)\left[\frac{-\hbar^2}{2m}\nabla^2 + V_{latt}(\mathbf{r})\right]w(\mathbf{r} - \mathbf{r}_{i+1}) \tag{2.31}$$

The tunneling energy J is related to the superposition of the Wannier functions localized to the i^{th} and the $(i+1)^{th}$ sites, and it represents the probability for an atom to hop from one lattice site to another. By solving the Eq.2.31, it is possible to find a relation between the tunneling energy J in and the lattice parameter s, i.e.

$$\frac{J}{E_r} = 1.43s^{0.98}e^{-2.07\sqrt{s}} \tag{2.32}$$

which implies that by tuning the intensity of the laser employed to realize the lattice it is possible to change the tunneling energy. The second term of the Hamiltonian is proportional to the interaction energy

$$U = g\int d\mathbf{r}|\Psi(\mathbf{r})|^4. \tag{2.33}$$

which quantifies the energy cost to put two particle in the same lattice site. It depends on the coupling parameter g, which must be substituted by g_{1D} in the presence of 1D lattice, and it can be tuned by using the Feshbach resonance. Note that this is the only term which takes into account the interaction among particles: interactions among atoms in different sites are neglected. The last term takes into account the presence of an external potential. In fact, in the experiment with ultracold quantum gases an external trap potential is usually present and it provokes an energy offset ϵ_i in the i^{th} site. If we have an harmonic trap, the energy offset is

$$\epsilon_i = \frac{\alpha}{2}\sum_i(i - i_0)^2 \tag{2.34}$$

where α is the harmonic trap strength and i_0 is the trap center. If one assumes that the trap potential varies smoothly across the lattice, ϵ_i can be considered as a constant.

2.4.4 Superfluid and Mott Insulator

Let's consider the Bose Hubbard Hamiltonian, by neglecting the last term due to the presence of an external potential. In this situation the two relevant energy scale are the tunneling energy J and the interaction one U. Depending on the interaction among particles, the system can undergo a phase transition from a conductive phase to an insulator one induced by interactions, which suppress the tunneling from site to site. In order to treat this phenomenon more in detail, let's consider the two different cases, $U \ll J$ and $U \gg J$.

If the interaction among the particles is negligible compared to the tunneling energy, $U \ll J$, all of the particles are free to move across the lattice and they occupies the Bloch ground state. In this situation, they are delocalized throughout the lattice and the system is said to be in a superfluid phase. By assuming that the Bloch ground energy state of a single delocalized particle is a superposition of the wavefunctions localized on each lattice site, $\sum_i b_i^\dagger |0\rangle$, the system ground state of N identical bosons is the product of N identical Bloch waves

$$|\Psi_S F\rangle \propto \left(\sum_i b_i^\dagger\right)^N |0\rangle \,. \tag{2.35}$$

In this regime, in agreement with the Heisenberg uncertainty principle, the number of particles per site is not determined but it follows a Poissonian distribution, while for each site the phase is perfectly defined, giving rise to narrow peaks in the multiple matter wave interference. If the interactions among the particles are strong enough to overcome the kinetic energy, $U \gg J$, for the bosons is energetically convenient to stay apart and localize at each lattice site, instead of flowing through the lattice. In fact an atom jumping from a site to a neighbour one would cause an energy cost for the system equal to U. As a consequence, the system is in an insulating phase, the Mott insulator, whose ground state is given by the product of the single-site Fock states

$$|\Psi_{MI}\rangle \propto \prod_i (b_i^\dagger)^N |0\rangle \,. \tag{2.36}$$

In this situation, the particle number per site is perfectly determined, but there is no phase correlation between wavefunction localized at each site. As a result, no macroscopic phase coherence holds. In order to have a pure Mott insulator, each lattice site must to be occupied by an integer number of atoms. On the contrary, the superfluid phase coexists with the insulating one.

The value at which the quantum transition from the superfluid phase to the insulating one

occurs, i.e. $(J/U)_c$, depends on the chemical potential μ and on the site filling n as it shown in Fig. 2.5.

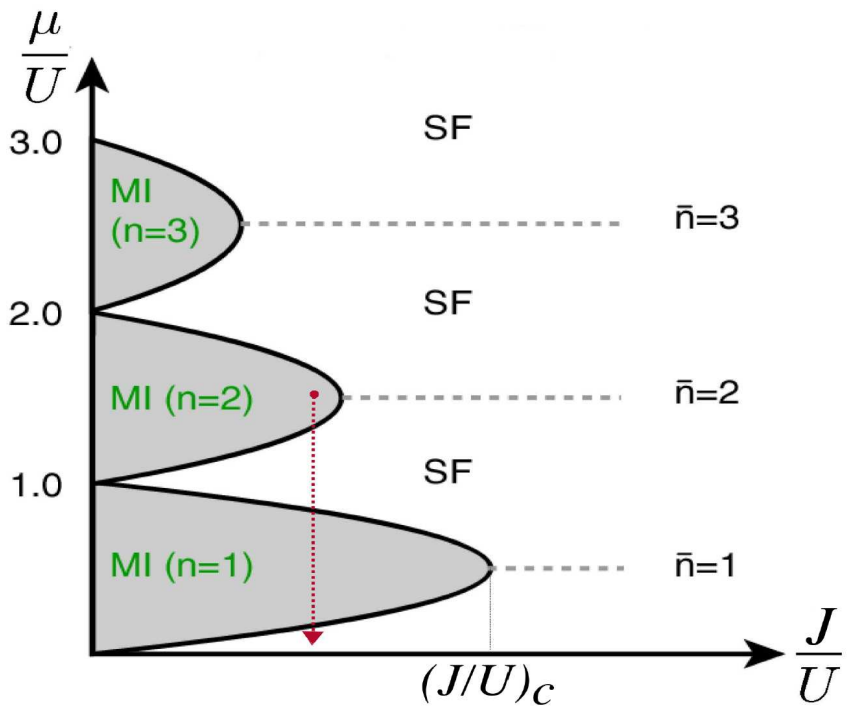

Figure 2.5: Phase diagram of the SF to MI transition in a homogeneous case as a function of μ and J, both normalized to U. The MI zones are characterized by an integer number of particles for each lattice site, whereas in the superfluid phase it is possible to introduce only a mean filling. Note that a larger average occupancy $\bar{n}$ implies a larger interaction energy to enter in the Mott phase and consequently a smaller critical value $(J/U)_c$. Red line: The decrease of the chemical potential μ/U at constant J/U along the trap implies a succession of MI zones and SF ones. Adapted from [38].

In the MI phase the site filling is well defined and it is an integer number, whereas in the superfluid phase only an average filling can be introduced, due to the fact that the number of particles for each lattice site is not determined. Note that a larger average occupancy $\bar{n}$ implies a larger interaction energy to enter in the Mott phase and consequently a smaller critical value $(J/U)_c$.

So far we have considered the homogeneous case. Anyway, in the experiments, it is difficult to have an homogeneous system, due to the presence of an external trapping potential. In fact, if the trap potential does not varies smoothly across the lattice, the last term in the BH hamiltonian cannot be neglected anymore, and the system has some regions with a commensurate filling and some with an incommensurate one. In this situation, the system can be thought to be characterized by a local chemical potential which slowly varies from site to site and reaches its maximum at the center of the harmonic potential. The variation of the chemical potential

provokes a change also in the local filling and in particular an increase of μ implies an increase of the local filling. For a given value $J/U < (J/U)_c$, the atoms alternate different phases depending on their position across the lattice and we observe a shell structure where shells of the Mott insulator are interchanged by shells of superfluid (Fig.2.6). In the limit case of $J = 0$, only the MI phase survives and the density profile of the trapped atoms shows the so called wedding-cake shape: all sites are filled with an integer number of particles and the central sites have the largest filling.

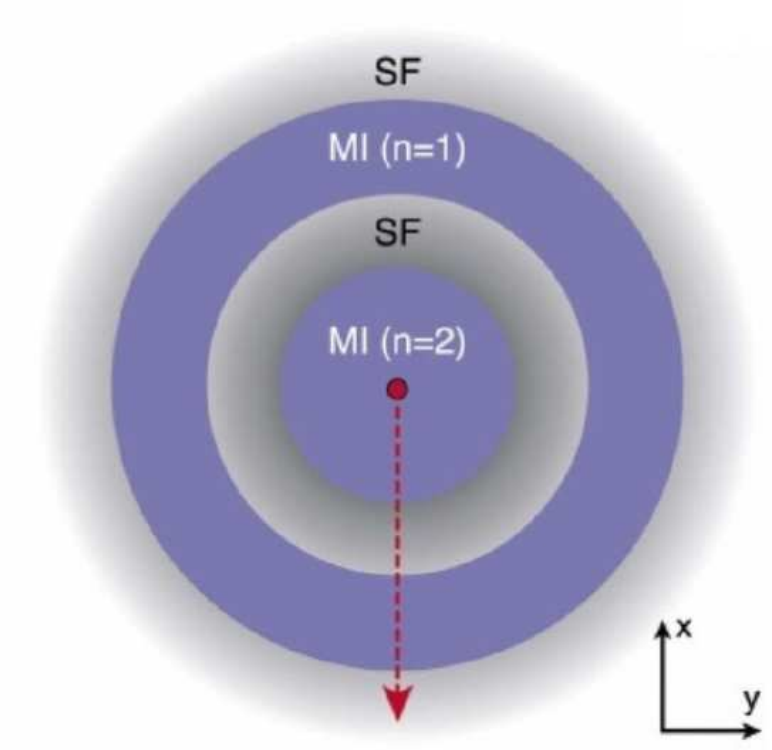

Figure 2.6: In an inhomogeneous system, for a given value $J/U < (J/U)_c$, the atoms alternate different phases depending on their position across the lattice and we observe a shell structure where shells of the Mott insulator are interchanged by shells of superfluid [38]

The Mott insulator phase was observed for the first time in an atomic systems in 2002 by Greiner et al.[24]. They increased the ratio U/J by increasing the lattice height s and they observed an loss of phase coherence in the momentum distribution, which confirmed the transition from a superfluid phase to an insulating one (Fig.2.7).

In the same experiments, they also verify the presence of the Mott insulator by probing the excitation spectrum. The superfluid phase and the insulating one, in fact, are characterized by a different spectra, which are related to their different conductivity properties. When the

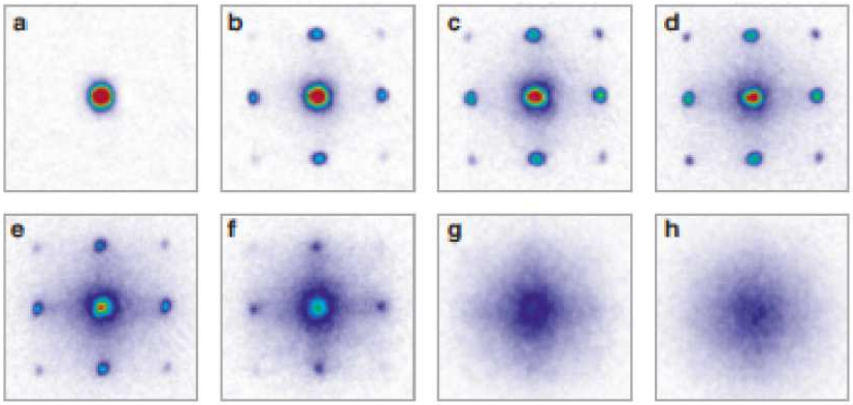

Figure 2.7: Momentum distribution for different value of 3D lattice height s. By increasing s (from (a) to (h)) the system undergoes a phase transition from the superfluid coherent phase to the Mott insulator incoherent phase. Adapted from [38].

system is in the superfluid phase, due to gapless energy spectrum, any amount of energy can be transfer in the system and the atoms are able to move from one lattice site to another one. Conversely, in the MI phase the atoms are not free to move due to discontinuous energy spectrum with a gap of the order of on site interaction energy U. A simple explanation for the origin of this gap is the following. The lowest lying excitation in a system with an atom in each lattice site is the creation of a particle-hole pair, where an atom in a lattice site is added into a neighbour one holding an other atom. The energy of this configuration, where two atoms are in the same lattice site, is raised by an amount U in energy above the configuration with a single atom in each lattice site, due to the on-site interaction energy U [1]. Consequently, in an homogeneous system, removing an atom from a site and adding it to a neighbouring one with the same occupancy has an energy cost equal to the on-site interaction energy U. Anyway, as it was introduced above, we may have an inhomogeneous system which has different lattice sites with different occupancy. In this situation it is possible to add an atom to a neighbouring site with different occupancy by paying an energy cost equal to $2U$.

2.5 Sine-Gordon Model

In the case of a weak optical lattice, the system dynamics is well described by the Sine-Gordon model, which consider the optical potential $V_{latt}(z) = V_0 \cos(Gz)$ as a perturbation [44]. The total Hamiltonian driving the system evolution can be obtained by starting from the general

[1] This explanation is valid also if the number of atoms in each lattice site is n

Hamiltonian (Eq.2.17) where a perturbation potential is added and where the expression in eq. 2.15 for the density it is used. In this situation, the Sine-Gordon Hamiltonian takes the form

$$\hat{H}_{sG} = \hat{H}_{LL} + \frac{g_{1D}}{\pi} \int dx cos(2p\hat{\phi}(x) + \delta x) \tag{2.37}$$

where $\delta = nG - 2p\pi n_{1D}$ measures the system degree of incommensurability and in particular $\delta = 0$ corresponds to a commensurate number of bosons for each lattice. In the δ, p is an integer number and the case $p = 1$ correspond to an integer number of bosons for each lattice site, whereas higher values of p correspond to a one boson every p lattice sites. In the presence of an integer filling, it is possible to recover the quantum transition from the superfluid phase to the Mott insulator one also by starting from the Sine-Gordon Hamiltonian. By using the renormalization group (RG) approach on the Sine-Gordon Hamiltonian, we find that the phase transition occurs at a universal value of the Luttinger parameter $K_c = 2/p^2$: for $K > K_c$ the system is in a superfluid phase and the optical lattice behaves as a negligible perturbation, whereas in the opposite case the system is in the Mott insulating phase.

Chapter 3

Phase Slips in one dimensional systems

3.1 Phase slips in superconductors

The intriguing phenomenon of superconductivity was observed for the first time by the dutch physicist Heike Kamerlingh Onnes in 1911 [48]. By studying the behaviour of the resistance of solid mercury at cryogenic temperatures, he found that below a critical temperature T_C, the resistance of mercury abruptly disappeared. In subsequent decades, the phenomenon of superconductivity was observed in several other materials and, since its discovery, it has been widely studied both from a theoretical point of view and an experimental one. Thanks to the advent of modern technology, such as lithographic techniques and thin film deposition, it has been possible to realize new experimental systems and answer to new theoretical questions. One of these questions is if it is possible to observe the phenomenon of superconductivity in one-dimensional (1D) systems. Obviously, the answer to this question has, important implications both in fundamental physics and practical applications. From a theoretical point of view, in a 1D system it is not possible to observe the phenomenon of superconductivity, due to the presence of thermally activated phase slips (TAPS) [1], which give rise to a finite resistance also for temperatures below T_C.

The first theoretical proposal for TAPS was made by Little in 1967 to understand the mechanism of the supercurrent decay in a ring made of a thin wire [1]. His starting point was that strong enough thermal fluctuations can provoke deviations from their equilibrium values of both modulus and phase of the complex order parameter $|\Psi(x)|e^{i\phi(x)}$ describing the superfluid state (Fig. 3.1a). Due to thermal fluctuation, the modulus of the order parameter in a point of the wire is suppressed and at the same time a $2\pi n$ phase jump is observed, with n an integer number (Fig. 3.1 b). After the formation of phase slips, the modulus returns to its initial value and the system gets back to its initial state with an accumulated phase shift of $2\pi n$ (Fig.3.1c).

Due to the rareness of the phase slip events, it is possible to considerer only the cases $n = \pm 1$.

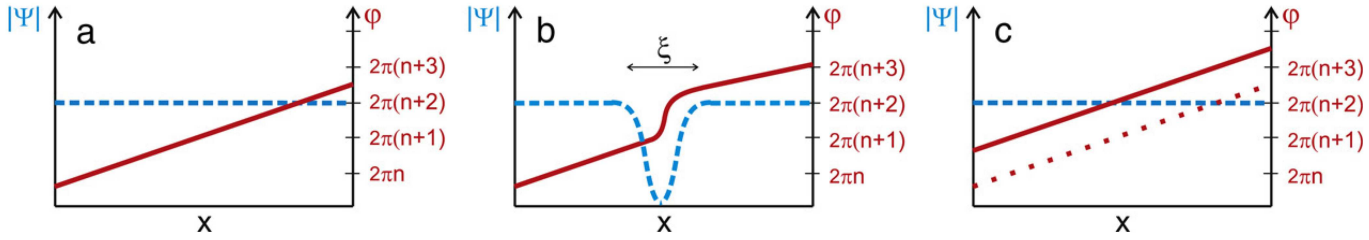

Figure 3.1: Cartoon of a phase slip event. (a) Before a phase slip event, the complex order parameter $|\Psi(x)|e^{i\phi(x)}$ is characterized by a modulus $|\Psi(x)|$ (dotted blue line) and a phase $\phi(x)$ (solid red line). (b) During a phase slip event, the modulus of the order parameter is suppressed and the phase makes a 2π phase jump. (c) After a phase slips event, the modulus is restored but both the phase gradient and the velocity $v(x)$ are reduced. Adapted from [49].

Following a phase slip event, a finite voltage V appears across the wire due to the Josephson relation between V and $\dot{\phi}$, i.e. $V = \frac{\hbar\dot{\phi}}{2e}$. If there is not a bias current, there are the same numbers of positive ($n = 1$) and negative ($n = -1$) phase slips and consequently the net voltage is zero. Instead, in the presence of a bias current $I \propto |\Psi(x)|\nabla\phi$, the system is more inclined to create positive phase slips, since the work performed by the current is positive for positive phase slips, and the system is subject to a finite voltage and, at the same time, to a finite resistance $R = V/I$.

The first quantitative theoretical model to estimate the resistance was developed by Langer and Ambegaokar [2] and it was modified by McCumber and Halperin [3], few years later. Their model was based on the idea that phase slips occur when the order parameter passes, via thermal activation, over the free energy barrier ΔF separating states whose value of $\Delta\phi$ differ by 2π. They estimated the free energy barrier height by using the mean-field Ginzburg-Landau equation, and they found that in a narrow superconducting channel, the free energy barrier depends on the condensation energy density H_c and on the volume $A\xi(T)$, where A is the wire's cross section area and $\xi(T)$ the Ginzburg-Landau coherence length, via

$$\Delta F = \frac{8\sqrt{2}}{3}\frac{H_c(T)^2}{8\pi}(A\xi(T)) \tag{3.1}$$

The rate of thermal activated phase slips is given by an Arrhenius type equation via $\Omega(T)e^{-\Delta F/k_BT}$ where

$$\Omega(T) = (\frac{L}{\xi(T)})(\frac{\Delta F}{k_BT})1/2(\tau_{GL})^{-1} \tag{3.2}$$

is the attempt frequency. Here L is the wire's length and $\tau_{GL} = \frac{\pi\hbar}{8k_B(T_c-T)}$ is the relaxation time of the time-dependent Gitzburg-Landau theory. By considering a narrow superconducting channels with a finite current I, the voltage due to the presence of TAPS is

$$V = \frac{\hbar\Omega(T)}{e} e^{-\frac{\Delta F}{k_B T}} \sinh(\frac{I}{I_0}) \tag{3.3}$$

where $I_0 = 4ek_BT/h$. In the limit of low current, i.e. $I \ll I_0$, the resistance is

$$R_{LAMH} = V/I \simeq R_q \left(\frac{\hbar\Omega(T)}{k_B T}\right) e^{-\frac{\Delta F}{k_B T}} \tag{3.4}$$

where $R_q = \frac{h}{(2e)^2}$.

The first measurement of a finite voltage for temperatures lower than T_C was performed by Lukens et al. [50] in 1970 by studying the voltage behaviour as a function of the current in a one dimensional single-crystal tin whiskers (Fig. 3.2). They found that the voltage as a function of the current near the transition behaved consistently with the Langer-Ambegaokar model, i.e. $V \propto \sinh(I/I_0)$, confirming the presence of thermally activated phase slips.

As the temperature decreases, due to the increase of the height of the free energy barrier ΔF, the probability of TAPS becomes very small and phase slips cannot occur due to thermal activation. Anyway, it has been suggested that at very low temperatures, phase slips should be induced by quantum fluctuation of the order parameter [51, 52]. The first heuristic model for quantum phase slips (QPS) in thin superconducting wires was proposed by Giordano [4] in 1988, in order to explain the discrepancy between the measured resistance of a narrow In strip as a function of the temperature and the LAMH model, in the case of very low temperature (Fig. 3.3).

He started by considering the motion of a damped particle moving in a tilted washboard potential and assuming that it can be considered as a harmonic oscillator in a well, with a natural frequency ω_0. In this situation, the tunneling rate has the form

$$\Gamma_{MQT} = B\sqrt{\frac{V_0\omega_0}{\hbar}} e^{\frac{-aV_0}{\hbar\omega_0}} \tag{3.5}$$

where a and B are constant and V_0 is the barrier height which coincides with the free energy barrier ΔF in the case of a thin superconducting wires. Since the natural frequency ω_0 can be identified with the inverse of the Gitzburg-Landau relaxation time τ_{GL}, the tunneling rate has the form

$$\Gamma_{MQT} = B\sqrt{\frac{\Delta F}{\hbar\tau_{GL}}} e^{\frac{-a\Delta F\tau_{GL}}{\hbar}} \tag{3.6}$$

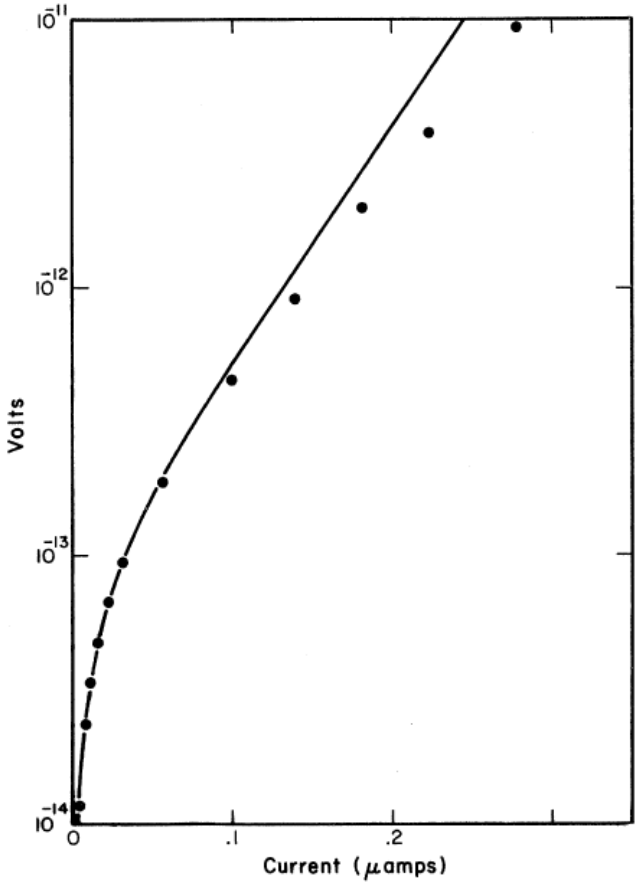

Figure 3.2: Voltage as a function of the current at fixed temperature. The data points (solid circles) are fitted by using the function $V = \sinh(I/I_0)$ (solid line). Adapted from [50]

and the resistance due to the presence of quantum phase slips becomes

$$R_{MQT} = B\frac{L}{\xi}R_q\sqrt{\frac{\Delta F}{\hbar\tau_{GL}}}e^{-\frac{a\Delta F\tau_{GL}}{\hbar}} \tag{3.7}$$

Consequently, in the case of thin superconducting wires, the total resistance has the form

$$R = R_{LAHM} + R_{MQT}. \tag{3.8}$$

As the collective state of a large number of electrons is involved, these phase slips are an example of macroscopic quantum tunneling, experimentally observed in Josephson junctions [53, 54, 55, 56] and superconducting loops [57]. It is interesting to note that the resistance R_{MQT} has the same form of R_{LAHM}, i.e. depends on the same manner on ΔF, but the temperature in the activation exponent is substituted by $\tau_{GL} \propto \Delta T$. Since τ_{GL}^{-1} can become larger than $k_BT/\hbar$, it is possible to find a range of temperatures where the phenomenon of macroscopic

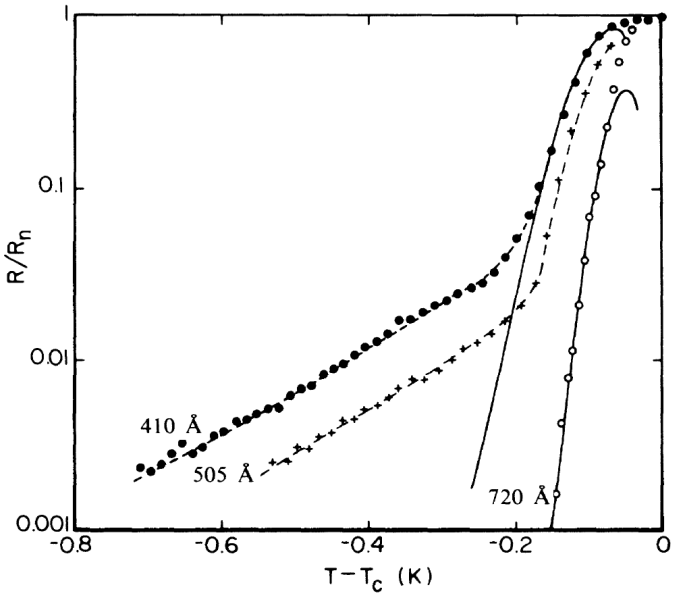

Figure 3.3: Resistance, normalized by the normal state value, as a function of the temperature, for three different values of the sample diameters. The solid curves are fits realized by using Eq. 3.4 which consider the presence of thermally activated phase slips , whereas the dotted curves are fits realized by using Eq.3.8 which consider also the presence of quantum phase slips. Adapted from [4]

quantum tunneling dominates on the thermal activation of phase slips.

Since their first observation, phase slips (both thermal and quantum) have been the objects of interest by the scientific community. They have been studied in different condensed-matter systems, such as superconducting nanowires [58, 59, 11, 60, 61, 62] and Josephson junction arrays [15], where the phase slips nucleation rate is controlled by tuning the temperature or the current. The phase slips phenomenon is interesting not only from a theoretical point of view but also from an experimental one. Since the last few years, theoretical proposal of devices based on the phenomenon of quantum phase slips have been made and it would be interesting to realize them experimentally. For example, it would be interesting to realize the quantum phase slip junction [63], or the superconducting phase slips oscillator [64] or topologically-protected qubits [63, 65] or a quantum standard for the electrical current [15]. These are just a few examples of possible applications of the phase slips. Additional applications will certainly be possible in the future, but a greater understanding of the phenomenon is needed in order to realize devices based on phase slips. Thanks to the easy control and manipulation of their key properties, the ultracold quantum gases are a good candidate to better understand this phenomenon.

3.2 Quantum phase slips in superfluids

The nucleation of phase slips is remarkably important also in the field of Becs, due to the fact that they can be subject to the presence of fluctuations which provoke the destruction of superfluidity. The phenomenon of phase slips in the field of BECs is interesting due to the fact that this system might in principle be employed to study aspects of phase slips that are not accessible in other systems, thanks to the control on key properties such as dimensionality, interaction and disorder.

The interplay between the superfluidity and the increase of thermal and quantum fluctuation has been studied extensively both theoretically [5, 6, 7] and experimentally [18, 19, 66, 67, 68] but an exhaustive experimental picture of quantum phase slips (QPS) in ultracold superfluids has not been obtained yet. The first signatures of QPS was observed in the group of Brian DeMarco in 2008 [18]. They employed a Rb BEC in a 3D optical lattice and they studied the phenomenon of quantum phase slips by performing transport measurements. They observed a regime of temperature-independent dissipation (Fig.3.4) which is consistent with the presence of quantum phase slips. Moreover, they also observed a motion-induced features reminiscent of vortices and vortex rings associated with phase slips in time-of-flight imaging.

The phenomenon of QPS has been also observed in our group by employing 1D atomic superfluid flowing along a periodic potential [19]. In particular, by performing transport measurements, we studied the phase slips nucleation rate for different value of velocity, interaction and temperature. We observe a crossover between a regime of temperature-dependent dissipation at small velocity and interaction which suggests a thermal activation of phase slips and a second regime of velocity-dependent dissipation at larger velocity and interaction which suggests a quantum activation of phase slips. We will discuss the experiments more in detail in chapter 4. The theoretical model for the phenomenon of QPS in 1D superfluids in a periodic potential will be shown in the following subsection.

3.2.1 Quantum phase slips in one-dimensional superfluids in a periodic potential: theorethical model in the Bose-Hubbard regime.

Superfluidity in ultracold bosonic gases presents many similarities with superconductivity and, as a superconductor, the superfluid state can be described by a complex order parameter $|\Psi(x)|e^{i\phi(x)}$. The superfluid state is a metastable state, and it corresponds to a local minimum of the Ginzburg-Landau free energy potential [69]. In fact, the absolute minimum, coincides with the state characterized by no flow. After a phase slip event, i.e. after a local fluctuation

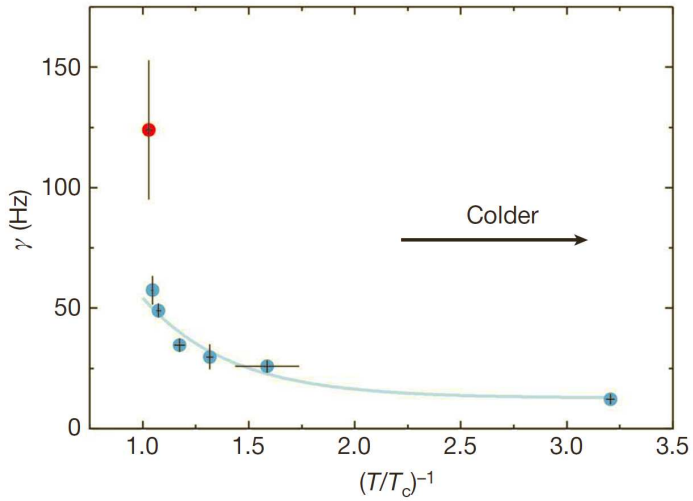

Figure 3.4: Damping rate γ as a function of temperature in the Bose-Hubbard regime ($s = 6$). Each data point is extracted from the time evolution of the center of mass velocity. The error bars are the uncertainty in the fit of the center of mass velocity. The data points are fitted (solid line)) by assuming the presence of quantum phase slips. The red data point at highest temperature is excluded from the fit and it is due to the presence of a thermal activated phase slips. Adapted from [18]

in $\Psi(x)$ corresponding to the suppression of its modulus and a simultaneous phase jump of 2π, the superfluid state can decay into another metastable state with lower velocity, due to the fact that the system velocity and the system phase are related via $v = \frac{\hbar}{m}\nabla\phi$. As in the case of superconductor, three main processes may activate a phase slip, depending on the temperature regime (Fig.3.5). If the temperature is much higher than the free-energy barrier between two metastable states, $T \gg \delta F/k_B$, the order parameter may overcome the barrier via thermal fluctuations, causing the formation of thermally activated phase slips (TAPS) with a nucleation rate following the Arrhenius law $\Gamma \propto ve^{-\delta F/k_B T}$ as predicted in the LAMH theory [2, 3]. When $T \leq \delta F/k_B$, the probability of TAPS becomes small and phase slips occur mainly via quantum tunneling through the free-energy barrier. As in the case of superconductors, one can find a characteristic temperature below which the QPS nucleation rate is temperature-independent [4, 49]. This is not a quantum phase transition, but a crossover, with an intermediate regime of thermally-assisted QPS (TAQPS).

In order to obtain the theoretical model of the quantum phase slips nucleation rate in one-dimensional superfluids in a periodic potential [5, 22], we need to start from the Bose-Hubbard Hamiltonian

$$H = \sum_{\langle jk \rangle} -J(a_j^\dagger a_k + a_k^\dagger a_j) + \sum_j \frac{U}{2} a_j^\dagger a_j (a_j^\dagger a_j - 1) \tag{3.9}$$

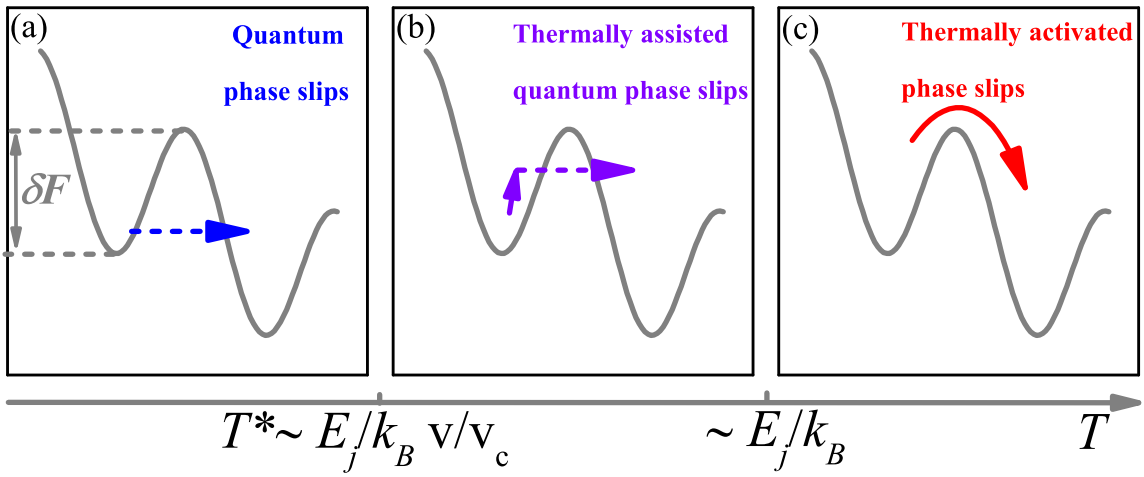

Figure 3.5: Cartoon of the phase slips activation mechanisms. a) At low temperatures, phase slips are activated by quantum tunneling; b) by increasing the temperature, the quantum phase slips are assisted by the temperature. c) At large temperatures, phase slips are activated only by thermal fluctuations.

where $a_j^\dagger$ and a_j are the boson creation and annihilation operators at the lattice site j, $\langle jk \rangle$ indicates pairs of nearest neighbours, J is the single-particle hopping amplitude and U is the on-site repulsive interaction energy. This Hamiltonian can be mapped into the O(2) quantum rotor model

$$H = \sum_{\langle jk \rangle} -2Jn \cos\left(\phi_k - \phi_j\right) + \sum_j \frac{U}{2} n_j^2 \tag{3.10}$$

where, n us the average number of bosons per site, ϕ_j and n_j are the conjugate phase and the number of particles on the site j. The importance of the quantum rotor model is due to the fact that it is possible to apply the instanton techniques on this model and by using the celebrated instanton formula [70, 71]

$$\Gamma \propto e^{-S} \tag{3.11}$$

it is possible to analytically predict the quantum phase slips nucleation rate Γ. Here S is the action for the bounce solution (instanton) of the classical equations of motion. For momentum lower than the critical velocity for breaking superfluidity in a periodic potential, v_c, the quantum phase slips nucleation rate depends on the quasi-momentum via

$$\Gamma \propto v^\alpha \tag{3.12}$$

where the parameter α depends on the interaction [22]. As it has discussed before, there is not a

quantum phase transition from TAPS and QPS regime, but there is a crossover, characterized by a crossover temperature T^*, where quantum phase slips are assisted by the temperature (TAQPS). In this situation, the nucleation rate of TAQPS depends also on the temperature T via

$$\Gamma \propto vT^{\alpha(\gamma)-1}. \tag{3.13}$$

Obviously, the specific form of δF and T^* depends on the specific type of obstacle experienced by the superflow, e.g. disorder [72], isolated defects [6] or periodic potentials [5]. In the case of ultracold quantum gases, the most controllable obstacles are optical lattices and in this situation the free energy barrier is

$$\delta F \simeq E_j, \tag{3.14}$$

with $E_j = \hbar v_s/\sqrt{2}d$ is the Josephson plasma energy and v_s the sound velocity, and the crossover temperature is

$$T^* \simeq \frac{E_j}{k_b}\frac{v}{v_c}. \tag{3.15}$$

The presence of phase slips strongly modifies the transport properties of a system, especially in 1D where the effect of thermal and quantum phase slips is significant. Experiments performed to study the transport properties of trapped gases in the presence of an obstacle, such as random [73, 74], single barrier [75], or periodic potentials [66, 76, 77, 78, 79], have shown that dipole oscillations, induced for example by a sudden displacement of a parabolic trap, are strongly damped, even if the system is in the superfluid state. Theory provides a direct relation between the damping rate G of the dipole oscillations and the phase slips nucleation rate

$$G(v) \propto \frac{\Gamma(v)}{v} \tag{3.16}$$

by using both qualitative consideration on energy loss during the damping, which will be shown in the following, and exact numerical simulations with time-evolving block decimation method at zero temperature [22].

The energy loss during the damping can be written in two different ways. The first one considers the energy loss due to the loss of potential energy in the first half period, which can be written as

$$E_{loss} = \frac{1}{2}M\omega^2(A_0^2 - A_1^2), \tag{3.17}$$

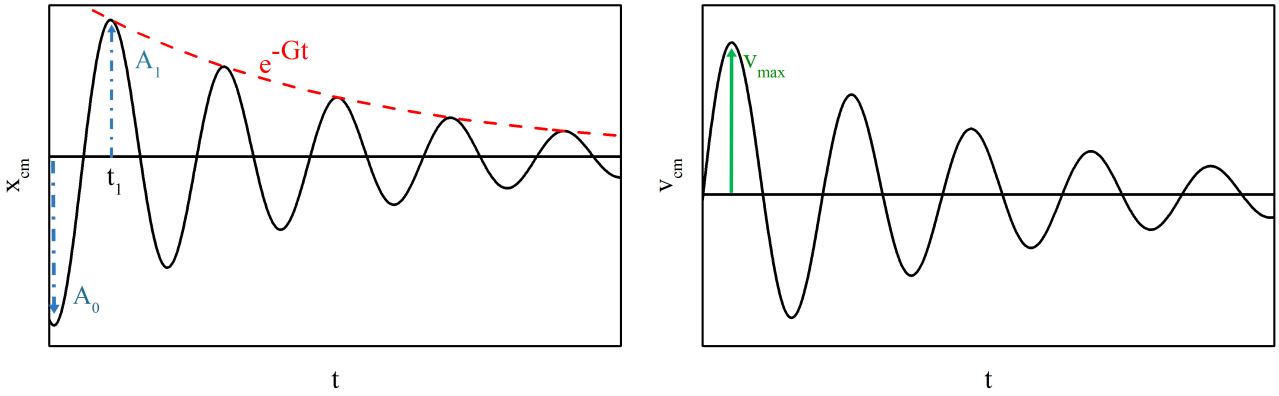

Figure 3.6: a)Cartoon of the time evolution of the center of mass position x_{cm}. A_0 and A_1 are the oscillation amplitude at $t = 0$ and after half period t_1 and G is the oscillation damping. b) Cartoon of the time evolution of the center of mass velocity v_{cm}. v_{max} is the maximum velocity reached during the first oscillation.

where ω is the oscillation frequency, M the total mass and A_0 and A_1 are the oscillation amplitude respectively at $t = 0$ and after half period, at $t_1 = \pi/\omega$. If one assumes the underdamped regime, i.e. $\delta = 1 - A_1/A_0 \ll 1$ or $Gt_1 \ll 1$, the energy loss can be written as

$$E_{loss} = \simeq M(\omega A_0)^2 \delta \simeq M v_{max}^2 G t_1, \tag{3.18}$$

where $\delta \simeq Gt_1$, due to the fact that $A_1 \simeq A_0 e^{-Gt_1} \simeq A_0(1 - Gt_1)$, and $v_{max} \simeq \omega A_0$ is the maximum velocity reached during the first oscillation. The second way considers the energy loss due to the Joule heat, which can be written as

$$E_{loss} = P t_1 \tag{3.19}$$

where P is the power of the system, which can be written in terms of the resistance of the system R and in terms of the particle current I as $P = RI^2$. If one takes into account the presence of phase slips as the source of the resistance, R assumes the form $R = \frac{2\pi\hbar\Gamma}{I}$[2], with $I \simeq n_{1D} v_{max}$. Under these assumptions, the energy loss can be written as

$$E_{loss} \simeq 2\pi\hbar n_{1D} v_{max} \Gamma t_1. \tag{3.20}$$

Equating the two different ways in which the energy loss can be written, a relation between the damping rate and the phase slips nucleation rate can be found

$$G \simeq \frac{2\pi\hbar n_{1D}}{Nm} \frac{\Gamma}{v_{max}}. \tag{3.21}$$

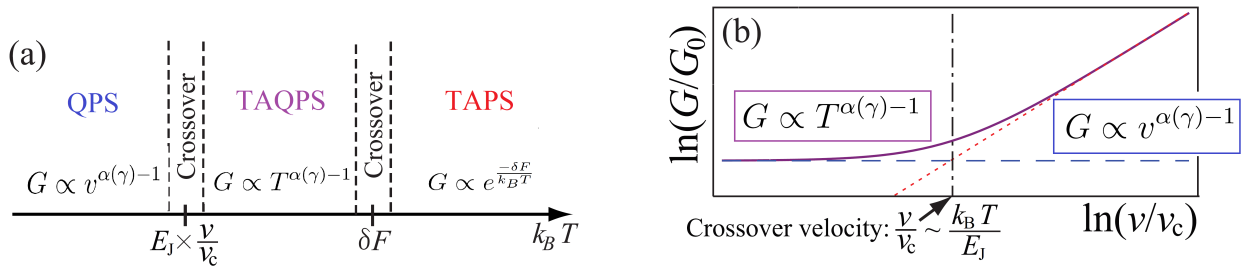

Figure 3.7: a) Scheme of the Damping rate G parameter dependence. G is velocity-dependent in the QPS regime, it is temperature dependent in the TAQPS regime and it is defined by an Arrhenius type equation in the TAPS regime. b) Damping rate G as a function of the velocity in the presence of quantum phase slips (pure and thermally assisted). Adapted by [22].

Consequently, as the phase slips nucleation rate Γ, aslo the damping rate G behaves differently in the case of thermal or quantum fluctuations, as it is shown in Fig.3.7.

In the presence of TAPS, the damping rate G is defined by an Arrhenius type equation

$$G \propto e^{\frac{-\delta F}{k_B T}} \tag{3.22}$$

and it shows a dependence on the temperature in the exponent, whereas in the case of QPS it is temperature-independent and it depends on the velocity via

$$G \propto v^{\alpha-1} \tag{3.23}$$

and it is temperature independent. In the intermediate case of QPS assisted by the temperature, the damping rate G behaves differently from the QPS case: it is velocity independent and it depends only on the temperature via

$$G \propto T^{\alpha-1}. \tag{3.24}$$

Another simple way to derive the relation between the damping rate G and the nucleation rate Γ is the following. The deceleration at the first maximum in the oscillation can be written in terms of the damping rate G as $dv/dt = -Gv$. In terms of individual phase slips, instead, this can be written as $\delta v/\delta t$, where $\delta v = -h/mL$ is the deceleration following a phase slip of 2π in a chain of length L and $\delta t^{-}1 = \Gamma$. By equalling the two expressions we obtain again the relation $G = \frac{h}{mL}\frac{\Gamma}{v}$.

Chapter 4

Exploring quantum phase slips in 1D bosonic systems

4.1 Experimental procedure

The goal of my thesis is to study the transport properties of 1D bosonic superfluids in an optical lattice, by focusing on how interaction and temperature affect the system behaviour. In our experiments we employ ^{39}K atoms which have a negative background scattering length, i.e. $a_{bg} = -44a_0$, and a broad Feshbach resonance[80], which gives us the possibility to tune the interactions among the particles, as shown in sec. 1.3. The production of a ^{39}K BEC is not trivial: due to the level structure of this atom and its collisional properties in the absence of a magnetic field, it is difficult to cool by evaporative cooling down to the temperature necessary for the condensation [81]. As a consequence, we use sympathetic cooling with the ^{87}Rb atoms in order to obtain the BEC. In particular, we initially trap the atoms in a magnetic optical trap where we perform the laser cooling in order to reach samples temperature (both Rb and K) of the order of hundreds of microkelvin. Than, the atoms are trapped in a magnetic trap where an evaporative cooling of Rb is performed, in order to obtain the temperature of few microkelvin. Finally, the atoms are transferred in an optical trap, where we can use the Feshbach resonance, and they can reach the right temperature for the condensation (few tens of nK) after an additional evaporative cooling for the rubidium atoms and a sympathetic cooling for the potassium atoms. In the following I will explain briefly the steps performed to achieve the condensation. More details can be found in the previous thesis of my group [82, 84, 83].

- **Laser cooling in a MOT**: The first step to obtain the ^{39}K BEC is to cool the atoms thanks to the *laser cooling* and to trap them into a magnetic optical trap (MOT).

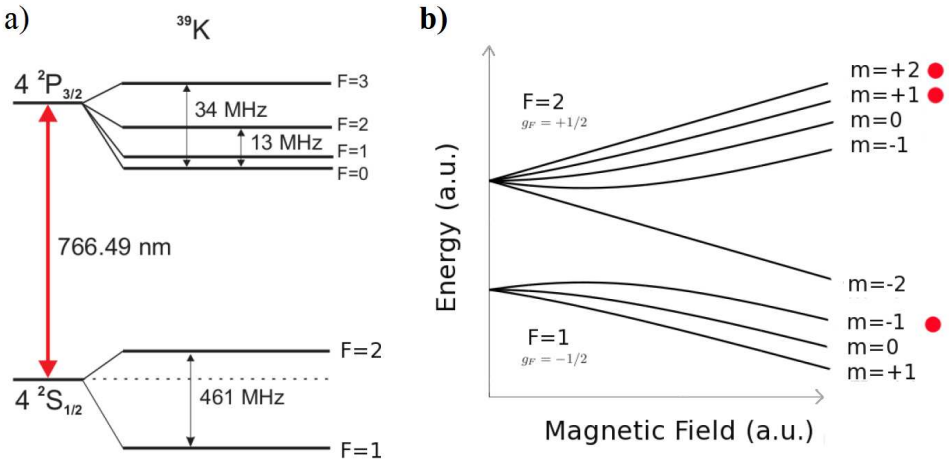

Figure 4.1: a)The hyperfine structure for the ^{39}K. The case of ^{87}Rb is analogous. b) Zeeman shift of the ground state levels. The red dots indicate the low-field seeking levels. Adapted from [40]

Fig. 4.1*a* shows the level structure for K; the case of ^{87}Rb is analogous. In our experiments we use the optical transitions from the level $F = 2$ to the level $F' = 3$, both for potassium and rubidium atoms. Due to the selection rules, some atoms may decay into the level with $F = 1$, which is not coupled with the laser light. As a consequence, we use a repumping beam to transfer the atoms from $F = 1$ to $F = 2$. In our setup there are two MOTs, in order to trap and cool a large number of atoms. A first chamber where the first MOT is loaded, is connected with the solid heated samples of potassium and rubidium atoms; here the pressure is about to 10^{-9} Torr. The atoms are then pushed into the second cell, by means of a push beam, where the pressure is lower than that in the first one (10^{-12} Torr) and the atoms are recaptured in the second MOT.

At the end of the cooling phase the atoms of K and Rb are cooled at a temperature $T \simeq 100\mu K$ and the densities are about 10^{10}cm^{-3}. However, the temperature is not low enough to obtain the condensate. The range of temperatures that can be reached by employing the laser cooling is in fact lower bounded, due to the fact that, by means of this technique, the already slowed atoms reabsorb the diffused photons from other atoms during the slowdown.

- **Evaporative cooling in a magnetic trap:** In order to lower even more the temperature, the atoms are trapped into a magnetic trap and cooled via evaporative cooling. At the end of the second MOT phase, the atoms are equally distributed on all Zeeman levels with $F = 2$, but not all the Zeeman levels can be trapped in a magnetic trap (Fig. 4.1 b). As a consequence we perform an optical pumping to the level $|F = 2, m_f = 2\rangle$,

which is a low-field seeking state, and then we load the K and Rb mixture in a pure magnetic trap with a QUIC configuration. The evaporative cooling is forced by removing selectively the hottest atoms of Rb with a microwave transition into the high-field seeking state $|F = 1, m_F = 1\rangle$. In fact, in this level, the atoms are no longer trappable and hence they are lost (Fig. 4.1 b). Rb is cooled down via evaporative cooling to $T \simeq 1\mu$K, while K is sympathetically cooled via K-Rb collisions, without relevant atom losses. It is important to know that after the forced and selective evaporation of Rb atoms on the microwave transition, some Rb atoms survive in the state $|F = 2, m_F = 1\rangle$ and they cannot be cooled. As a consequence, it is necessary to use another frequency to eliminate these atoms in order to reach the temperatures necessary to have a condensate.

- **Optical trapping and evaporation in the optical trap**: In order to further cool down the potassium atoms and to reach the condensation temperature, we transfer K and Rb atoms into a dipole trap, which is realized with two crossed laser beams at a wavelength $\lambda = 1064$ nm, which provide an average trap frequency of about 50 Hz. When the atoms are trapped into the dipole trap, they are transferred from the state with $|F = 2, m_f = 2\rangle$ into the ground state with $|F = 1, m_f = 1\rangle$. In this state K atoms are characterized by an intraspecies Feshbach resonance at $B_0 \simeq 400$ G and interspecies Feshbach resonance with Rb and K atoms at $B_0 \simeq 315$ G (4.2). The remaining Rb atoms into the level $|F = 2, m_f = 2\rangle$ are removed by using resonant light pulse. The optical evaporation of the atoms is performed in two step, by exponentially lowering the intensity of the two trap beams. During the first part, a homogeneous magnetic field is turned on at the value $B = 316$ G, in order to increase the collisions between Rb and K atoms and to obtain a more efficient thermalization between the two species. The shape of the evaporation ramps has been chosen in order to obtain evaporation mostly on the vertical direction. In this way we lose mainly the heavier rubidium atoms. In the second part, the intensity of the two trap beams is lowered again until it reaches a vertical depth that allows the formation of a pure K condensate. In this situation, the heavy rubidium atoms cannot be trapped anymore and they are completely lost. In this phase, the magnetic field is increased to the value $B = 395$ G, in order to increase the K scattering length and the intraspecies collisions. At the end of the evaporation we have a ^{39}K condensate, which is characterized by a number of atoms of N and a temperature T.

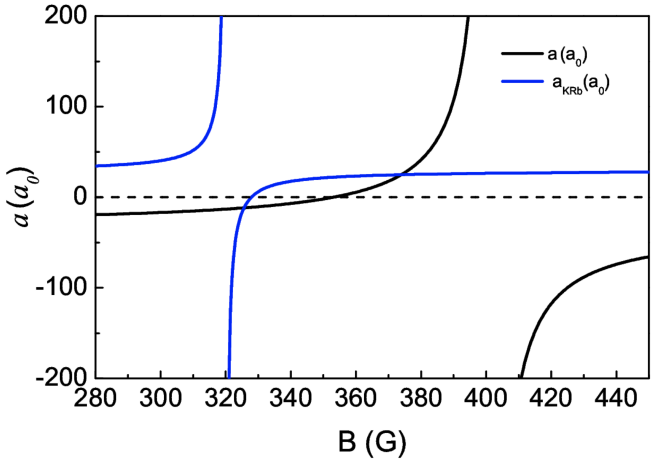

Figure 4.2: Heteronuclear (blue line) and homonuclear (black line) scattering lengths as a function of the magnetic field. At $B = 316$ G the ^{39}K atoms have a interspecies Feshbach resonance with the ^{87}Rb atoms whereas at $B = 395$ G the ^{39} K atoms have a intraspecies Feshbach resonance.Adapted from [40].

4.2 Realization of 1D systems

We realize the 1D systems by splitting the 3D Bose-Einstein condensate with $N_{tot} \simeq 30000$ atoms by using a strong horizontal 2D optical lattice (with depth 20 E_R). More in detail, the 2D lattice is ramped up in a fixed time ($t = 400$ ms) such that an array of independent potential tubes direct along the vertical z axis is created, as it is shown in Fig. 4.3. In our conditions, few hundred subsystems are created and each subsystem contains an average of 30-40 atoms.

The radial trapping energy $\hbar\omega_\perp = h \times 40$ kHz is much larger than all other energy scales, realizing effectively 1D system. Along the longitudinal direction z, a 1D optical lattice with a lattice spacing $d = 532$ nm is then added. The potential depth V_0 can be tuned in the range from $s = V_0/E_R = 1$ to $s = 5$, where $E_R = \hbar^2k^2/2m$ is the recoil energy, with $k = \pi/d$ the lattice wave vector. Along the z direction a harmonic potential ($\omega_z = 2\pi \times 150$ Hz), required from an experimental point of view to realize the 1D systems, is also present.

Due to the presence of the harmonic trap during the loading of the 2D lattice, the atoms prefer to stay into the center of the trap rather than being distributed in an isotropic way, making our system inhomogeneous. As a consequence, when we split the 3D BEC into a matrix of 1D systems, we obtain that the most populated tubes are those at the centre of the external optical trap.

At the same time, the gaussian laser beams that we employ to realize the 2D optical lattice

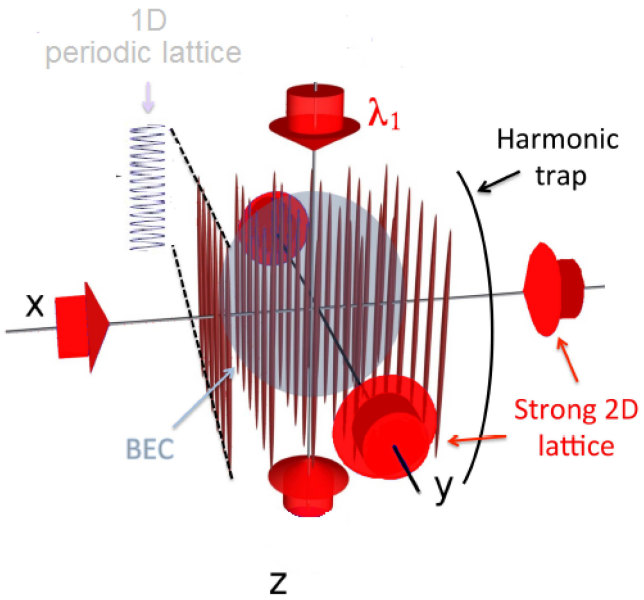

Figure 4.3: The 1D systems are realized by splitting the 3D BEC into few hundreds of tubes by using 2D deep optical lattices in the horizontal plane. Along the z direction a 1D optical lattice and a harmonic potential trap are present. Figure adapted from [85]

induce an inhomogeneity not on the full system scale as the harmonic trapping potential, but in each 1D tube: in each 1D system, in fact, the density of bosons is greater in the centre of the tubes due to the fact that in the presence of the external harmonic confinement, the energy levels of the system are modified. In particular, if the interaction energy E_{int} between the atoms is lower than the trapping energy, the particles prefer to share the same lattice site rather than occupies different sites. As a consequence, due to the fact that the energy of the external lattice site due to the harmonic trap is higher respect the energy of the central sites, the more favourable energetic configuration is that where the atoms occupies the central sites of the lattice.

In order to change the interparticle interaction, we tune the 1D scattering length a_{1D} by using a magnetic field, as it was shown in sec 2.2. The value of the scattering length a_{load} when the lattices are loaded determines the size of the condensate, therefore also the number of populated tubes and the number of atoms in each tube. In particular, in the tube (i,j) the number of atoms is given by

$$N_{i,j} = N_{0,0}\left[1 - \frac{2\pi N_{0,0}(i^2 + j^2)}{5N_{tot}}\right]^{3/2}. \tag{4.1}$$

This expression is obtained by integrating the Thomas-Fermi profile of the interacting sample along the tubes.

The atom number in the central tube $N_{0,0} = 5N_{tot}d^2/2\pi R_x R_y$ depends on the Thomas-Fermi radii R_x and R_y along the horizontal directions, and on the spacing of the tubes $d = \lambda/2$ [86]. From the atom number for each tube it is possible to obtain the mean atomic density in each 1D system. The density distribution in individual tubes is expected to vary from Thomas-Fermi to Tonks, depending on the atom number and interaction strength [87]. To calculate the mean site occupation for each tube, we choose the distribution that gives the largest density at the center of the tube [87]. Then, we estimate the mean site occupation $\bar{n}$ by averaging overall the tubes. In particular, once that ω_z and N_{tot} are known, we are able to tune the mean filling $\bar{n}$ by tuning the scattering length a_{load} during the loading of the 2D optical lattice. In the last part of the loading procedure, the scattering length is set with a slow ramp to its final value a_{meas} and kept there for the rest of the experiment. This value of a determines the interaction energy among the particles.

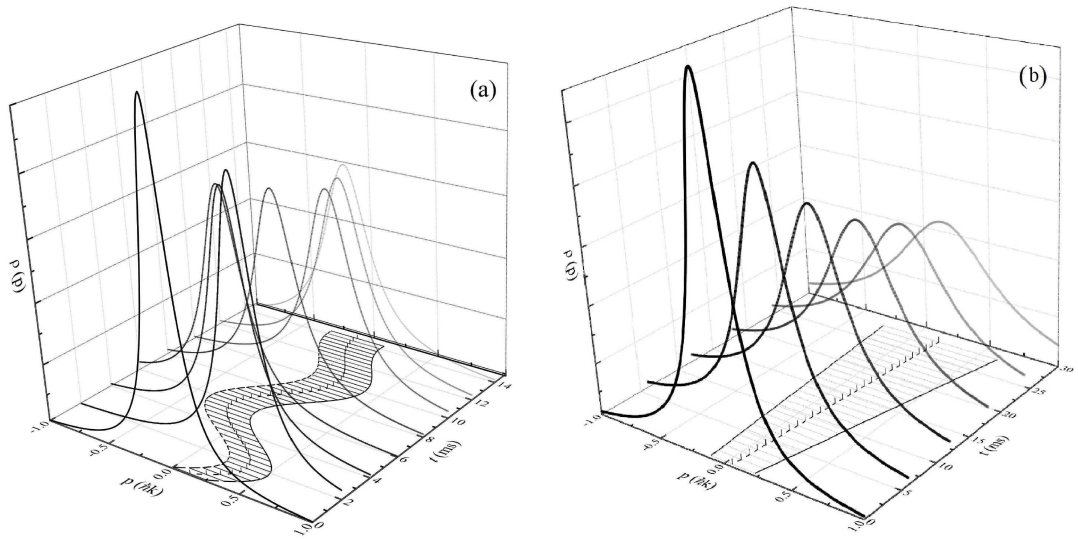

Figure 4.4: (a) Cartoon of the first technique. By suddenly displacing the harmonic trap center at $t = 0$, we excite an oscillation of the 1D systems. The momentum distributions are equispaced in time (2 ms). The dashed line shows the trajectory of p and the grey area exhibits the increase of δp. (b) Cartoon of the second technique. By moving the harmonic trap center at constant velocity, the system dissipates and δp increases linearly. The momentum distributions are equispaced in time (6 ms). The dashed line shows the trajectory of p and the grey area exhibits the increase of δp.

4.3 Exciting the 1D motion

As it was introduced it sec 2.3, the experimental observable is the momentum distribution $\rho(p)$, which is obtained performing time-of-flight absorption imaging, i.e. by releasing the atomic cloud from all potentials and letting it free to expand before the image acquisition. By fitting $\rho(p)$ with a Lorentzian function, we are able to measure the quasimomentum p, which we identify with the averaged momentum acquired by the atoms, and the half-width-at-half-maximum δp.
In order to probe the transport properties of our systems we perform transport measurements, by employing two different procedures. The first procedure consists in suddenly displacing the center of the trap by abruptly switching off the magnetic field gradient which compensate for gravity. The atoms are no longer in the minimum of the potential and start to oscillate in the new potential configuration. After a variable evolution time, we record $\rho(p)$ and we study the time evolution of p, which is affected by the presence of dissipation (Fig. 4.4a). By tuning the magnetic field gradient, we change the trap displacement and we excite oscillations with different amplitude.

The second procedure consists in displacing the center of the trap at constant velocity by linearly changing the magnetic field gradient. After a variable time in the trap, we record $\rho(p)$ (Fig. 4.4b). In this kind of measurements, we investigate the time evolution of δp, whose increase is related to the dissipation. The energy dissipated during the harmonic potential movement is in fact converted into momentum spread. In fig. 4.5 a scheme of the magnetic field gradient behaviour for both procedures is shown.

Both procedure can be better understood by considering the analogous in the electric circuits physics. The first procedure is analogous to excite an oscillation into an RLC circuit. Initially, the electric circuit is at the equilibrium and there is not charge transport into the circuit. Subsequently, a current start to flow with a sinusoidal behaviour when the capacitor is charged and / or a current is induced in the inductor: this correspond to the sudden shift of the harmonic trap. As in the case of our system, also in the case of a RLC circuit, if there is a finite resistance, the current does not keep oscillating forever, but the oscillation amplitude slowly diminishes with time and eventually the motion stops altogether. In the second procedure we instead impose a constant velocity. This is analogous to imposing a continuous current into a circuit. In both of the system we observe a Joule heating.

4.4 Dissipation in the presence of oscillations

Dissipation in the presence of oscillations: evidence of quantum phase slips

In this section we will focus the attention on the experiments with an oscillating system. As it was explained in the previous section, the oscillations are induced by suddenly shifting the center of the harmonic trap. By working in the semiclassical framework, the oscillating motion of the system in the trap in the presence of an optical lattice can be obtained by solving the system of equations

$$\begin{cases} \dot{p} = -k_e z - \beta \dot{z} \\ \dot{p} = m^*(p)\ddot{z} \end{cases}$$

The first equation describes a damped oscillation along the z direction; it contains the coefficients k_e and β which are the elastic constant and the viscous friction coefficient, respectively. The first term, k_e, is related to the axial trapping frequency ω_z via $\omega_z = \sqrt{k_e/m}$, whereas the second coefficient, β, is related to the damping rate G via $G = \beta/2m$. The damping rate G is a parameter of interest, which gives informations about the dissipation in the system.

The second equation takes into account the presence of an optical lattice in the effective mass m^* term, which is related to the curvature of the energy band of the lattice, as it was shown in sec. 1.5.2.

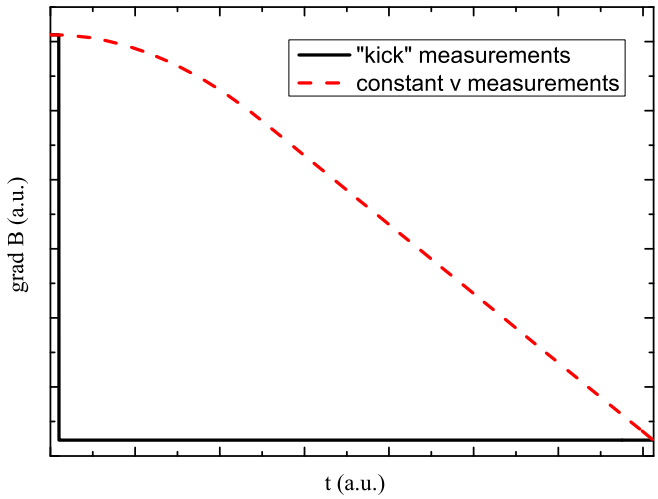

Figure 4.5: Scheme of the magnetic field gradient behaviour for both experimental procedures employed to perform transport measurements. In the first procedure (solid black line) we abruptly switch off the magnetic field gradient which compensate the gravity in order to excite the system oscillation. In the second one (red dashed line) we change linearly the magnetic field gradient in order to perform measurements at constant velocity.

In the presence of an optical lattice, both the oscillation frequency and the damping depends on the effective mass m^*. In particular, the oscillation frequency takes the form $\omega' = \sqrt{\omega^{*2} - 4\pi G^{*2}}$, where $\omega^* = \omega_z\sqrt{\frac{m}{m^*}}$ is the oscillation frequency in the absence of any dissipative effect, and $G^* = G\frac{m}{m^*}$ is the damping rate in the presence of the lattice.

In the presence of a finite damping rate $G*$, the time evolution of p can be approximated with a damped oscillation function of the form

$$p = m^*\tilde{v}e^{-Gt}\sin(\omega' t + \varphi) \tag{4.2}$$

with amplitude $p_0(t) = m^*\tilde{v} = m^*\omega^{*2}\Delta z/\omega'$ and frequency $\omega' = \sqrt{\omega^{*2} - 4\pi^2 G^2}$. Here Δz is the trap displacement.

It is important to know that the system behaves according to the eq. 4.2 only if the maximum momentum reached during the oscillation is smaller than the critical momentum for the dynamical instability p_c. If $p < p_c$ we observe a damping in the oscillations which is due to the presence of phase slips.

For momenta larger than p_c the system behaves differently from the previous case and the system does not oscillate anymore. We observe, instead, an overdamped motion, which we attribute to the occurrence of the dynamical instability that can be described in term of a divergence of the phase-slips rate at the critical velocity v_c of the superfluid.

In the subsection 4.4.1 we will treat the phenomenon of the dynamical instability, whereas we will focus on the phenomenon of phase slips in the subsection 4.4.2.

4.4.1 Dynamical instability

A time evolution of the momentum distribution peak p for $s = 2$ and for $a = 8.4a_0$ is shown in Fig. 4.6 a. In this picture, we observe an initial increase of p up to a certain critical value p_c, which is followed by a subsequent decrease. More in detail, for $p < p_c$, the oscillation is weakly damped and the data points can be fitted by using the damped oscillation equation shown in the previous section (Eq.4.2). This behaviour is consistent with the presence of phase slips, as we will see more in details in the next subsection. For $p > p_c$, instead, the system enters into a dynamically unstable regime driven by a divergence of the phase slip rate, and the oscillation is strongly damped. In order to estimate the critical momentum p_c, which separates the weakly dissipated regime from the strongly unstable one, we plot the difference between the fit of the weakly damped oscillation and the experimental data, as shown in Fig. 4.6 b. In fact, the critical momentum p_c for the occurrence of the dynamical instability is identified as the value where the experimental data points deviate with respect to the theoretical curve. The interception of the

two linear fits identifies the time at witch the system enters the unstable regime, corresponding to the critical momentum p_c. We also observe the presence of two different regimes into time evolution of the momentum distribution width δp: initially δp is almost constant, whereas it abruptly starts increasing when the system enters into the unstable regime (Fig. 4.6 c)

Thus behaviour can be explained in terms of the phenomenon of the dynamical instability. An intuitive explanation of this instability in the absence of interaction can be given in term of the effective mass m^*.

As it was discussed in section 1.5.2, it is possible to describe the system dynamics in the presence of an optical lattice by using the semi-classical model, provided that the mass of the system is replaced with the effective mass m^*, which takes into account the presence of the lattice. The effective mass is not constant, but it depends on the quasimomentum p of the system, and, in particular, it can become negative at a certain value of the quasimomentum. The critical value corresponds to one-quarter of the reciprocal lattice constant, i.e. $\pi/2$ at zero interactions, only for a lattice strengths in the tight-binding regime ($s \geq 5$).

When the effective mass of the system changes its sign, the BEC behaves as if it was subject to a negative scattering length and, due to a such attractive interaction, the BEC collapses [88].

Another interpretation of this mechanism can be given in term of divergence of the phase slips rate. When the system enters into the dynamical unstable regime, it is observed a rapid growth of excitations (phase slips), which provoke a strongly dissipation and the system stops oscillating. In this situation, the phase coherence of the system is broken due to the fact that the tunnelling is not fast enough to lock the phases of adjacent sites, which start to run independently. As a consequence, the system enters into an insulating incoherent regime.

So far we have considered the case of $U = 0$. For non-negligible interaction the situation changes, and the critical momentum is not equal to $\pi/2$ (i.e. the theoretical value in the tight binding regime). As it was shown in subsection 2.4.4, when the interaction among the particles is strong enough to overcame the kinetic energy, the system undergoes a phase transition from the SF to the MI regime, and this happens even for very small velocity. In this scenario, we thus expect that the critical velocity decreases as the interactions increase, i.e. $p_c < \pi/2$, vanishing at the SF-MI transition [89].

As it is shown in Fig 4.7, we have excited the sloshing motion of the system for different values of interactions and lattice depth. By increasing the scattering length, we observe that the damping rate at short times increases, as the phase slips nucleation rate increases (Fig. 4.7 a), while p_c decreases (Fig. 4.7 b). However, as it is show in Fig. 4.7 b, by increasing the interactions, the measured p_c reaches a finite constant value, but it does not vanish. The

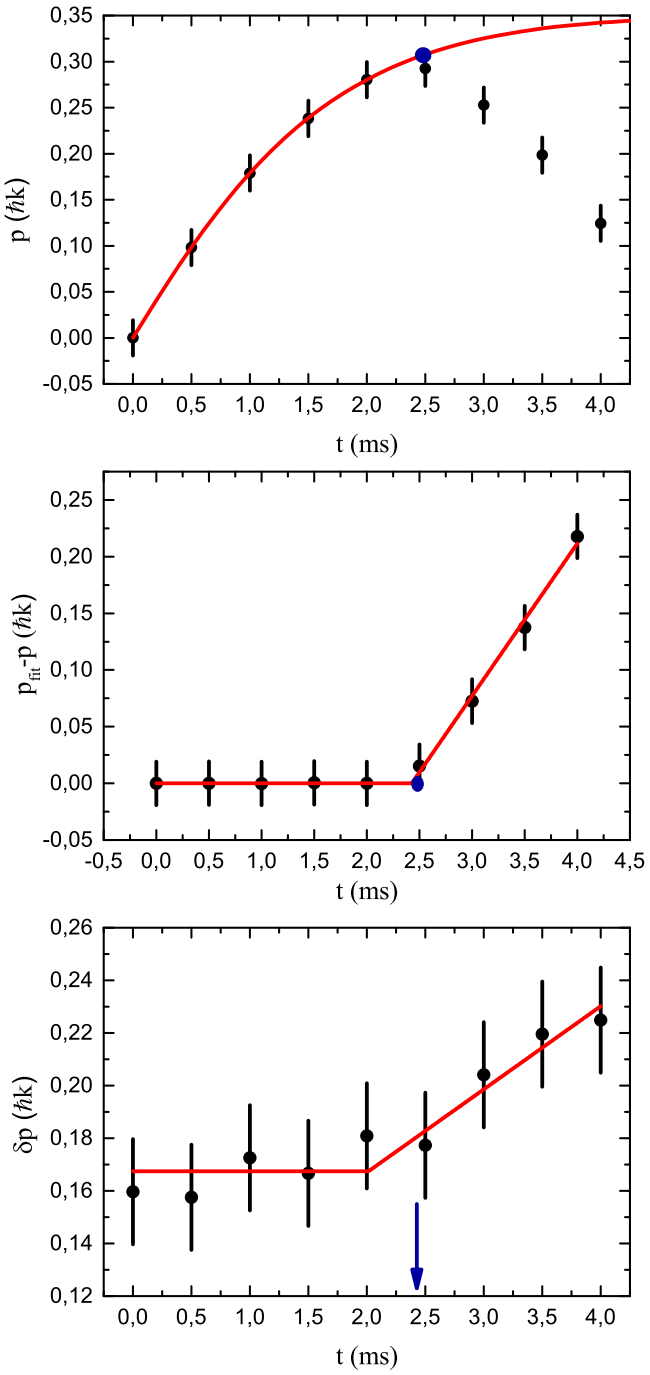

Figure 4.6: (a) Time evolution of the momentum distribution peak p at $s = 2$ for $a = 8.4a_0$. The solid line is the damped oscillation fitting the data for $p < p_c$ before the dynamical instability sets in. The blue circle marks the critical momentum p_c. The error bars comprise the imaging resolution and the statistical uncertainties. (b) Difference between the fit to the initial damped motion and the experimental data (dots). The continuous line is the fit to estimate the critical momentum. (c) Time evolution of the momentum width. The blue arrow marks the time t corresponding to the critical momentum p_c.

onset of this plateau can be interpreted as the critical scattering length a_c to enter the Mott regime for the commensurate regions of the system. As it was introduced in sec. 4.2, the presence of a trap during the loading of the 2D lattice makes the 1D systems inhomogeneous and some tubes contain commensurate regions, as well as incommensurate regions where the critical density is always lower than unity. The transport along the tubes with a commensurate regions is globally suppressed driving the system into an effective insulating regime, i.e. within in each tube a part of the atoms reaches the localization condition $n = 1$ stopping also the remaining adjacent parts with different occupation. The fraction of tubes that does not reach the critical density $n = 1$ keeps instead moving also for $a > a_c$, originating the observed plateau for p_c. We estimate that about one quarter of the atoms resides in tubes where the occupation is always $n < 1$. For a given lattice depth when increasing the scattering length in the Mott phase, $a > a_c$, this fraction of delocalized atoms remains constant because in the tubes where the Mott domains form, the density is fixed.

This interpretation seems confirmed by the observed increase of the plateau for decreasing lattice depth (Fig. 4.7 b). In fact, the increase of the interaction strength that is necessary to reach the insulating regime, produces an overall decrease of the density of the 1D systems, hence an increase of the fraction of tubes that does not reach the critical density for the Mott insulator transition. For each set of measurements with a given value of s, we determine the

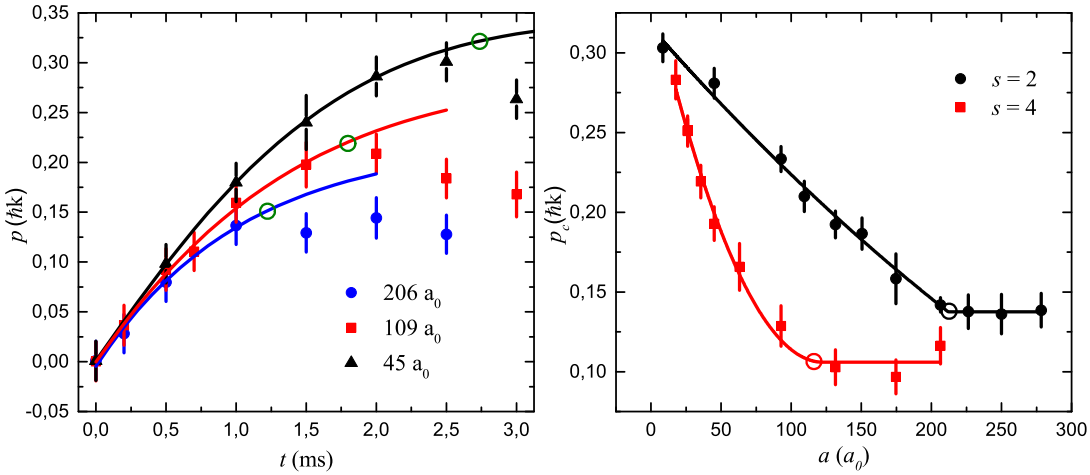

Figure 4.7: (a) Time evolution of the momentum distribution peak p at $s = 2$ for different values of scattering length. The solid lines are the theoretical damped oscillation fitting the data for $p < p_c$ before the dynamical instability sets in. The green circles mark the critical momentum p_c. The error bars comprise the imaging resolution and the statistical uncertainties. (b) Critical momentum p_c versus scattering length for two lattice depth: $s = 4$ (red squares) and $s = 2$ (black circles). A piecewise fit (solid lines) determines the critical values for the SF-MI transition (empty circles) for $n = 1$: respectively $a_c/a_0 = 122(8)$ ($\gamma_c = 1.08(7)$) and $a_c/a_0 = 214(6)$ ($\gamma_c = 1.88(5)$).

critical value of the scattering length, a_c, by using a piecewise fit [90]. More in detail, we use a second-order polynomial fit, which is justified by the phase-slip based model [5, 90]. As it is shown in Fig.4.7 b, as the lattice depth decreases, the critical scattering length increases. This behaviour is in agreement with the numerical results with Monte Carlo simulation [90].

In conclusion, by studying the critical quasimomentum behaviour as a function of the interactions, the onset of the Mott regime can be easily detected from a vanishing p_c, and this kind of measurements can be performed both in the presence of a shallow lattice [90] and a deep one [68].

4.4.2 Observation of velocity-dependent quantum phase slips

For momenta lower than the critical one, far from the dynamical instability, the system never enters in the unstable regime, but it keeps oscillating with a dissipation due to phase slips nucleation. As it was shown in sec. 3.2.1, the damping rate G is related to the phase slips nucleation rate Γ via $G \simeq \frac{h}{mL}\frac{\Gamma}{v}$. As a consequence, in order to understand the phase slips phenomenon, we studied the behaviour of G for different values of velocity, interaction and temperature.

Despite the first theoretical model regarding the damping behavior of dipole oscillations of

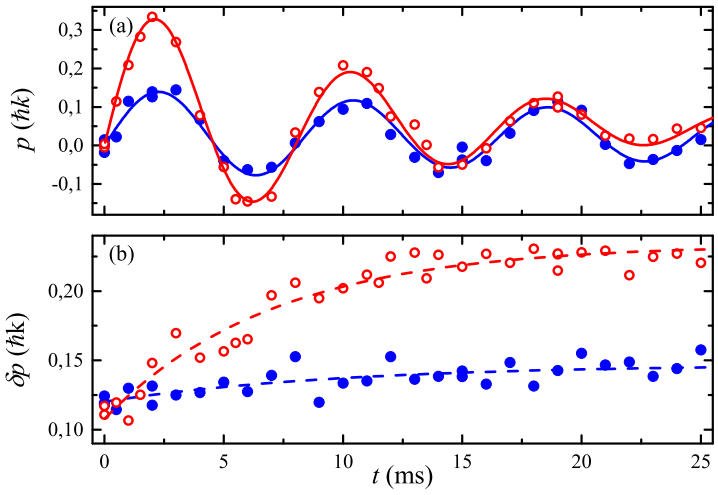

Figure 4.8: (a) Time evolution of the quasi-momentum p and (b) of the momentum distribution width δp for the interaction strength $\gamma = 1.22$, the temperature $T = 22(4)$ nK and two maximum velocities: $v = 1.4(4)$ mm/s (blue filled circles) and $v = 2.2(4)$ mm/s (red open circles), respectively corresponding to trap displacements $\Delta z = 1.5$ μ and $\Delta z = 4$ μm. The lines in panel (a) are fits to measure the damping rate, which is $G = 28(9)$ Hz and $G = 84(6)$ Hz for the blue and red data, respectively. The lines in panel (b) are fits to measure the time constant τ , which is $\tau = 10(7)$ ms and $\tau = 7(1)$ ms for the blue and red data, respectively.

one-dimensional ultracold gases due to the presence of phase slips [22] was performed in the Bose-Hubbard regime, we have decided to study this phenomenon in the presence of a weak optical lattice ($V = 1E_R$). The reason is that we want to perform measurements far from the dynamical instability, which occurs for velocity larger than a critical velocity, and to increase the range of velocities investigated. In the previous chapter we have shown the behaviour of the critical velocity for the dynamical instability for different values of interaction and lattice depth. We have observed that, for a fixed interaction value, the critical velocity decreases as the lattice depth increases (Fig. 4.7). As a consequence, by increasing the lattice depth, we decrease the range of velocities that we can investigate far from the phenomenon dynamical instability. In the presence of an optical lattice with depth $s = 1$, the critical velocity varies in the range [0.74,0.56] $\hbar k$, depending on the interaction value.

The idea is that a weak lattice in the Sine-Gordon limit shifts the critical velocity towards the band edge, thus enlarging the range of accessible v for studying the phase-slips phenomenon. In the weak interaction limit, in fact, the critical velocity is defined as the point in which the curvature of the Bloch band is zero, so that the critical velocity tends to the Bragg velocity for vanishing lattice strengths.

The damping rate is measured by fitting the time evolution of p with the model presented previously, as shown in Fig. 4.8. We observe that, at the same interaction $\gamma = 1.22$, the damping rate G is different for two different value of velocity, which we identify in this kind of measurements with the velocity reached during the first oscillation as in the theoretical model [22], suggesting the presence of phase slips with a nucleation rate that depends on the velocity. In fact, a small velocity v (blue filled circles) typically leads to a very weakly damped oscillation. In this case, δp is almost constant showing that the system is just slighting dissipating and that its coherence properties are almost preserved. Instead, at high velocity (red open circles), the oscillation is strongly damped and δp greatly increases during the evolution, showing a strong effect of excitations.

We fit the growth of δp with an inverted exponential,

$$\delta p(t) = \delta p(0) + p_\infty[1 - exp(-t/\tau)], \tag{4.3}$$

where τ is the constant time and p_∞ is the relative saturation value. We found that the damping rate G is directly related to τ via $2\tau \simeq 1/G$, and this can be interpreted considering that the mechanical energy dissipated in the oscillation is converted into momentum spread.

We have repeated this type of measurement for a wide range of velocities, interaction strengths and temperatures. The temperature is estimated from the momentum distribution at

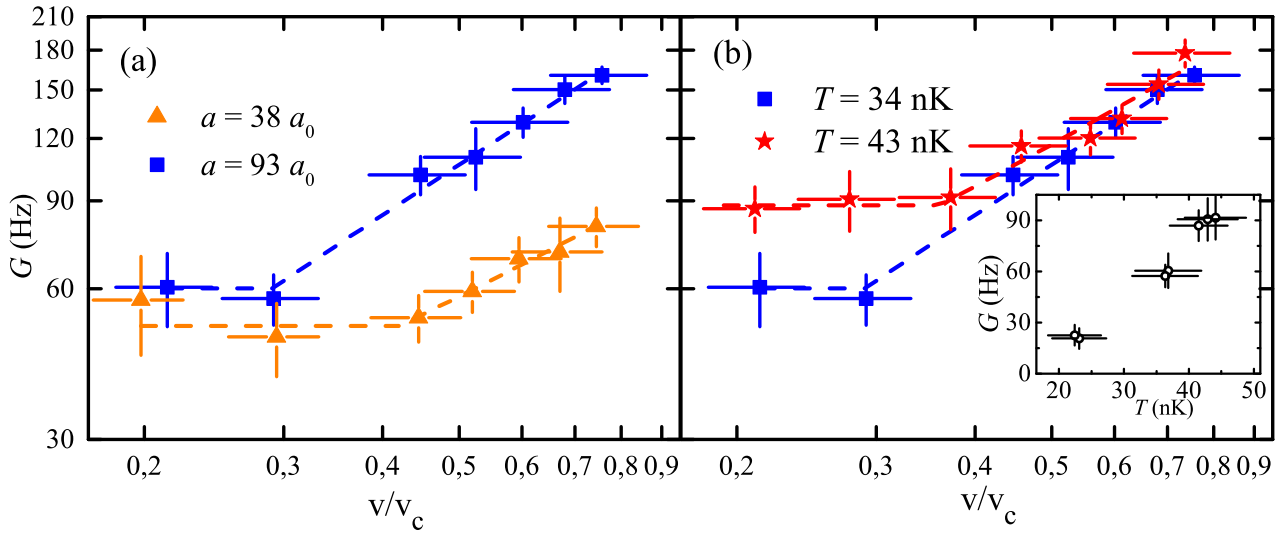

Figure 4.9: (a) Damping rate G is plotted versus the maximum velocity v normalized to the critical velocity v_c, for three interaction strengths and constant temperature: $\gamma = 0.13$ and $T = 37(7)$ nK (black circles), $\gamma = 0.19$ and $T = 39(7)$ nK (orange triangles) and $\gamma = 0.64$ and $T = 34(5)$ nK (blue squares). (b) G versus v/v_c for two different temperatures and approximately constant interaction energy: $T = 34(5)$ nK and $\gamma = 0.64$ (blue squares) and $T = 43(5)$ nK and $\gamma = 0.70$ (red stars). The lines are fits to measure the crossover velocity v^* .

$t = 0$ and the mean atom number per site $\bar{n}$ via the established relation $k_B T = \hbar \bar{n} \delta p_0 / 0.64 m^* d$ [91, 92], where m^* is the effective mass which takes into account the presence of an optical lattice. In our measurements the temperature T changes from 20 to 35 nK and the interaction strength γ changes form 0.13 to 1.22. Some measurements of the evolution of G with velocity and interaction at the same temperature are shown in fig 4.9. Each data set is rescaled to the corresponding critical velocity v_c for dynamical instability, which is measured according to the technique introduced in the previous subsection.

In Fig.4.9 a, two different dataset at the same temperature and different interaction are reported. For strong interaction (orange, blue), we observe a clear crossover from a regime of constant G to a regime where G grows with the velocity.

We fit the data by using a piece-wise linear function and we determine the crossover velocity v^*, which we define as the minimum velocity required to enter the velocity-dependent regime. The crossover velocity seems to depend on the interaction and in particular it apparently decreases for increasing interaction.

By repeating the same measurements for different values of temperature and at the same interaction, we observe a similar behaviour similar to the one introduced earlier (Fig. 4.9 b). Also in this case, in fact, we observe a crossover from a regime where G is velocity independent

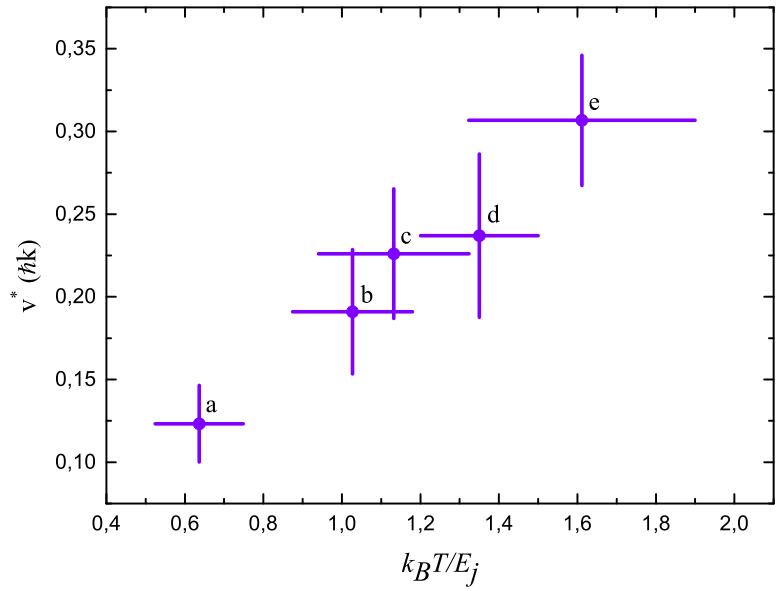

Figure 4.10: Crossover velocity as a function of the temperature normalized to the Josephson plasma energy. The crossover velocity increases as the temperature rises. The individual datapoints have been taken for different temperatures and interaction energies: a) $\gamma = 1.22$ and $T = 22(2)$ nK, b) $\gamma = 0.64$ and $T = 34(5)$ nK, c) $\gamma = 0.37$ and $T = 30(5)$ nK, d) $\gamma = 0.70$ and $T = 43(5)$ nK, e) $\gamma = 0.19$ and $T = 39(7)$ nK.

to a regime where G grows with velocity.

Moreover, as shown in Fig. 4.9 b , in the regime where G does not depend on the velocity, i.e. for $v \ll v^*$, the damping rate G is strongly affected by temperature and we observe a monotonic increase of G with T (as shown in the inset in Fig. 4.9 b). In this regime the dependence on interaction (Fig. 4.9a) is weaker. On the contrary, in the v-dependent regime, interaction effects are apparently dominant (Fig. 4.9 a), whereas we cannot measure a clear dependence on T (Fig. 4.9 b). As a consequence of the combination of these effects, the crossover velocity increases as the temperature increases. The behaviour of the crossover velocity as a function of the temperature normalized to the Josephson plasma energy is shown in fig.4.10.

These observations appear consistent with the predicted crossover from a regime where the nucleation of phase slips is due to thermal effect to a regime of quantum phase slips. We do not control this crossover by changing the temperature T, but by varying the crossover temperature

$$T^* \propto E_j/k_B v/v_c \tag{4.4}$$

by tuning velocity and interaction strength. For $T^* \ll T$, i.e. at small velocity and small interaction, G depends only on T and it is velocity-independent, suggesting a thermal activation of phase slips. For $T^* \gg T$, i.e. at large velocity and large interaction, the system

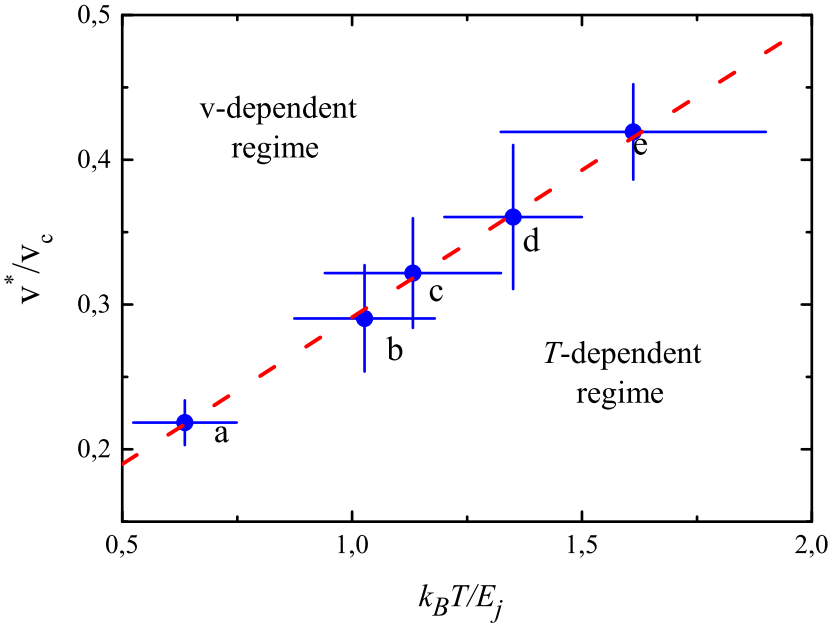

Figure 4.11: Crossover velocity v^*/v_c versus k_BT/E_j. The individual datapoints have been taken for different temperatures and interaction energies: a) $\gamma = 1.22$ and $T = 22(2)$ nK, b) $\gamma = 0.64$ and $T = 34(5)$ nK, c) $\gamma = 0.37$ and $T = 30(5)$ nK, d) $\gamma = 0.70$ and $T = 43(5)$ nK, e) $\gamma = 0.19$ and $T = 39(7)$ nK. The dashed line apparently separates the thermal and the quantum regimes for phase slips.

enters in a regime where G is linearly dependent on the velocity and temperature independent, suggesting a quantum activation of phase slips. A further indication that our measurements are in agreement with the crossover from thermal assisted to quantum phase slips is the linear scaling of the crossover velocity normalized to the critical velocity v^*/v_c as a function of temperature normalized to the Josephson energy k_BT/E_j. As shown in fig. 4.11, despite the individual datapoints have been measured for scattered values of γ and T, they show a clear linear scaling, which is consistent with the theoretical prediction

$$\frac{k_BT^*}{E_j} \propto \frac{v}{v_c}. \tag{4.5}$$

From the fit we get the relation for the crossover velocity T^* as a function of v, E_j and v_c

$$k_BT^* = 4.9(14)E_j\frac{v}{v_c} - 0.4(4)E_j. \tag{4.6}$$

Unfortunately, the agreement with the theory is only qualitative since we cannot reproduce the theoretical exponent α. In our experiments we observe a damping rate that is proportional to $T^{\alpha-1}$ in the case of thermally activated phase slips and to v^α in the quantum phase slips one, but our experimental exponents α are interaction independent and they are of the order

of unity [19], as it is shown in fig.4.12.

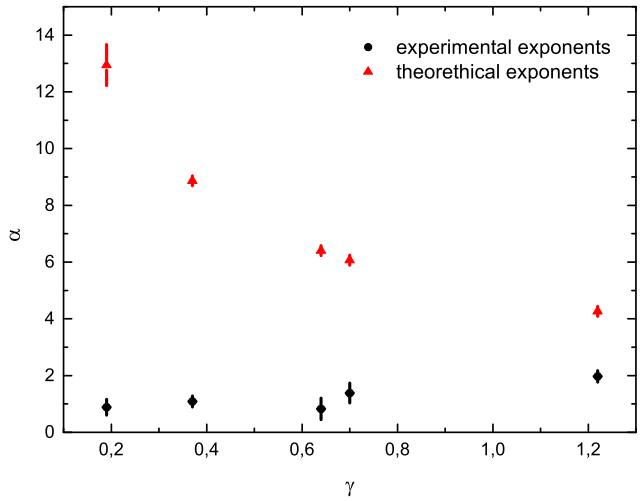

Figure 4.12: Experimental (red circles) and theoretical (black triangles) exponents α as a function of the interaction γ. Our exponents are about constant (and of the order of the unit) and they do not depend on the interaction. On the contrary, the theoretical exponents depend on the interaction and they can be an order of magnitude larger than the experimental exponents.

On the contrary, according to the theoretical model [22], the theoretical exponents depend on the interaction. By using the relation between the Luttinger parameter K and the Lieb-Liniger parameter γ in the limit of no lattice potential ($s = 0$) and for small interactions ($\gamma < 10$)

$$K \sim \pi\sqrt{\gamma - \gamma^{3/2}/(2\pi)} \tag{4.7}$$

we estimate the theoretical exponents and we find that they varies from about 13 to 4.5 in the same range of interaction strengths, i.e. they can be an order of magnitude larger than the measured exponents [22]. Possible reasons for the disagreement are the range of velocities explored, much larger than in the theory , and the lattice strength ($s = 1$), much lower than in the theory [22]. More in detail, the power-law behavior I showed above is valid only for very low velocities ($p < hk/10$), while in the experimental range ($hk/10 < p < hk/2$) a different, exponential behavior has been predicted [22, 5]. On the experimental side, the limited range of accessible velocities, which is limited by the finite T on the low-v side, does not allow us to distinguish a power law from an exponential.

4.4.3 Comparison between our experimental results and the theoretical model of thermally activated phase slips of one-dimensional Bose gases in the Sine Gordon limit.

Recently M.Kunimi and I. Danshita from the Yukawa Institute for Theoretical Physics, have performed a theoretical study of thermally activated phase slips of one-dimensional Bose gases in a shallow optical lattice, motivated by our experimental results.

They find, at low velocity and weak interaction, damping rates comparable with our experimental values, by assuming the presence of thermal activated phase slips rather than thermally assisted quantum phase slip [23]. In the following I will briefly show a summary of the methods that they have used and a comparison between their theoretical and our experimental results.

Under the mean-field approximation, they initially consider a ring shape system with an optical lattice and they estimate the energy barrier between the stable and the unstable solutions of the stationary Gross-Pitaevskii equation, the frequency of the unstable mode and the curvature of the energy landscape around the stationary solutions. By employing the Kramers formula, they use the previous results to calculate the behaviour of nucleation rate of TAPS as a function of the filling factor $n = n_{1D}d$ and the velocity. Finally, they estimate the damping rate G by using the local density approximation, in order to taking into account the inhomogeneity of the system, due to the presence of an harmonic trap, and the temporal change of the velocity. More in detail, to include these effects, they substitute the power P in the eq. 3.19 with the power per unit length $\tilde{P} = \tilde{P}[n(x,t), v(t;G)] = 2\pi\hbar\tilde{\Gamma}[n(x,t), v(t;G)]n(x,t)v(t;G)$ at time t. Here, $\tilde{\Gamma} = \Gamma/L$ is the nucleation rate per unit length. The spatial and temporal dependences of the power and the nucleation rate is originated by the local particle density $n(t,x) = n_{TF}(x - x_{cm}(t))$, which depends on the 1D Thomas-Fermi density profile n_{TF} and on the position of the center of mass during the damped oscillation $x_{cm}(t)$, and by the velocity $v(t;G) = e^{-Gt}v_{max}sin(\omega_L t)$.

In this scenario, the energy loss in eq. 3.19 can be substituted by

$$E_{loss} = \int_0^{t_1} dt \int dx \tilde{P} = \tilde{P}[n(x,t), v(t;G)] \tag{4.8}$$

which is obtained by integrating the power $\tilde{P}[n(x,t), v(t;G)]$. By equaling Eq. 4.8 and Eq. 3.17, with $A_1 \simeq A_0 e^{-Gt_1}$, they obtained a relation between the damping rate G and the nucleation rate Γ

$$\frac{N}{2}mv_{max}^2(1-e^{-2Gt_1}) = \int_0^{t_1} dt \int dx\tilde{P} = \tilde{P}[n(x,t), v(t;G)]. \tag{4.9}$$

Once known the filling factor and as the nucleation rate Γ depends on the velocity, one can estimate the damping rate G for thermal activated phase slips by solving Eq. 4.9.

It is important to note that in order to estimate G, they used the peak density, i.e. the density of the central tube, for sake of simplicity. From an experimental point of view, we use instead the mean density due to the fact that when we record the images of the momentum distribution, we obtain information on the mean properties of all subsystems. As a consequence, the theoretical G gives only a bound of the damping rate, which is a lower bound due to the fact that G decreases as the number of particles increases.

Figs. 4.13 and 4.14 show the comparisons between the theoretical behaviour of the damping rate G as a function of the velocity v normalized to the critical velocity v_c, and the experimental one for different values of interactions, temperature and atom numbers. As it is shown in figs. 4.13 (a,b,d,e) and in figs 4.14 (a,b,d,e) the theoretical G is comparable with our experimental values in the regime of low velocity, where the Kramers formula is efficient, and in the regime of

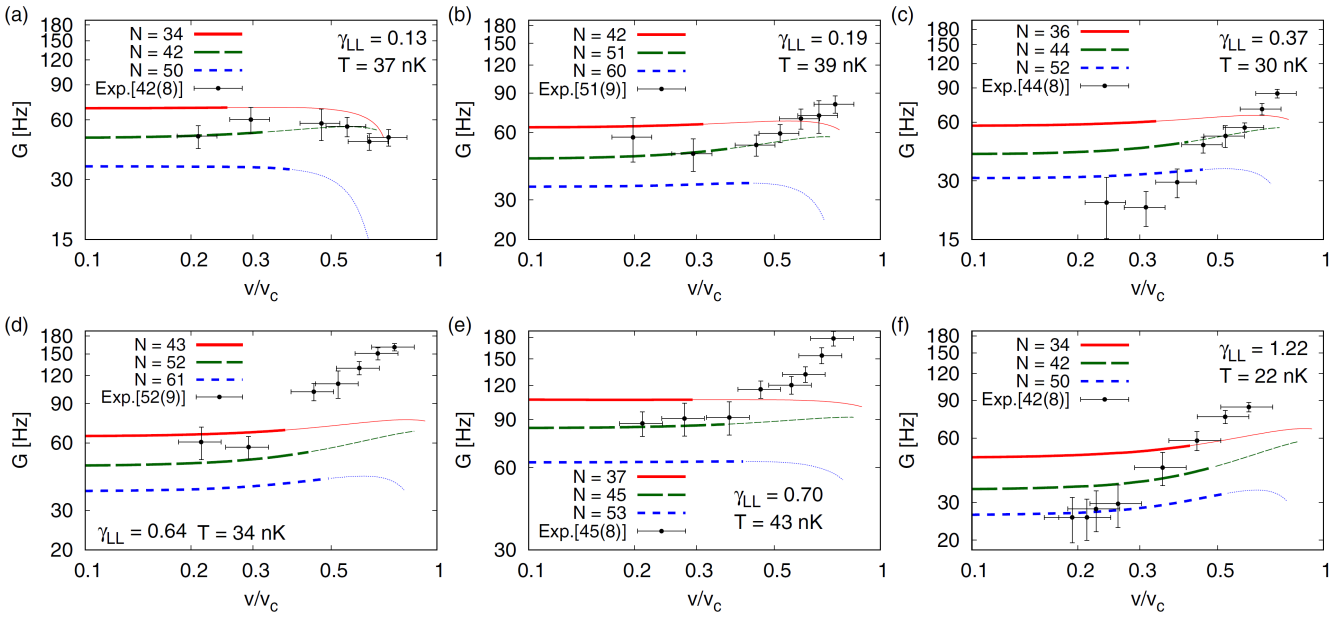

Figure 4.13: Theoretical amping rates for (a) $(\gamma, T) = (0.13,37$ nK), (b) $(\gamma, T) = (0.19,39$ nK), (c) $(\gamma, T) = (0.37,30$ nK), (d) $(\gamma, T) = (0.64,34$ nK), (e) $(\gamma, T) = (0.70,43$ nK), and (f) $(\gamma, T) = (1.22,22$ nK). The black points represent our experimental data. The thick lines represent the region in which the system at the trap center satisfies $E_B > 2k_BT$. Adapted from [23]

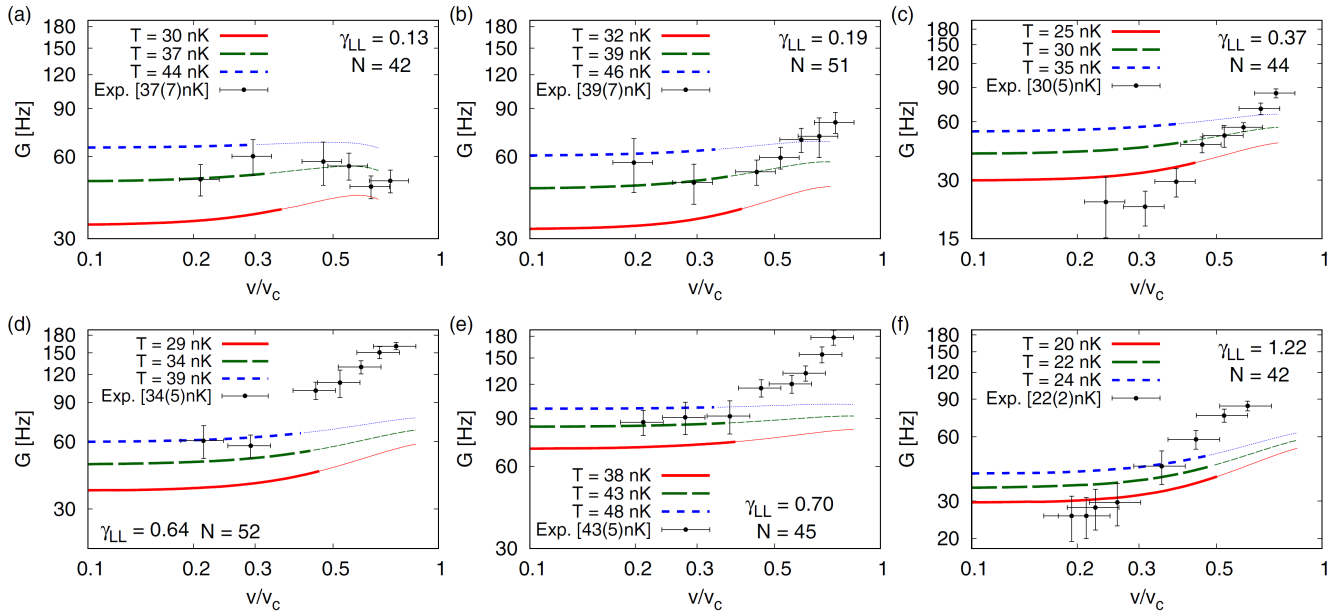

Figure 4.14: Damping rates for (a) $(\gamma, N) = (0.13,42)$, (b) $(\gamma N) = (0.19,51)$, (c) $(\gamma N) = (0.37,44)$, (d) $(\gamma N) = (0.64,52)$, (e) $(\gamma N) = (0.70,45)$, and (f) $(\gamma N) = (1.22,42)$. The black points represent our experimental data. The thick lines represent the region in which the system at the trap center satisfies $E_B > 2k_BT$. Adapted from [23]

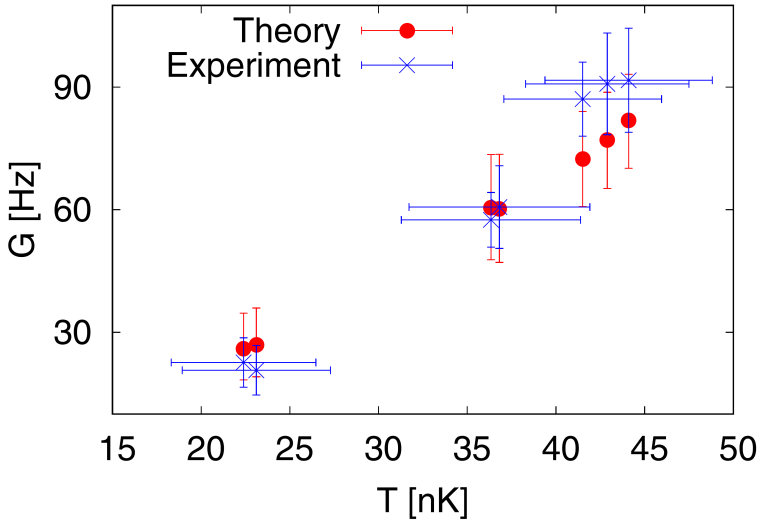

Figure 4.15: Theoretical (red dots) and experimental (blue x) damping rate as a function of temperature for $(\gamma, N) = (0.67,49)$. The error bars in the theoretical data points are estimated by the value of G at the lower and upper bounds of the experimental temperature, whereas the error bars in the experimental data points represent the statistical uncertainties. Adapted from [23]

weak interaction, where the GP mean-field theory is valid. This agreement suggests a thermal nature of the phase slips and in particular for low velocity and weak interaction the damping in the system oscillations seems be due to thermally activated phase slips, rather than thermally assisted quantum phase slips.

In figs.4.13 (c,f) and figs. 4.14 (c,f), we see that our experimental data are not in agreement with the theoretical model and in particular they are not included into the region between the upper and lower theoretical curves. The disagreement in figs. 4.13 f and 4.14 f is probably due to the fact that the interaction $\gamma = 1.22$ is too large to use the GP mean-field theory, whereas the disagreement in figs. 4.13 c and 4.14 c is not clear. As shown in fig. 4.15, the experimental values of G for different temperatures are in good agreement with the theoretical values and this can be considered a further indication that in the regime of weak interaction and low velocity the nature of phase slips is purely thermal. Nevertheless, it is still missing a comparison for large velocity and large interaction regime, where the experiment observed a damping rate G which depends on the velocity but not on the temperature. This behaviour is compatible with a quantum activation of phase slips.

In conclusion, our results provide for the first time the experimental evidence of quantum phase slips in one-dimensional superfluids, and consists also in the first observation of the crossover from a regime of phase slips due to thermal fluctuation to a phase slips due to quantum fluctuations. Moreover, in the regime of low velocities and low interactions, our measurements are in agreement with the theoretical model for thermally activated phase slips. However, the quantitative comparison between theory and experiment in the QPS regime is still missing.

One important feature of our setup is that the quantum regime can be reached at constant temperature, by tuning the velocity or the interaction. This offers the possibility to control the quantum phase slips nucleation rate and opens new perspectives for the study of QPS-related phenomena in ultracold quantum gases.

4.5 Dissipation at constant velocity

Dissipation at constant velocity: exploring the strongly interacting regime

In this section I will describe a second series of experiments, where we have investigated the dissipation during a shift of the trap at constant velocity. By employing this new experimental technique, we have the advantage of being able to study the phase-slips dissipation rate at interaction strengths larger than those investigated for oscillating systems.

As it was shown in the previous section, the range of velocity that can be investigated by

performing oscillation measurements is limited by the phenomenon of dynamical instability. In particular, the critical velocity v_c for this phenomenon limits above this range of velocity, which decreases when the interaction increases as the critical velocity v_c. As a consequence, experimental measurements at lower velocity are required. Nevertheless, in the oscillation measurements, the range of velocity is also limited below due to an experimental limit that is related to the finite temperature of the system. In fact, if the velocities are too small, the thermal effect provokes a finite damping which prevent the observation of a complete oscillation and thus the measurement of the dissipation rate.

Instead, by shifting the trap at constant velocity we can extend the range of the velocities investigated and, at the same time, also the range of interactions. The idea is the following: by imposing the trap displacement at constant velocity, we are able not only to reach velocity lower than those achieved in the case of an oscillating system, but we are also able to approach velocity close to the critical velocity without ever reaching it. This is an important difference respect tp the measurements performed with an oscillating system: here in fact the dynamical instability occurs when the maximum velocity is close to the critical velocity, regardless of whether the mean velocity of the system is lower than the critical one. Due to the fact that in this kind of measurements we can impose the system velocity, we can perform measurements at velocity chosen appropriately. As it was shown previously, in fact, by increasing the interactions we decrease the critical velocity. As a consequence, we perform measurements at low velocity in order to stay far from the dynamical instability also in the presence of a strongly interacting system. In particular, while in the measurements shown in subsection 4.4.2 we have reached the lowest maximum velocity of 1.2 mm/s and the highest interaction $\gamma = 1.22$, by shifting the center of the trap at constant velocity we can reach a velocity of 0.4 mm/s and an interaction $\gamma = 8.4$.

In the measurements performed by shifting the trap at constant velocity, the experimental observable is the momentum spread. In particular we measure the dissipation rate from the increase of the momentum spread, due to the fact that the energy dissipated during the system dynamics is converted into momentum spread.

In this kind of measurements we expect that a superfluid should follow the trap displacement and dissipate due to the presence of phase slips, resulting in an increase of δp. A Mott insulator should not instead follow the trap displacement and should not dissipate, unless a trap shift large enough to break the insulator is applied[24], as it will be explained more in detail in the following subsection.

For a superfluid, the dissipation rate R is related to the nucleation rate of phase slips Γ and to the system velocity v via a relation of the form $R \propto v\Gamma$.

This result can be obtained as follows. As it was shown in section 3.2.1, for a 1D system of length L the rate of change of velocity due to the presence of phase slips is related to the dissipation rate Γ via the relation

$$\frac{dv}{dt} = \frac{-h\Gamma}{mL}. \tag{4.10}$$

Therefore, for N particles, the rate of change of kinetic energy due to phase slips is

$$\frac{dE_k}{dt} = Nmv\frac{dv}{dt} = -Nhv\Gamma/L. \tag{4.11}$$

From this relation one obtains the energy dissipation rate

$$-\frac{dE_k}{dt} = h\rho v\Gamma \tag{4.12}$$

where $\rho = N/L$. By assuming the variation of the kinetic energy as an effective temperature, and using the known relation between T and δp, [91, 92], we estimate a linear increase in time of the momentum spread $\delta p = \delta p_0 + Rt$, with a rate

$$R \simeq 4vm^*\Gamma. \tag{4.13}$$

4.5.1 Shallow lattice

The first measurements that we have performed with this technique are in the presence of a shallow lattice with $s = 1$, across the SF-MI transition, for a trap velocity of 0.8 mm/s. In fig.4.16 the time evolution of δp for different values of scattering length is reported. We observe that δp increases linearly with time, as expected. In particular, when the system is in the superfluid phase, for $\gamma < \gamma_c$, δp is almost constant, showing that the system is just slightly dissipating due to phase slips, and that its coherence properties are almost preserved. By increasing the interaction, the system undergoes a phase transition to the insulator phase and we observe that δp greatly increases during the evolution. It is important to remember that the critical interaction for the transition from the superfluid phase to the insulating ones, γ_c, is estimated independently by measuring the critical scattering length with the technique shown in sec. 4.4.1 and by using the relation Eq. 2.23 between γ and g_{1D}.

With a linear fit of the data we find the dissipation rate R, which increases by increasing the interaction as shown in Fig. 4.16 b. In particular, the dissipation rate shows a roughly linear dependence on the interaction, except for the point at very low interaction ($\gamma = 0.038(4)$). In order to have an indication about the nature of the phase slips on the basis of the diagram in

fig. 4.11, we estimate T, E_j and v_c when the system is in the superfluid regime. We find a temperature $T = 27 \pm 5$ nK except for the data set at $\gamma = 0.038(4)$ which is at $T = 60 \pm 10$ nK. The higher temperature for the data set at the lowest interaction is probably due to the fact that when we use a slow ramp to set a_{load} to the final value a_{meas}, we are not really adiabatic and the system heats up. We find that the point at high temperature is in the T-dependent region suggesting that its dissipation may be due to the presence of thermally activated phase slips. By increasing the interaction, we find that the point at $\gamma = 1.8$ is close to the crossover between the T-dependent region and the v-dependent one whereas the last point in the superfluid regime ($\gamma = 3.2$) is in the v-dependent region, suggesting that the dissipation may be due to the presence of quantum phase slips. Surprisingly, we observe a finite dissipation also when the system is in the insulating regime, as shown in fig. 4.16. This dissipation may be due to two different phenomena. The first phenomenon is related to the coexistence of a superfluid and a Mott insulating phase, due to the inhomogeneity of our system. As it was described in sec. 4.2, the presence of an harmonic trap, when splitting the BEC in an array of 1D tubes, makes our system inhomogeneous and in particular we observe that de population decreases from the tubes in the center of the array to the ones in the tails. As a consequence, we may have some tubes reaching a commensurate filling and other ones where there are not commensurate regions. By increasing the interaction, the transport along individual tubes reaching a commensurate filling

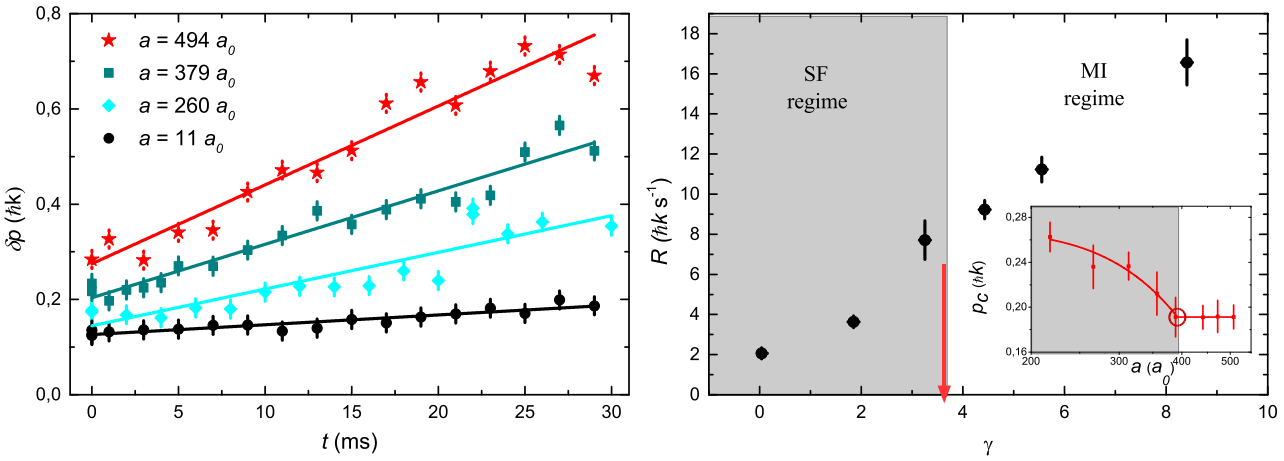

Figure 4.16: (a) Time evolution of the momentum width δp for $s = 1$ at various interaction strengths: $\gamma = 0.038(4)$ (black circles), $\gamma = 3.25(4)$ (cyan diamonds), $\gamma = 5.55(4)$ (blue squares) and $\gamma = 8.40(8)$ (red stars). Trap velocity $v = 0.8$ mm/s (i.e. $\Delta z = 24\mu$m and $t = 30$ ms). Solid lines are linear fits to extract the dissipation rate R. (b) Dissipation rate versus the interaction strength for $s = 1$. Inset: critical momentum versus scattering length. The piecewise fit (solid line) determines the experimental critical value for the SF-MI transition (empty circle) $a_c/a_0 = 392(12)$. The grey zone indicates the superfluid regime, whereas the white zone the Mott insulator regime. The solid arrow marks the experimental interaction value for the SF-MI transition ($\gamma_c = 3.44(16)$).

is globally suppressed and the system does not behave as a superfluid anymore, whereas tubes with no commensurate regions keep moving and dissipate due to the presence of phase slips.

The second phenomenon is the excitation of the gapped Mott phase. Let us analyse it more in detail. Experimentally, when we move the harmonic trap, we apply a potential gradient $\nabla V(\delta z)$, whose form can be obtained by starting from the total potential energy of the system $V(z) = \frac{1}{2}m\omega^2 z^2 + \nabla V(z)z$. By putting $V'(z) = 0$, we find that the potential gradient has the form

$$\nabla V(\delta z) = m\omega^2 \delta z. \tag{4.14}$$

By tilting the optical lattice, we change the energy difference between neighbouring lattice sites, i.e $\nabla V d$. If this energy difference equals the on-site interaction energy U in the Bose-Hubbard limit (Fig. 4.17 a), we can excite the Mott insulator and lead it to the breakdown (Fig. 4.17 b), as already exploited in the first exploration of the Mott phase with ultracold atoms in 2002 [24].

For shallow lattices in the Sine Gordon regime a quantitative description of the phenomenon is more complex, since the tunnelling is not limited to the neighbouring sites and the Mott gap is small [76]. In our case the maximum gradient $\nabla V(\Delta z)$ is of the order of $h\times 2.2(3)$ kHz/μm which is probably large enough to excite the Mott insulator. For $s = 1$, in fact, the tunnelling is not negligible up to the third neighbouring site and we expect that the Mott gap is smaller than $h\times 0.4$ kHz [76]. This suggests that the excitation of the Mott insulator in our system is highly probable. In the absence of a quantitative modelling it is not possible to discriminate which

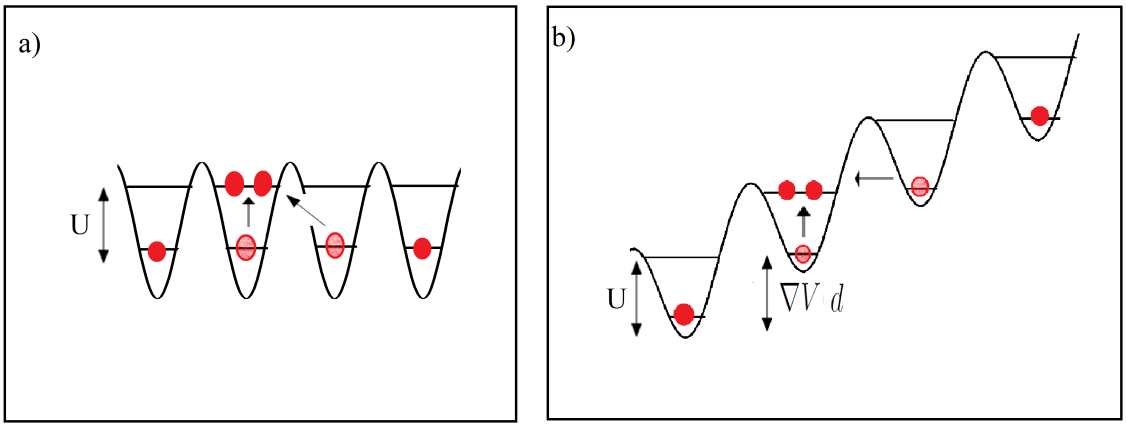

Figure 4.17: Sketch of the excitation of MI.(a) The MI is a gapped insulator and removing an atom from a site and adding it to a neighbouring one with the same filling, has an energy cost equal to the on-site interaction energy U. (b) If the energy acquired during the harmonic potential displacement, $\nabla V d$, is equal to the MI energy gap U, it become possible to excite the insulator at no energy cost.

one of the two effects dominates the observed dissipation. Further measurements, in a different regimes, are required in order to understand which effect provokes the observed dissipation also when the system is in the insulating phase. As a consequence, we decided to repeat this kind of measurements in the Bose-Hubbard regime. In this situation, in fact, the Mott insulator gap is well defined and we can compare it with the energy acquired during the harmonic trap displacement.

4.5.2 Deep lattice

We have repeated this type of experiments at constant velocity in the presence of a deeper lattice with s= 5. In this case we expect a clearer distinction between the Mott insulator and superfluid fractions of the system, since in the Bose-Hubbard limit the Mott gap is larger and the tunnelling is essentially only to the neighbouring sites.

In fig. 4.18 a the time evolution of δp, for a trap velocity of 0.4 mm/s and for different values of scattering length, is shown. Also in this case we observe a linear scaling of δp with time, in both superfluid and Mott insulator regimes. We now calculate that the Mott gap U/h

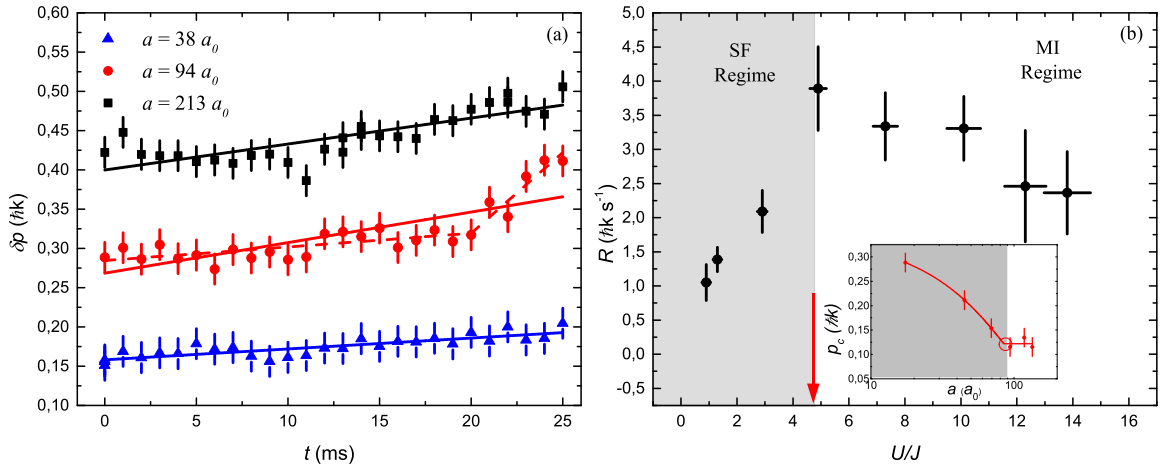

Figure 4.18: (a) Time evolution of δp for $s = 5$ and different interaction strengths: $U/J = 1.9(1)$ (blue triangles), $U/J = 4.9(3)$ (red circles) and $U/J = 12.3(7)$ (black squares)). The data set at $U/J = 4.9(3)$ is shifted by 0.1 $\hbar k$ and the data set at $U/J = 12.3(7)$ is shifted by 0.2 $\hbar k$. Trap velocity $v = 0.4$ mm/s (i.e. $\Delta z = 10\mu$m and $t = 25$ ms). The solid lines are linear fits to extract the dissipation rate R. The data set at $U/J = 4.9(3)$ show an activation mechanism, i.e. for $t > t^* \simeq 20$ ms the time evolution of δp can be fitted with a linear function with a larger slope (dashed line). (b) Dissipation rate R versus the interaction strength for $s = 5$. Inset: critical momentum versus scattering length. The piecewise fit (solid line) determines the experimental critical value for the SF-MI transition (empty circle) $a_c/a_0 = 85(15)$. The grey zone indicates the superfluid regime, whereas the white zone the Mott insulator regime. With the solid arrow we mark the experimental interaction value for the SF-MI transition ($\gamma_c = 4.5(3)$).

varies from 2.2(2) to 4.2(3) kHz, while the maximum energy shift $V'(\Delta z)d$, which is calculated by using Eq.4.14, is just $h\times 0.46(6)$ kHz, therefore an order of magnitude smaller. This excludes that the observed dissipation is due to the excitation of the Mott insulator. Consequently, the increase of δp may be due only to the excitation of the superfluid fraction that, as already discussed, coexists with the Mott phase due to the inhomogeneity of our system.

In fig.4.18 b the behaviour of the damping rate R, as a function of the interaction strength, is reported. When the system is in the superfluid regime, R increases with the interaction strength, as in the case of shallow lattices. For larger interactions we observe instead a saturation or even a decrease of R for increasing interaction strength. This behavior confirms the expectation of a freezing of the tubes where MI is forming and a residual transport on the ones never reaching commensurate density. We note that the data set near the SF-MI transition (fig. 4.18 a with $a/a_0 = 94$) behaves differently from the other data sets, as it shows an apparent activation mechanism at long times, hence at large energy shifts. This suggests that the Mott insulator might be excited for interaction strengths close to the SF-MI transition, since the gap is not yet fully developed. At larger interaction strengths we do not observe such increase at long times, confirming that the observed dissipation is entirely due to the superfluid tubes. Since the fraction of superfluid/insulating tubes is independent of the interaction strength, due to the fact that we split the BEC in the array at fixed scattering length, the decrease of R for increasing interaction indicates a decrease of the dissipation rate in the superfluid for increasing correlations.

The measurements performed at constant velocity open the way for a deeper understanding of the effect of phase slips also in the strongly interacting regime. It would be interesting to study the dissipation rate behaviour by employing systems where the presence of the Mott insulator can be excluded a priori. This condition can be reached, for example, by reducing the maximum occupation at the center of the trap below unity or by realizing an homogeneous system with a square-well trap, but both cases are not trivial from an experimental point of view. Once that the Mott phase is excluded, it would be possible to study how the phase-slip rate evolves for increasing interactions in the strongly correlated regime and in the presence of different kind of obstacles, such as isolated impurities or disordered potential.

Conclusions

The goal of this thesis is to investigate the phenomenon of phase slips in one dimensional Bose-Einstein condensates by probing the system superfluidity in the presence of an obstacle in different ranges of velocities, interactions and temperature.

The system we use is a one-dimensional Bose-Einstein condensate of ^{39}K atoms, in the presence of a 1D optical lattice along the axis of the system, which acts as an obstacle. The BEC, being a superfluid, should flow without dissipation, even in the presence of an obstacle. Anyway, by performing transport measurements, I observe a finite dissipation. I focused my attention on the dissipation phenomena that cause the superfluity breakage.

In the first part of my work, I focused my attention on the system dissipation and I investigated the system oscillation for different values of velocity. More in detail, I tuned the system velocity in a range between $v_C/5$ and v_C, where v_C is the critical velocity the dynamical instability.

Depending on the velocity, the systems behaves differently: close to the occurrence of the dynamical instability, we observed an overdamped motion, which is a consequence of the divergence of phase slips.

For velocity smaller than v_c, instead, we observed how phase slips act on our system: in this situation, we observed that our system oscillates with a damping due to the presence of phase slips. We measured the damping rate G due to the presence of phase slips for different values of interaction, velocity and temperature, far from the dynamical instability. In this situation the system never enters in the unstable regime but keeps oscillating with a finite dissipation. The damping rate G, which is related to the phase slips nucleation rate, according to the theory should behave differently depending on the nature of phase slips: in the presence of phase slips due to thermal fluctuation, the damping rate depends on the temperature, whereas it depends on velocity if phase slips are due to quantum fluctuations. This change of behaviour seems consistent with the predicted crossover from phase slips due to thermal fluctuations to the phase slips due to purely quantum fluctuations and provides the first experimental evidence of

quantum phase slips in a 1D atomic superfluid.

In the second part of experiments, we employed a different method to study the dissipation, by performing transport measurements at constant velocity, also for velocities lower than $v_C/5$, both in the regime of shallow lattices and a deep one. When the system is in the superfluid phase, the system dissipation is related to the presence of phase slips, both thermal and quantum depending on the interaction value. Surprisingly, we observed a finite dissipation also when the system is in the insulating phase. In this case it should not dissipate. This dissipation may be due to two different phenomena. The first one is related to the coexistence of a superfluid and a Mott insulating phase, due to the inhomogeneity of our system, whereas the second phenomenon is related to the excitation of the gapped Mott phase. In the presence of a weak optical lattice, it is difficult to discriminate which one of the two effects dominate the observed dissipation. As a consequence, we have repeated the same measurements in the presence of a deep lattice and also in this case we observed a dissipation both in the superfluid phase and in the insulating phase. As in the case of a weak optical lattice, when the system is in the superfluid phase, the system dissipation is related to the presence of phase slips. By comparing the gap of the Mott insulator and the energy acquired during the harmonic potential trap displacement, we found that the MI gap was an order of magnitude larger than the energy due to the trap shift. As a consequence, we excluded that the finite damping was due to the excitation of MI, and it seems due to the dissipation of the superfluid phase coexistent with the insulating ones.

Our results open the way for a deeper understanding of the intriguing phenomenon of phase slips, which is still an open topic. Since the last few years, theoretical proposal of devices based on the phenomenon of quantum phase slips have been made and it would be interesting to realize them experimentally. One of the proposed device is the quantum phase slip junction, which can be considered the dual of the Josephson junction [63]. The interest on this device is due to the fact that it may be employed to investigate the open topic of coherent quantum phase slips or can be used as resonators or as fundamental current standards. Moreover it could be also possible to realize experimentally a superconducting phase slips oscillator[64], which could be employed not only to study the phenomenon of coherent phase slips but also to obtain a few-photon non linearities, which is an important phenomenon in different branches of physics. Therefore, it is important to have a more comprehensive view of this phenomenon in order to realize devices based on phase slips. As a consequence, it would be also interesting to understand how the presence of different obstacles affects the nucleation of phase slips.

As shown in the thesis, it would be useful to employ the Bose Einstein condensate as

quantum simulator in order to answer some of the open questions about the phenomenon of phase slips. For example, it would be interesting to excited the dipole oscillations in our system in the presence of individual defects or controlled disorder. Moreover, further studies of the system dissipation during a shift of the harmonic potential trapping the atoms at constant velocity, in the absence of the Mott insulator may give information about the phase slips phenomenon in the very strongly interacting regime.

Appendix A

Disordered systems

So far I have shown how the interplay of interaction and temperature strongly affects the transport properties of a 1D bosonic superfluid in an optical lattice. The next step is to understand if also the presence of disorder may affect the transport properties. Actually, originally in three-dimensional systems and then in lower dimensional systems, it has been observed that the presence of the disorder modifies the transport properties,and lot of theoretical and experimental investigations have been performed in order to better understand this phenomenon. The main motivation to study the effect of disorder is due to the fact that it is widespread in nature. In fact, any physical structure is disordered, if observed on small enough length scales (e.g. crystal imperfections). Thanks to the fact that BECs have key properties which can be easily controlled, we can use this kind of platform also to study how the disorder affects the properties of 1D systems.
Originally the case of a 3D system of interacting bosons in a clean optical lattice in the presence of an external potential has been consider. As we have seen in sec. 2.4.3, this system can be described by the Bose-Hubbard Hamiltonian (Eq.2.30). In the presence of a disordered potential, we can still describe the system behaviour by using the Bose Hubbard model, but we need to add another term in the Hamiltonian that takes into account the presence of disorder. In this situation, the Hamiltonian takes the form

$$\hat{H}_{DBH} = -J \sum_{\langle i,i' \rangle} a_i^\dagger a_{i'} + \Delta \sum_i e_i \hat{n}_i + \frac{U}{2} \sum_i \hat{n}_i(\hat{n}_i - 1). \tag{A.1}$$

Here ϵ_i is the on-site energy given by an external potential. It depends on the disorder strength Δ via $\epsilon_i = \Delta e_i$, where e_i is a number in the interval [-1,1] and its distribution across the lattice depends on the details of disorder.

The presence of the disorder influences the nature of the system. A system of non-interacting

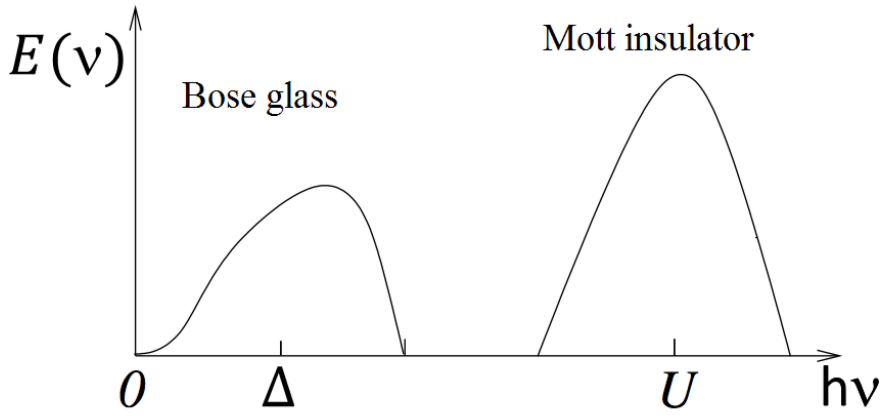

Figure A.1: Sketch of absorption energy spectrum for strongly interacting particles system in a disordered optical lattice. The peak at $h\nu \sim U$ is due to the Mott insulator whereas the peak at low frequency $h\nu \sim \Delta$ is due to the BG. Adapted from [97]

particles in a disordered potential can be described by the Hamiltonian in Eq. $A.1$, where the interaction term U is equal to zero. In this situation, if the disorder amplitude Δ exceeds a critical value of the order of tunnelling energy J, non-interacting particle can be localized due to the presence of disorder, which tends to break the coherence of the system. This phenomenon is known as Anderson localization and was predicted by Anderson in 1958 [93]. In particular, for strong enough disorder, only the lowest energy levels are populated and the wavefunction is exponentially localized. The first observation of Anderson localization in ultracold quantum gases has been achieved in 2008 in two experiments. Despite two different disordered potential have been employed (speckle in one experiment [94], quasi-periodic potential in the other [95]), both experiments have shown a suppression of the transport of matter due to the presence of disorder and the exponential shape of the tails of the atomic spatial distribution.

The next question is how the interactions among particles and disorder influence each other. Interactions among particles play a crucial role in a disordered system. In particular, for bosonic particles, the interactions mask the effect of disorder and tend to restore the coherence. For finite interaction strengths, smaller than the disorder energy, the many-body states are substantially deformed and start to occupy more than one single particle state. In this situation the interaction tends to create islands of superfluid that are not connected together so the coherence across the entire system is not yet restored. This regime is known as Bose glass [96]. When interaction strength becomes comparable with the disorder energy the coherence across the entire system is restored and the system goes in the superfluid phase.

In the Bose glass phase, the system behaves differently from the Mott insulator one if

we measure the energy absorbed by the system, due to the gapless nature of the Bose glass excitations [98]. A sketch of the excitation spectrum is reported in Fig. *A*.1 for $U \gg \Delta$. Two different excitation peaks may arise by measuring the energy absorbed by the system, one centred at the energy $h\nu \sim U$ and the other one at $h\nu \sim \Delta$. Such a spectrum is due to the fact that in a disordered inhomogeneous system, the commensurate regions of the system form a MI with an energy gap of the order of U, while the regions with incommensurate filling form a Bose glass that fills the low-energy gap.

The first observation of the Bose glass in 1D systems has been achieved in 2014 by the group of Giovanni Modugno in one experiment with bosonic ultracold atoms in the presence of a quasi-periodic optical lattice [86]. They studied the whole $\Delta - U$ diagram, in order to understand the interplay between the interactions and disorder from weak to strong interaction. By studying coherence and transport properties of the system, they traced out a draft of the complete diagram showing an incoherent regime extending from weak to strong interactions and surrounding a region of higher coherence similar to a SF. Then, in order to distinguish the Mott insulator phase from the Bose glass one, they performed a lattice modulation spectroscopy [77] and measured the excitation spectra.

The experimental procedure they used is the following. After loading the 1D quasi-condensate in the quasi-periodic lattice the main lattice is modulated in amplitude for a time t (which is chosen as long as possible, as allowed by the system background heating), in order to have the maximum sensitivity at low frequencies. The depth of the main lattice thus becomes

$$V(t) = V_0(1 + A\sin(2\pi\nu t) \tag{A.2}$$

where A is the modulation amplitude, which is kept constant and ν is the modulation frequency, which is tuned to scan the excitation spectrum. After the excitation, the lattice potentials are exponentially ramped down and the system thermalizes via atom-atom collisions. The amount of energy $E(\nu)$ absorbed by the atoms as a function of ν is obtained looking at the increase of the system temperature which can be estimated by measuring the reduction of the BEC fraction (Fig. *A*.2) or the increase of system δp.

As it is shown in Fig. *A*.2*a*, in the non-disordered case, the predicted Mott insulator response of a strongly interacting system is observable. At low frequency, for $h\nu < U$, there is not energy absorption whereas a first excitation peak appears at the Mott-gap $h\nu \sim U$. This peak is due to excitations within individual MI domains with commensurate filling. In fig *A*.2*a* another peak at $h\nu \sim 2U$ is shown. This is due to the particles hopping between a lattice site with filling n and another site with filling $n + 1$ and it is a consequence of the system inhomogeneity. By

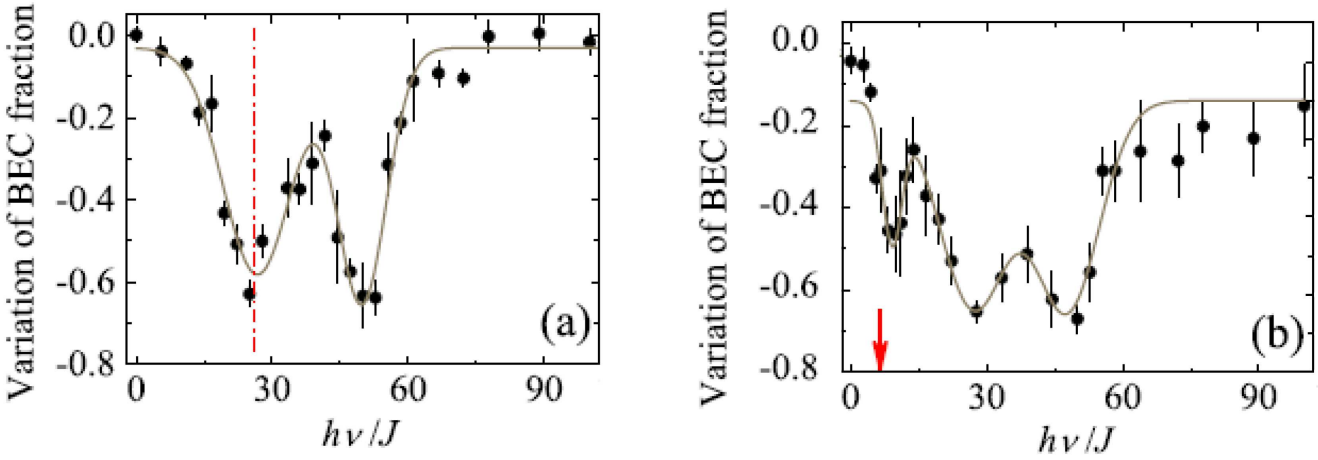

Figure A.2: Excitation spectrum for the $U = 26$ J and $\Delta = 0$ and for $U = 26$ J and $\Delta = 6.5$ J realized by measuring the variation of the condensed fraction. In the absence of the disorder, only the peaks at $h\nu = U$ and at $h\nu = 2U$ are present. In the presence of disorder, another peak appears. The red arrow is at $h\nu \sim \Delta$. Adapted from [86]

introducing a finite disorder Δ, an extra excitation peak appears (Fig. $A.2$ b) in the excitation spectra for $h\nu \sim \Delta$. This peak is consistent with the presence of a Bose glass. It is however not easy to study the Bose glass properties due to the coexistence of Bose glass and Mott insulator in the same system.

During my Ph.D I started to study and characterize the Bose glass phase in the absence of a Mott insulator. To remove the Mott insulator contribution to the excitation spectra we tune the atoms number density in order to have 1D systems with $\bar{n} < 1$. In this situation, also for strong interaction, only the Bose glass insulator is present. The idea is to characterize the Bose-glass excitation spectra for different value of disorder, temperature and interaction. During the last months I performed preliminary measurements in this regime by using the experimental technique which I described above. In order to reach the atoms number density $n < 1$ we decompress the optical dipole trap during the optical lattices. The main lattice is modulated in amplitude for a time t=200 ms with a modulation amplitude $A = 0.01$. Due to the fact that the condensate fraction is too small in this measurements, we extracted the absorbed energy by measuring the increase of δp . As it is shown in fig.$A.3$, we see an increase δp (which has the features of a excitation "peak") at $h\nu \sim 1.5$ kHz close to the theoretical value $h\nu \sim 1.26$ kHz. Unfortunately, the peak is not clear yet. Further measurements are required to find the experimental condition to see a distinct Bose-glass excitation spectrum. Once that the Bose glass phase is isolated, it would be interesting to study this insulating phase for different

value of interaction, disorder and temperature in order to understand the interplay of all energy scales.

The study of the Bose glass phase may give us the possibility to better understand the phenomenon of many body localization [86, 99, 100, 101], i.e. localization of disorder interacting system for finite temperature and interactions, due to the fact that our system is in the

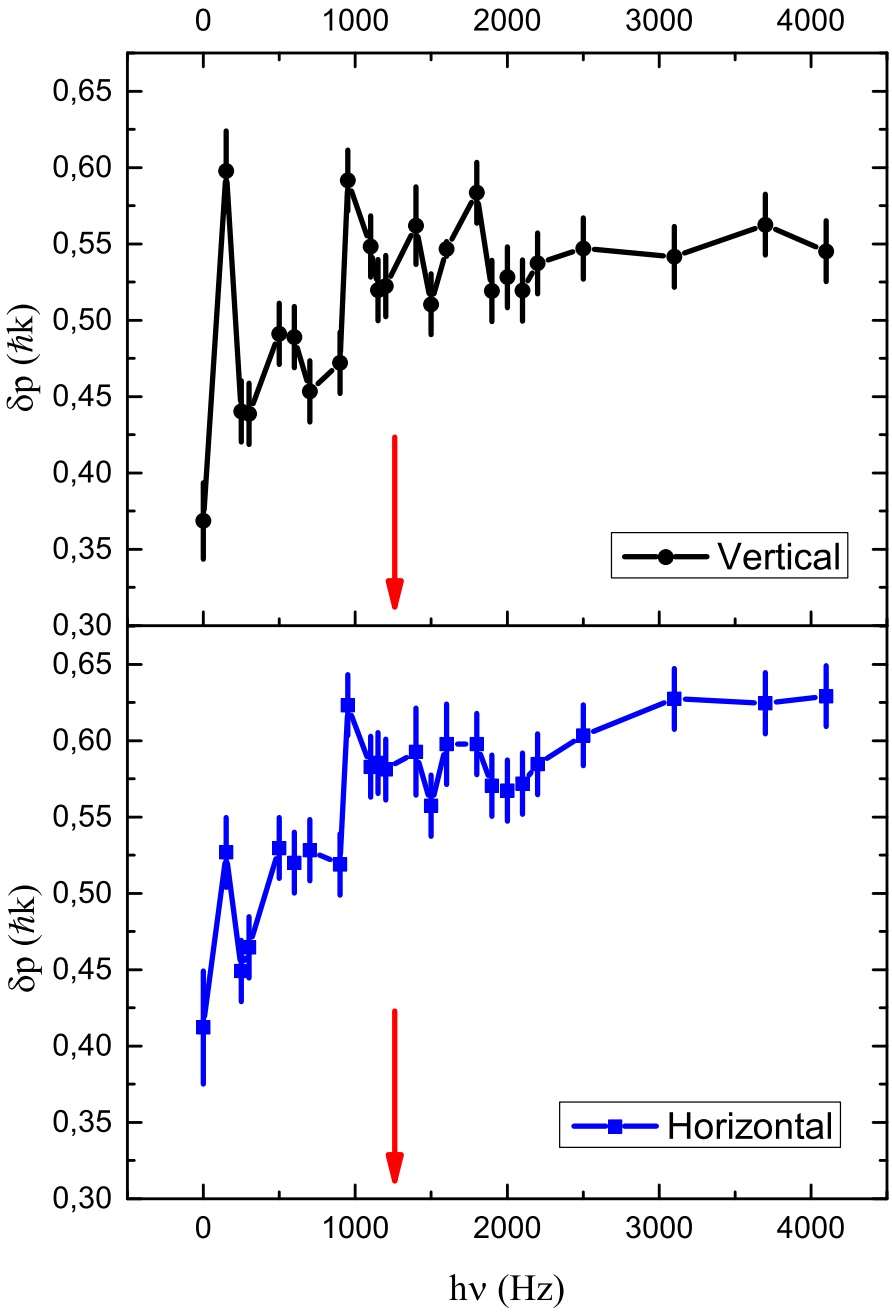

Figure A.3: Excitation spectrum for $\Delta = 1.26$ kHz realized by measuring the increase of δp along the vertical and horizontal directions. The red arrows mark the energy value $h\nu \sim \Delta$

same regime of many body localization. Consequently, it will be interesting to study the possible relation of this persisting insulating behaviour at finite T with the proposed many-body localization[100].

Appendix B

Landau instability

In the presence of an obstacle, we may observe another dissipation mechanism, different from the phenomenon of quantum phase slips or the phenomenon of dynamical instability. This phenomenon is known as energetic (or Landau) instability and it is related to the Landau's criterion for the superfluidity. According to this criterion, a system can flow without viscosity in the presence of an obstacle only if its velocity v is lower than the critical velocity

$$v_L = \min_{\mathbf{p}} \frac{\epsilon(\mathbf{p})}{p} \tag{B.1}$$

where $\epsilon(\mathbf{p})$ is the dispersion law (energy vs momentum) of the system. In this scenario, due to the fact that the presence of an obstacle does not perturb the system and does not transfer energy to collective excitations of the condensate, the system behaves as a superfluid.

In the opposite case, when the velocity is larger than v_L, for the system is more convenient to create elementary excitations rather than behave as a superfluid.

In the case of a uniform, weakly interacting BEC, the elementary excitation are described according to the Bogoliubov model [102] and the dispersion law of this excitations consists of two terms and takes the form

$$\epsilon(p) = \sqrt{\frac{gn}{m}p^2 + \left(\frac{p^2}{2m}\right)^2} \tag{B.2}$$

where g is the interaction coupling and n is the density. More in detail, the first term under the square root takes into account the effects of interactions, whereas the second one represent the free particles contribution. In the limit of small momenta, i.e. for $p \ll \sqrt{\frac{gn}{m}}m$, the second term in eq. $B.2$ can be neglected and the excitations dispersion law is linear in p and takes the form

$$\epsilon(p) = \sqrt{\frac{gn}{m}}p = v_s p \tag{B.3}$$

which is a phonon-like form where $v_s = \sqrt{\frac{gn}{m}}$ is the sound velocity. The Bogoliubov excitations are therefore plane waves which propagate in the Bose Einstein condensate with a frequency $\omega_k = v_s p$. In the other limit, i.e. for $p \gg v_s m$, it is possible to neglect the first term and to obtain the free particle dispersion law

$$\epsilon(p) = \frac{p^2}{2m}. \tag{B.4}$$

In this scenario, a weakly interacting Bose Einstein condensate satisfies the Landau's criterion for the superfluidity only if the system velocity is lower than the sound velocity v_s, which then coincides with the critical velocity v_L for the Landau instability. As it is shown in Eq. $B.3$, the sound velocity depends on the interaction g, and in particular it decreases as the interactions decrease until it vanishes at zero interactions. In the presence of an optical lattice, the sound velocity is modified since it depends on the effective mass m^* rather than the inertial mass of the system m.

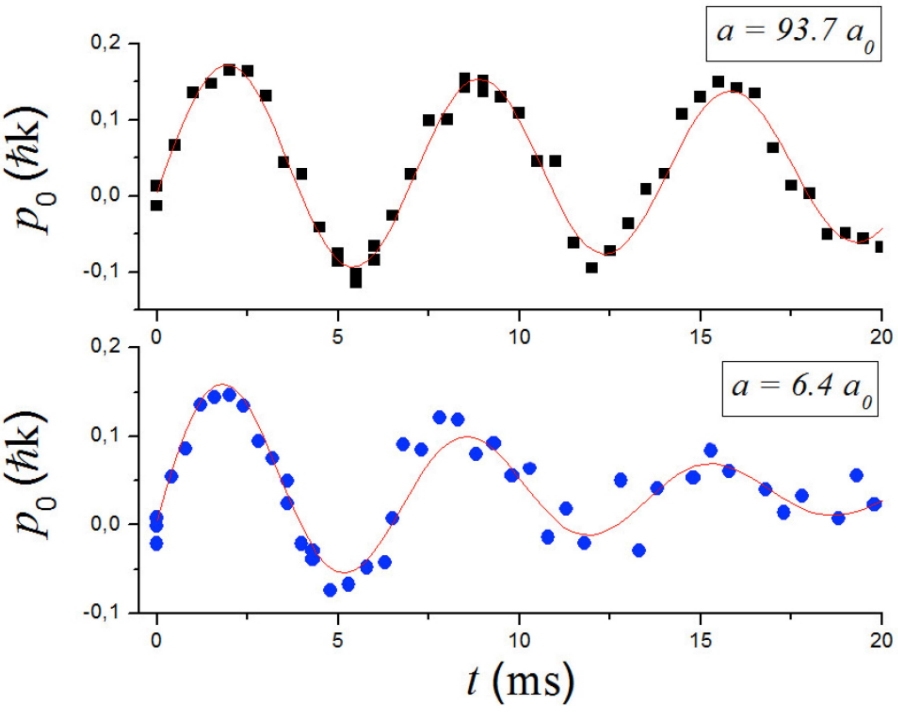

Figure B.1: Damped oscillations in 1D systems for two interaction values, $a = 93.7a0$ (black squares) and $a = 6.4a0$ (blue circles). The red solid lines are the fit realized by using Eq. 4.2. By increasing the interaction, we increase the sound velocity v_s and we observe a decrease in the oscillation damping.

From an experimental point of view, we have performed transport measurements in the absence of an optical lattice for different value of interactions, in order to observe how our system behave in the presence of phenomenon of the Landau instability. The goal of these measurements is to relate the dissipation due to this dissipation mechanism and the interaction energy in order to undestrand if the dissipation observed in the measurements reported in sec. 4.4 are due to the phenomenon of Landau instability rather than the QPS phenomenon.

More in detail, we excite the sloshing motion of the system by using the technique introduced in sec. 2.2, and we study the time evolution of the quantimomentum p_0 for different values of interaction at the same velocity $v = (1.64 \pm 0.16)$ mm/s. As it is shown in fig. $B.1$, we observe a damped oscillation, whose damping rate can be estimated by using eq.4.2 in sec.4.4. The measurements in fig. $B.1$ suggest a damping rate G which depends on the interaction, and in particular, it seems to decrease as the interaction increases. In fig. $B.2$ a, the behaviour of the damping rate G as a function of the interaction is shown. As mentioned previously, by increasing the interaction, the damping rate decreases. This behaviour seems consistent with the observations of the Landau instability: in the presence of an obstacle, the BEC behaves as a superfluid only if its velocity is lower than v_S. In our experiment, the obstacle is not an optical lattice, but an imperfection in our 2D lattice. Let us analyze it.

As it was shown in eq.$B.3$, the sound velocity depends on the interaction via the interaction

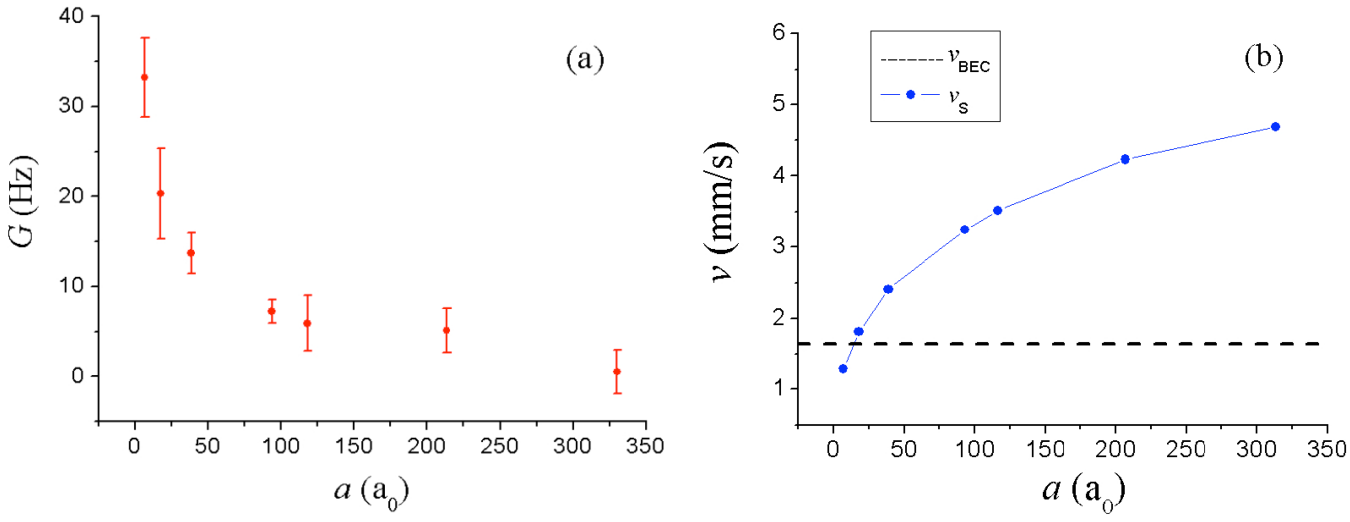

Figure B.2: (a) Damping rate G as a function of the scattering length a. The damping rate decreases as the interaction increases. (b) Calculated sound velocity v_s as a function of the scattering length a. The dashed line shows the maximum system velocity $v_{BEC} = (1.64 \pm 0.16)$ mm/s. For large scattering lengths G is small due to the fact that $v_{BEC} < v_s$. For small interactions values, where $v_{BEC} > v_s$, G is large due to the occurrence of the Landau instability.

coupling g. In particular, by increasing the interaction we increase the sound velocity (Fig $B.2$ b). As a consequence, we increase the range of velocities where the system behaves as a superfluid. For very low interaction ($a < 10a_0$) the sound velocity is smaller than the system velocity. For the BEC is easy to overcome the critical limit and we observe a larger damping rate. In this situation, the system prefers to emit phonons and dissipate rather than behave as a superfluid. By increasing the interaction we increase the critical velocity for the Landau instability above the system velocity. As a consequence, we observe a considerable decrease of the damping rate G, until it becomes negligible in the limit of strong interaction. This behaviour confirm the fact that in this situation the system prefers to behave as a superfluid. Therefore the dissipation rate that we observe in the case of 1D superfluids in the presence of an optical lattice cannot be related to the Landau instability. In fact, its behaviour as a function of the interaction is different from the case described above. As I mentioned above, by increasing the interaction we observe a decrease of the damping rate G. In the measurements shown in sect boh, instead, we observe that at low velocity, for $v \ll v_s$ the damping rate G is constant. For large velocity, instead, the damping rate G increases as the interaction increases. In both regimes of small and large velocity of the system compared to the sound velocity, the behaviour of the damping rate G as a function of the interaction is different and this confirms our idea that the observed dissipation cannot be due to the presence of phonons but is due to the presence of phase slips.

Bibliography

[1] W. A. Little., Phys. Rev. , **156**, 398, (1967).

[2] J.S. Langer and V. Ambegaokar, Phys. Rev. **164**, 498(1967).

[3] D. E. McCumber and B.I. Halperin, Phys. Rev. B **1**,1054 (1970).

[4] N. Giordano, Phys. Rev. Lett. , **61**, 18, 2137(1988).

[5] I. Danshita and A. Polkovnikov, Phys. Rev. A **85**, 023638 (2012).

[6] H. P. Büchler, V. B. Geshkenbein and G. Blatter, Phys. Rev. Lett. **87**, 100403 (2001).

[7] T. Roscilde, M. F. Faulkner, S. T. Bramwell and P. C. W. Holdsworth, New J. Phys. **18**, 075003 (2016).

[8] I. Bloch, J. Dalibard and W.Zwerger, Rev. Mod. Phys. **80** (2008).

[9] A. Bezryadin, C.N. Lau M. and Thinkham, Nature **404**, 971 (2000).

[10] C.N. Lau, N. Markovic, M. Bockrath, A. Bezryadin and M. Tinkham, Phys. Rev. Lett. **87**, 217003 (2001).

[11] F. Altomare, A. M. Chang, M. R. Melloch, Y. Hong and C. W. Tu, Phys. Rev. Lett. **97**, 017001 (2006).

[12] M. Sahu, M. H. Bae, A. Rogachev, D. Pekker, T. C. Wei, N. Shah, P. M. Goldbart and A. Bezryadin, Nature Phys. **5**, 503 (2009).

[13] Y. Chen, Y. H. Lin, S. D. Snyder, A. M Goldman and A. Kamenev, Nature Phys. **10**, 567 (2014).

[14] A. Bezryadin, J. Phys.: Condens. Matter **20**, 043202 (2008).

[15] I. M Pop, I. Protopopov, F. Lecocq, Z. Peng, B. Pannetier, O. Buisson and W. Guichard, Nature Phys. **6**, 589 (2010).

[16] S. Inouye, M. R. Andrews, J. Stenger, H. J. Miesner, D. M. Stamper-Kurn, and W. Ketterle, Science **392**, 151 (1998).

[17] H. Feshbach, Ann. Phys. **5**, 357 (1958).

[18] D. McKay, M. White, M. Pasienski and B. DeMarco, Nature **453**, 76 (2008).

[19] L. Tanzi, S. Scaffidi Abbate, F. Cataldini, L. Gori, E. Lucioni, M. Inguscio, G. Modugno and C. D' Errico, Sci. Rep. **6**, 25965 (2016).

[20] S. Scaffid Abbate, L. Gori, M. Inguscio, G. Modugno and C. D' Errico, Eur. Phys. J. Spec. Top. **226**, 2815 (2017)

[21] C.D' Errico, S. Scaffidi Abbate, G. Modugno, DOI: 10.1098/rsta.2016.0425.

[22] I. Danshita, Phys. Rev. Lett. **111**, 025303 (2013).

[23] M.Kunimi and I. Danshita, Phys. Rev. A **95**, 033637 (2017).

[24] M. Greiner, O. Mandel, T. Esslinger, T. W. Hänsch and I.Bloch, Nature, **415**, 39 (2002).

[25] L. D. Landau and E. M. Lifshitz. Statistical Physics. Pergamon Press, Oxford (1969).

[26] L.D. Landau and E.M. Lifshitz. Fluid Mechanics. Pergamon Press, Oxford (1987).

[27] S. N. Bose, Z. Phys. **26** , 178 (1924).

[28] A. Einstein, Sitzber. Kgl. preuss. Akad. Wiss.,**261** (1924); ibidem, 3(1925).

[29] M. H. Anderson, J. R. Ensher, M. R. Matthews, C. E. Weiman, and E. A. Cornell, Science **269**, 198 (1995).

[30] K. B. Davis, M. O. Mewes, M. R. Andrews, N. J. vanDruten, D. S. Durfee, D. M. Kurn, and W. Ketterle, Phys. Rev. Lett. **75**, 3969 (1995).

[31] C. C. Bradley, C. A. Sackett, J. J. Tollet, and R. G. Hulet, Phys. Rev. Lett. **75**, 1687 (1995).

[32] C. J. Pethick and H. Smith. Bose-Einstein condensation in Dilute Gases, Cambridge University Press (2001).

[33] J. Giacomelli, Localizzazione di uncondensato di Bose-Einstein in potenziali ottici, Tesi di diploma,Universit di Firenze(2007).

[34] F. Dalfovo, S. Giorgini, L. Pitaevskii and S. Stringari, Rev. Mod. Phys. **71**, 463 (1999).

[35] S. L. Cornish, N. R. Claussen, J. L. Roberts, E. A. Cornell, and C. E. Wieman, Phys. Rev. Lett. **85**, 1795 (2000).

[36] C. Chin, V. *Vuletić*, A. J. Kerman, and S. Chu, Phys. Rev. Lett. **85**, 2717 (2000).

[37] R. Grimm, M. Weidemller, and Y.B.Ovchinnikov, Advances in Atomic, Molecular and Optical Physics **42**, 95(2000).

[38] Markus Greiner, Ultracold quantum gases in three-dimensional optical lattice potential,Ludwig-Maximilians-Universitt Mnchen (2003).

[39] C. Kittel, Quantum Theory of Solids, John Wiley and Sons, New York (1963).

[40] Lorenzo Gori, 1D bosons in optical lattices: from Superfluid to Bose glass, PhD Thesis, LENS and University of Florence (2015).

[41] M. Olshanii, Phys. Rev. Lett. , **81** ,938.

[42] F. D. M. Haldane, Phys. Rev. Lett. **47**, 1840 (1981).

[43] T. Giamarchi, Quantum Physics in One Dimension, Oxford University Press, 2004.

[44] M. A. Cazalilla, R. Citro, T. Giamarchi, E. Orignac, and M. Rigol, Rev. Mod. Phys., **83**, 1405 (2011).

[45] M. Girardeau, J. Math. Phys. **1**, 516 (1960).

[46] E.H. Lieb, Phys. Rev. **130**, 1616 (1963).

[47] E. H. Lieb and W. Liniger, Phys. Rev. 130, 1605 (1963).

[48] H. K. Onnes, Leiden Comm., **120b,122b,124c** (1911).

[49] K. Y. Arutyunov, D.S. Golubev, and A.D. Zaikin, Phys. Rep. **464**, 1 (2008).

[50] J. E. Lukens, R. J. Warburton, and W. W. Webb, Phys. Rev. Lett.**25**, 1180 (1970).

[51] J. Kurkijärvi, *SQUISD-80: Superconducting Quantum Interference Devices and Their Applications* (de Gruyter, Berlin, 1980)

[52] A. O. Caldeira and A. J. Leggett, Phys. Rev. Lett., **46**, 211 (1981).

[53] J. M. Martinis, M. H. Devoret, and J. Clarke, Phys. Rev. B **35**, 4682 (1987).

[54] G. H. Lee, D. Jeong, J. H. Choi, Y.J. Doh, H.J. and Lee, Phys. Rev. Lett. **107**, 146605 (2011).

[55] H. F. Yu, X. B. Zhu, Z. H. Peng, Y. Tian, D. J. Cui, G. H. Chen ,D. N. Zheng, X. N. Jing , L. Lu, S.P. Zhao, and S. Han, Phys. Rev. Lett. **107**, 067004 (2011).

[56] L. D. Jackel, J. P. Gordon, E. L. Hu, R. E. Howard, L. A. Fetter, D. M. Tennant, R. W. Epworth, and J. Kurkijrvi, Phys. Rev. Lett. **47**, 697 (1981).

[57] O. V. Astafiev, L. B. Ioffe, S. Kafanov, Y. A. Pashkin, K. Y. Arutyunov, D. Shahar, O. Cohen, and J. S. Tsai, Nature **484**, 355 (2012).

[58] A. Bezryadin, C.N. Lau M. and Thinkham, Nature**404**, 971 (2000).

[59] C.N. Lau, N. Markovic, M. Bockrath, A. Bezryadin and M. Tinkham, Phys. Rev. Lett. **87**, 217003 (2001).

[60] M. Sahu, M. H. Bae, A. Rogachev, D. Pekker, T. C. Wei, N. Shah, P. M. Goldbart and A. Bezryadin, Nature Phys. **5**, 503 (2009).

[61] Y. Chen, Y. H. Lin, S. D. Snyder, A. M Goldman and A. Kamenev, Nature Phys. **10**, 567 (2014).

[62] A. Bezryadin, J. Phys.: Condens. Matter **20**,043202 (2008).

[63] J. E. Mooij and C. J. P. M. Harmans, New J. Phys. **7**,219 (2005).

[64] A. M. Hriscu and Yu. V. Nazarov, Phys. Rev. Lett. **106**, 077004 (2011).

[65] A. Belkin, M. Belkin, V. Vakaryuk, S. Khlebnikov and A. Bezryadin, Phys. Rev. X **5**,021023 (2015).

[66] C. D. Fertig, K. M. O'Hara, J. H. Huckans, S. L. Rolston, W.D. Phillips and J.V. Porto, Phys. Rev. Lett. **94**, 120403 (2005).

[67] J. Mun, P. Medley, G. K. Campbell, L. G. Marcassa, D. E. Pritchard and W. Ketterle, Phys.Rev.Lett. **99**, 150604 (2007).

[68] L. Tanzi, E. Lucioni, S. Chaudhuri, L. Gori, A. Kumar, C. D' Errico, M. Inguscio and G. Modugno Phys. Rev. Lett. **111**, 115301 (2013).

[69] L. D. Landau and V. L. Ginzburg, Zh. Eksp. Teor. Fiz. **20**, 1064 (1950).

[70] C. G. Callan and S. Coleman, Phys. Rev. D, **16**, 1762 (1977).

[71] S. Coleman, Phys. Rev. D, **15**, 2929 (1977)

[72] S. Khlebnikov and L. P. Pryadko, Phys. Rev. Lett. **95**, 107007 (2005).

[73] B. Gadway, D. Pertot, J. Reeves, M. Vogt, and D. Schneble, Phys. Rev. Lett. **107**, 145306 (2011)

[74] M. Pasienski, D. McKay, M. White, and B. DeMarco, Nat. Phys. **6**, 677 (2010)

[75] M. Albiez, R. Gati, J. Flling, S. Hunsmann, M. Cristiani, and M. K. Oberthaler, Phys. Rev. Lett. **95**, 010402 (2005)

[76] E. Haller, R. Hart, M. J. Mark, J. G. Danzl, L. Reichsöllner, M. Gustavsson, M. Dalmonte, G. Pupillo, and H. C. Nägerl, Nature **466** , 597 (2010)

[77] T. Stöferle, H. Moritz, C. Schori, M. Köhl, and T. Esslinger, Phys. Rev. Lett. **92**, 130403 (2004)

[78] S. Burger, F. S. Cataliotti, C. Fort, F. Minardi, M. Inguscio, M. L. Chiofalo, and M. P. Tosi, Phys. Rev. Lett. **86**, 4447 (2001)

[79] D. McKay, M. White, M. Pasienski, and B. DeMarco, Nature **453** , 76 (2008)

[80] C. D' Errico, Osservazione di Risonanze di Fano-Feshbach in miscele atomiche K-Rb, Master Thesis, University of Florence (2005).

[81] M.Landini, S.Roy, L.Carcagni, D.Trypogeorgos, M.Fattori, M.Inguscio, and G. Modugno, Phys. Rev. A **84**, 043432 (2011).

[82] G. Roati, Quantum degenerate Potassium-Rubidium mixtures, PhD Thesis, University of Trento (2003).

[83] M. Zaccanti, Tuning of the interactions in ultracold K-Rb quantum gases, PhD thesis, University of Florence (2007).

[84] C. D' Errico, Anderson localization of a weakly interacting Bose-Einstein condensate , PhD Thesis, University of Florence (2008)

[85] L. Gori, T. Barthel, A. Kumar, E. Lucioni, L. Tanzi, M. Inguscio, G. Modugno, T. Giamarchi, C. D' Errico, and G. Roux, Phys. Rev. A **93**, 033650 (2016).

[86] C. D' Errico, E. Lucioni, L. Tanzi, L. Gori, G. Roux, I. P. McCulloch, T. Giamarchi, M. Inguscio and G. Modugno, Phys. Rev. Lett. **113**, 095301 (2014).

[87] V. Dunjko, V. Lorent and M. Olshanii, Phys. Rev. Lett. **86**, 5413 (2001).

[88] L. De Sarlo, L. Fallani, J. E. Lye, M. Modugno, R. Saers, C. Fort, and M. Inguscio, Phys. Rev. A **72**, 01360 (2005).

[89] E. Altman, A. Polkovnikov, E. Demler, B. I. Halperin, and M. D. Lukin, Phys. Rev. Lett. **95** 020402 (2005)

[90] G. Boéris, L. Gori, M. D. Hoogerland, A. Kumar, E. Lucioni, L. Tanzi, M. Inguscio, T. Giamarchi, C. D' Errico, G. Carleo, G. Modugno and L. Sanchez-Palenchia, Phys. Rev. A **93**, 011601(R) (2016).

[91] S. Richard, F. Gerbier, J. H. Thywissen, M. Hugbart, P. Bouyer and A. Aspect, Phys. Rev. Lett. **91**, 010405 (2003).

[92] F. Gerbier, Ann. Phys.Fr. **29** 1, 1 (2004).

[93] P. W. Anderson, Phys. Rev. 109, 1492 (1958).

[94] J. Billy, V. Josse, Z. Zuo, A. Bernard, B. Hambrecht, P. Lugan, D. Clment, L. Sanchez-Palencia, P. Bouyer and Alain Aspect, Nature **453**,891(2008)

[95] G. Roati, C. D' Errico, L. Fallani, M. Fattori, C. Fort, M. Zaccanti, G. Modugno, M. Modugno and M. Inguscio, Nature **453**, 895 (2008).

[96] M. P. A. Fisher, P. B. Weichman, G. Grinstein, and D. S. Fisher, Phys.Rev.B 40, 546 (1989).

[97] G. Orso, A. Iucci, M. A. Cazalilla, and T. Giamarchi, Phys. Rev. A, **80**, 033625 (2009).

[98] L. Fallani, J. E. Lye, V. Guarrera, C. Fort, and M. Inguscio, Phys. Rev. Lett. **98**, 130404 (2007).

[99] D. M. Basko, I. L. Aleiner and B. L. Altshuler, arXiv:cond-mat/0602510

[100] I. L. Aleiner, B. L. Altshuler and G. V. Shlyapnikov, Nature Physics **6**, 900 (2010).

[101] M. Schreiber, S. S. Hodgman, P. Bordia, H. P. Lschen, M. H. Fischer, R. Vosk, E. Altman, U. Schneider and I. Bloch, Science **349**, 842 (2015).

[102] N. N. Bogoliubov, J. Phys. (USSR) **11**, 23 (1947)..